DUAL MODE SUSPENDED SUBSTRATE STRIPLINE (SSS) FILTER

NORAZWANA BINTI MOHD NAJIB

Submitted in accordance with the requirements for the degree of
Doctor of Philosophy

**The University of Leeds,
School of Electronic & Electrical Engineering.
May 2018**

Declaration

The candidate confirms that the work submitted is her own, except where work which has formed part of jointly-authored publications has been included. The contribution of the candidate and the other authors to this work has been explicitly indicated below. The candidate confirms that appropriate credit has been given within the thesis where reference has been made to the work of others.

The details of chapter 3 of the thesis are based on the following published paper:

[1] N. Binti Mohd Najib, N. Somjit, and I. Hunter, "Design and Characterisation of Dual-Mode Suspended-Substrate Stripline Filter," *IET Microwaves, Antennas Propag.*, pp. 1–7, 2018.

The candidate (Norazwana binti Mohd Najib) performed the experimental work and prepared the initial draft along with the graphical and tabular presentation, calculation and summarization of the paper.

The co-author (Prof. Ian Hunter and Nutapong Somjit) supervised the work, proof read the drafts and made suggestions and corrections to the draft paper.

Norazwana binti Mohd Najib

Acknowledgement

I would like to thank to Professor Ian C. Hunter and Dr Nutapong Somjit for their endless knowledge, encouragement, patience and support given throughout my study. I am very thankful to have a supervisor and co-supervisor whom really concern about my research work and very responsive to all my queries throughout this period. It was also not complete without expressing the gratitude towards my husband, my lovely daughter any all my family for their continuous support, encouragement, understanding and patience to all the ups and downs during my study period. I would also like to express gratitude to my friend Zahari for all his help as well as the moral support.

Finally, I would like to thank the Malaysian Government for providing the funding which allowed me to conduct this research.

Abstract

Evolution of wireless communication systems towards high flexibility, low cost and high efficiency leads to tremendous activity in the area of microwave filters. In an RF front-end of a cellular radio base station, signals are being transmitted and received simultaneously. In the receive band, there are chances of intermodulation products from the power amplifier being fed to the receiver, thus the transmit filter must have a very high level of signal rejection. Furthermore, the transmit filter must also have low passband insertion loss since it impacts the power transmitted and the overall transmit system efficiency. Recently, filters with dual-mode operation were being investigated due to their ability to produce two degenerate modes using a single physical structure; therefore, the size and cost of the filter can be reduced without compromising any figure-of-merits.

A dual mode suspended substrate stripline filter is presented in this thesis. These filters enable achieving low insertion loss, high Q, high selectivity and good spurious response. Initially, a dual mode ring resonator structure is investigated using suspended substrate stripline technology. This technology is used due to its advantages which are comparable to microstrip or any other planar transmission lines. The HFSS three dimensional finite element method (FEM) is used to evaluate the resonant frequency, quality factor and the first harmonics.

A second order suspended substrate stripline filter was designed with capacitive coupled input and output feeding method. The input and output feed were positioned 90 degree from each other while a notch was used in this filter to couple two degenerate modes which also control the bandwidth of the filter. A high performance Generalized Chebychev filter was designed to meet the stringent electrical requirement in the RF front-end of a cellular radio base station. With this fourth order filter, four finite frequency transmission zeros were achieved due to phase cancellation between two paths which results in high selectivity filter response. Metal tuning screws were added to improve any practical imperfections. Finally an asymmetrical Generalized Chebychev filter was designed with real frequency transmission zeros positioned on one side of the passband. With this design, the aim of achieving higher selectivity filter response above the passband was demonstrated.

Table of Contents

List of Figures

Abbreviations

BPF – Band pass filter

BS - Base station

BW – Bandwidth

CMS – Coupling matrix synthesis

CPW – Co-planar waveguide

DSS – Defected stripline structure

GHz – Gigahertz

HFSS – High frequency structure simulator

IL – Insertion loss

LPF – Low pass filter

MHz – Megahertz

PLR – Power loss ratio

RF – Radio Frequency

RL – Return loss

SSS – Suspended substrate stripline

TEM – Transverse electromagnetic

TZ – Transmission zero

WLAN – Wireless local area network

Chapter 1 Introduction

1.1 Introduction to Microwave Filters

Microwaves are electromagnetic waves as are radio waves, infrared (IR), visible light, ultraviolet (UV), X-rays and gamma-rays. The term *microwave* refers to the region of electromagnetic spectrum ranging from 300 MHz to 300 GHz with a corresponding free space wavelength between 1m and 1mm respectively. A microwave filter is a two-port network used to control the frequency response of systems, by passing the desired signals and attenuating unwanted signals. Microwave filters play a vital role in the development of RF/microwave applications. Some of the major applications are communication systems, terrestrial, mobile & satellite, radar systems, environmental remote sensing and medical systems. In recent decades, the significant development of communication systems due to the increasing demands for high flexibility, low cost and high efficiency have led to much research on microwave filters. For example, Figure 1 shows the RF front end of a cellular base station where

diplexers are commonly used to combine transmitter and receiver into a single antenna.
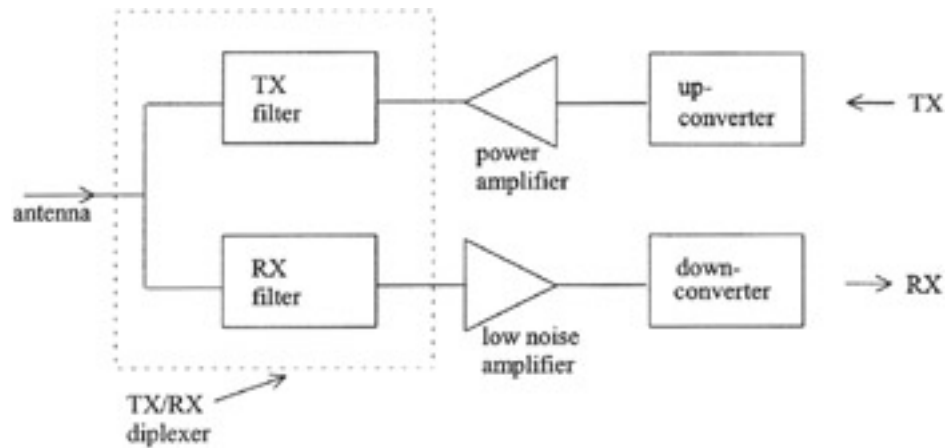
Figure 1 RF Front end of a cellular base station [2]

Because signals are being transmitted and received simultaneously, the transmit filter must have a very high level of rejection in the receive band in order to eliminate the chances of intermodulation products from the power amplifier being fed to the receiver. Furthermore, the transmit filter must also have low passband insertion loss since it impacts the power transmitted and the transmit system efficiency. Therefore, the biggest challenge in achieving an ideal cellular base station is to design a filter structure which is capable to handle high power, gives high out of band rejection as well as low losses. In this research, a focus will be given to designing a dual-mode ring resonator filter using suspended substrate stripline (SSS) technology. Adapting and utilising the key features of suspended substrate stripline (SSS) into dual-mode filter design results in a low-loss and high selectivity miniaturised planar filter for the application of modern communication systems.

1.2   Review of Ring Resonators

A simple and straight-forward structure of ring resonator consists of the feed lines, coupling gaps and the resonator itself. Figure 2 shows an example of a simple ring resonator structure where the resonator is loosely coupled to the feeding lines. In this figure, power is fed in and out of the feeding line and coupling gaps. Meanwhile, the coupling gap represents the capacitance value which influences the resonant frequency of the ring. The bigger the coupling gap, the lesser it influences the resonant frequency. In other words, stronger coupling will give more effect on the resonant frequency. In a single ring resonator, resonance occurs when the mean circumference of the ring is equal to an integral multiple of the guided wavelength.
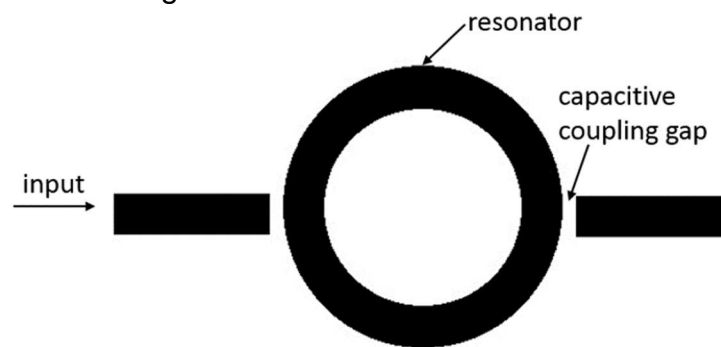
Figure 2 Single Ring Resonator
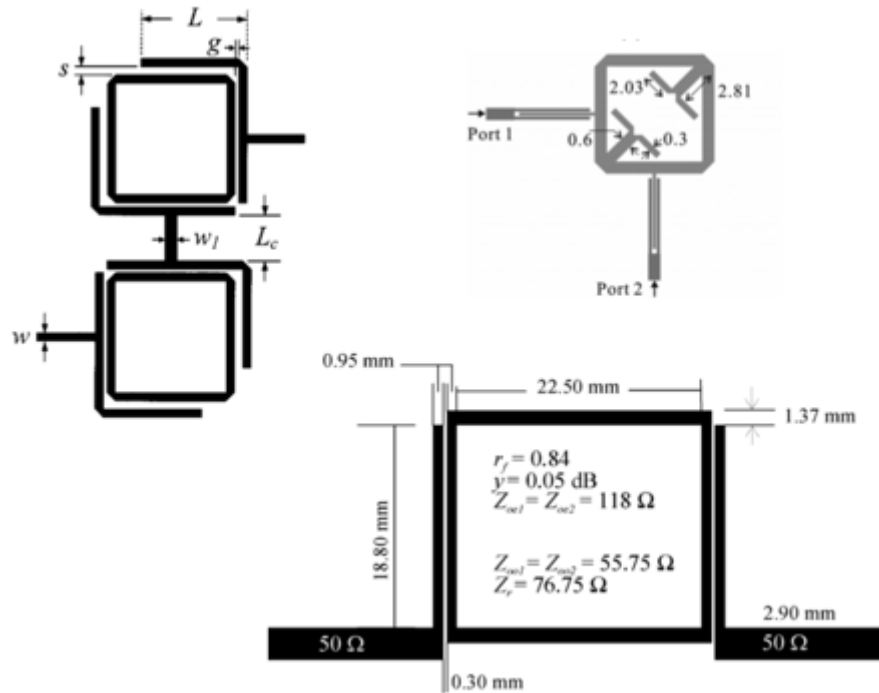
Figure 3 Past research on ring resonator filters [3]–[5]

For the past few decades, much work has been conducted on ring resonator filter. Some of them were mentioned in [3]–[7] and some of the structures are demonstrated in Figure 3. Ring resonators can be classified into the single-mode and multi-mode resonator. The single-mode ring resonator is often used in the theory and design of simple lowpass, bandpass, highpass and bandstop filters. In modern communication systems, filters are normally designed with more than one element; thus, resulting in lossy and bulky resonator filter due to the combination of more than one resonator. Therefore, utilizing multimode resonator such as dual-mode ring resonator is always considered as the best solution. This is because each of the dual-mode ring resonators acts like a double tuned circuit; hence the number of resonators required can be reduced by half. In a single ring resonator, dual-mode can be achieved with few steps as follows:

1) Input and output ports should be perpendicular

2) Perturbation which may take the form of patch, notch or stub added symmetrically 135 degrees from both input and output port

3) A plane of symmetry should exist within circuit

1.2.1 Coupling Methods for Ring Resonators

The performance of ring resonator filter can be enhanced or degraded by the method of coupling. Therefore, choosing a suitable coupling technique is very important to achieve the best filter performance. Basically, there are few coupling techniques can be applied to ring resonator such as (1) loose coupling, (2) matched stub, (3) enhanced coupling, (4) annular coupling, (5) direct connection and (6) side coupling [8]. Loose coupling is the simplest coupling method where it is an illustration of the negligibly small capacitance of the coupling gap. Figure 4a portrayed the arrangement of loose coupling where a feed line is connected to the ring through a small gap spacing.
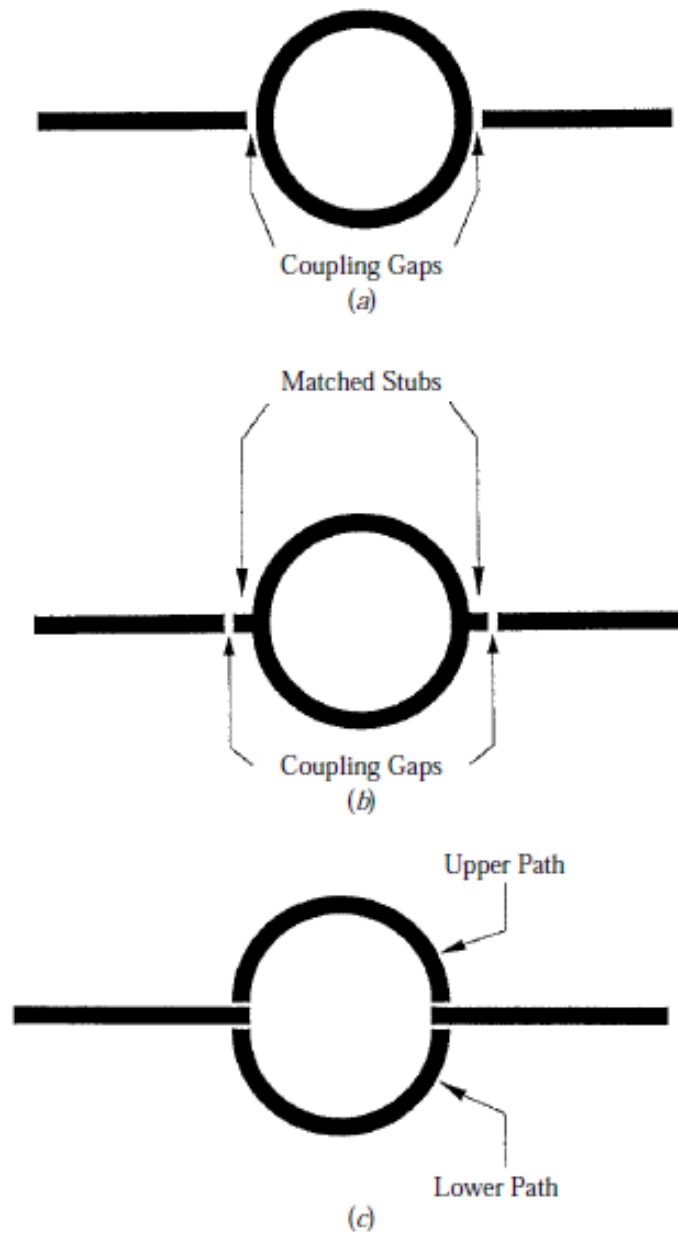
Figure 4 Coupling methods (a) loose coupling; (b) matched stubs; (c) enhanced coupling

Figure 4b demonstrated the arrangement of matched stubs coupling where the gaps are formed between the feed lines and the matched stubs. The enhanced coupling showed in Figure 4c is implemented by punching the feed lines into the annular ring element.
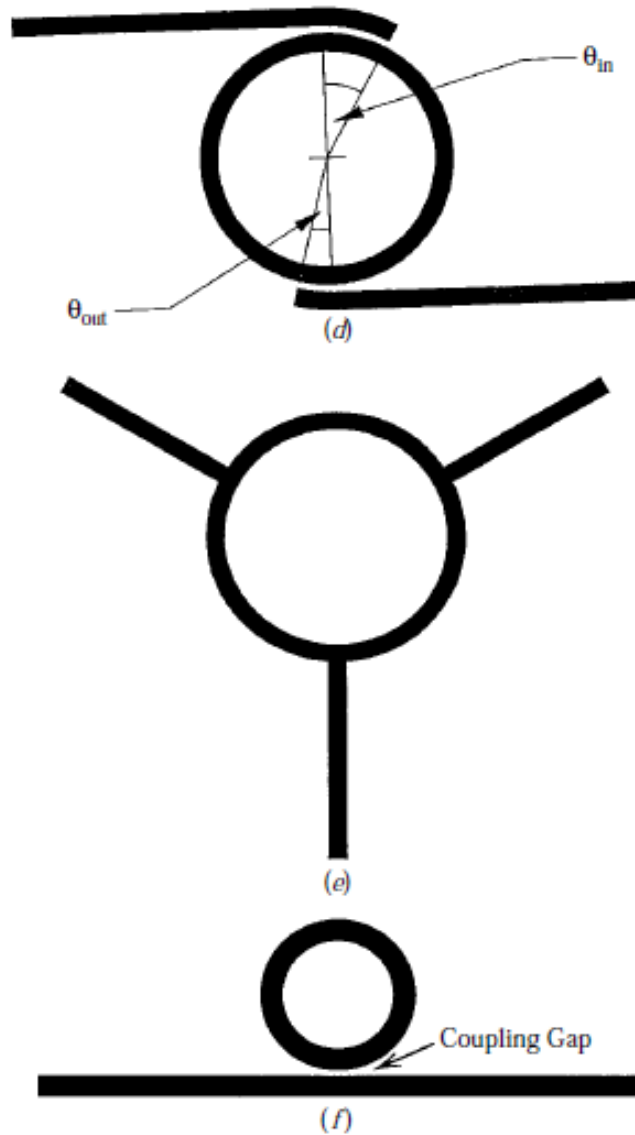
Figure 5 Coupling methods (d) annular coupling; (e) direct connection; and (f) side coupling

There are two coupling gaps on each port which are formed between the enhanced feed lines and the ring. An advantage of using the enhanced coupling technique compared with the loose coupling technique is that the resonant frequency does not change significantly by changing the gap size. The annular coupling arrangement is presented in Figure 5d where the coupling length is presented by two annular angles that is θ_{in} and θ_{out}. Figure 5e and Figure 5f

demonstrated the direct connection and side coupling arrangement of a ring resonator respectively. In [9], a study has been performed to investigate different coupling techniques which can be applied to a ring resonator considering loose coupling, enhanced coupling and matched stub coupling. Of all techniques analysed, the loose coupling turned to be the most preferable technique due to its simplicity to implement.

1.3   Review of Suspended Substrate Stripline (SSS)

Suspended substrate stripline (SSS) is a variant of stripline that offers higher Q factor and wider value range of realisable characteristic impedances compared to microstrip. Many RF and microwave components such as directional couplers, power dividers and transistor amplifiers are manufactured using SSS technology. SSS is a printed circuit technology that can be used for both broadband and narrowband filters; typical frequency range 500 MHz to 40 GHz. SSS consists of a conducting strip supported on a thin dielectric substrate that is located between a pair of ground planes between two air gaps [10]. Figure 6 shows a cross-section of a suspended substrate stripline (SSS). The most interesting aspects of SSS are the circuit patterns can be printed on both sides of the stripline that enables broadside strong coupling, as well as the use of a metal housing that prevents the fields from radiating to the external of the circuit. SSS also offers high Q factor due to the dielectric which is mainly the air, and no surface waves as in microstrip.

Filtering circuits implemented using SSS offers greater advantages such as high selectivity, lower insertion loss and good temperature stability. Since SSS is a purely transverse electromagnetic (TEM) transmission line media, it is

non-dispersive, and this makes SSS such an interesting medium for the implementation of all types of filters.
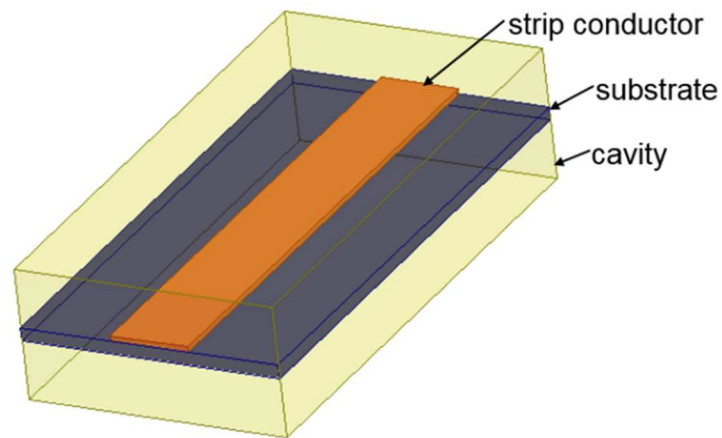
Figure 6 Cross-section of Suspended Substrate Stripline (SSS)

The impedance of a TEM transmission line can be written as

$$Z_o\sqrt{\varepsilon_r} = \frac{377}{C/\varepsilon}$$

1.1

where ε_r is the dielectric constant and C/ε is the normalised static capacitance per unit length of the transmission line.
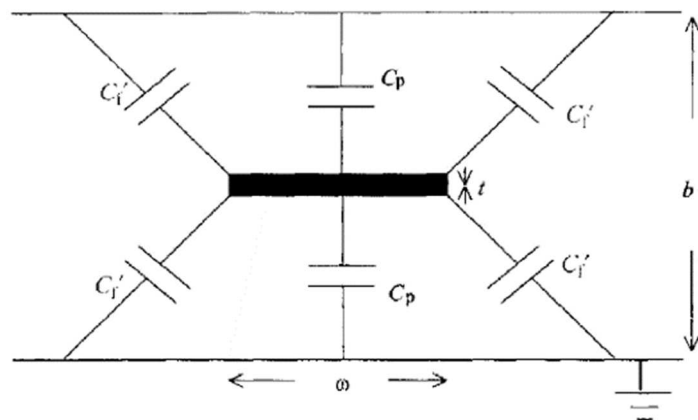
Figure 7 Single suspended transmission line [2]

Figure 7 shows a single suspended transmission line where the fringing effect is normally taken into account in the normalised static capacitance equation, thus gives [11]:

$$\frac{C}{\varepsilon} = 2C_p + \frac{4C'_f}{\varepsilon} \qquad 1.2$$

where C'_f is the fringing capacitance to ground which is plotted in Figure 8.

$$C_p = \frac{\frac{w}{b-t}}{2} \qquad 1.3$$

From the above equation, b is the ground plane spacing, w is the width and t is the thickness of the strip conductor. In a printed circuit, t is normally assumed as 0; hence, from Figure 8

$$\frac{C'_f}{\varepsilon} = 0.46 \qquad 1.4$$

Thus the equation becomes

$$\frac{C}{\varepsilon} = \frac{4w}{b} + 1.84 \qquad 1.5$$

Rearranging the equation represents the width of the transmission line as:

$$w = \frac{b}{4}\left(\frac{377}{Z_0} - 1.84\right) \qquad 1.6$$

where Z_o is the characteristic impedance. The effective dielectric constant of SSS is approximately unity because dielectric is thin with respect to the ground plane spacing b.
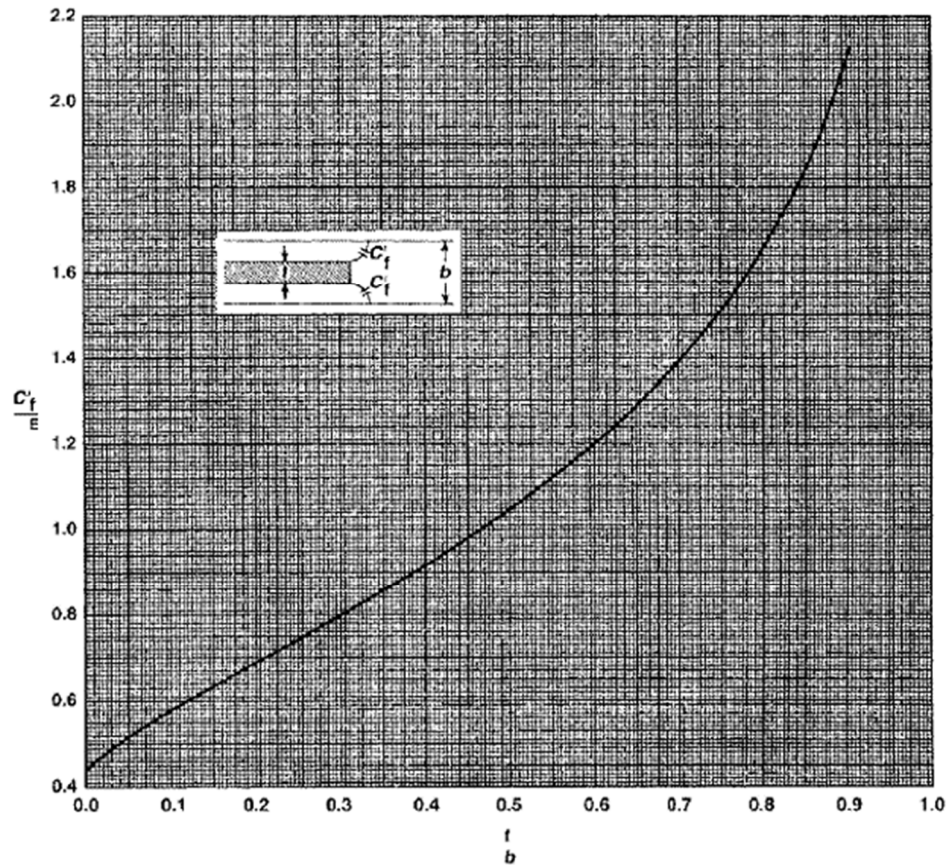
Figure 8 Fringing capacitance from a rectangular bar [12]

1.4   Literature Reviews

A concise overview of past research about recent advancements in filter design which is relevant to the objectives of this project is presented. It covers dual-mode filter design using microstrip and other filter technologies as well as some research on suspended substrate stripline filters.

1.4.1   Dual-mode Filters

A dual-mode filter basically is a filter with resonators which exhibit two degenerate modes using a single physical structure. In other words, a dual-mode filter behaves in theory as a pair of coupled resonators. Consequently, the size and cost of the filter can be reduced without compromising any figure-of-merits.

Recently, the interest in the design of low-insertion loss, low-cost, and high-quality dual-mode filters has grown, especially given the large filter numbers needed in modern base station. There are many research works using a different type of technologies such as planar, coaxial, cavity and waveguide filters. Some dual-mode filters found in the research literature include the coaxial filter [13]–[15], waveguide filter [16]–[19], dielectric resonator filter [20]–[22] and patch based resonator filters [23]–[25].

Microstrip technology is frequently used in designing dual-mode filters due to its advantages such as low profile and fabrication cost. The dual-mode resonator for microstrip filter applications was firstly introduced in [26] using ring resonators in the early 1970s. A dual-mode rotational symmetric resonator filter was developed with two transmission zeros generated near the upper and lower passband [27]. Besides, a fourth-order dual-mode microstrip filter with interdigital capacitive loading element was developed in [28]. In [29] and [30], compact dual-mode microstrip filters were designed, fabricated and evaluated by using parallel coupled resonators and meander loop resonators, respectively. Furthermore, a triangular microstrip dual-mode filter based on the coupling matrix synthesis method was developed with a good rejection performance obtained [31]. Also, a dual-mode filter with source-load coupling was designed in [32] and [33] with which demonstrated good filter performance. In [34], a dual-mode microstrip bandpass filter was designed and tested, in which slots and metallic via were used to reduce the overall filter size and introduce another resonant mode. Besides, cross-coupling from source to load were used in the design to introduce transmission zeros, hence improved the out-of-band rejection level. In [35], Yatendra and Ajay designed a miniaturised dual mode circular patch bandpass

filter. It was clearly shown that the introduction of slots on the circular patch with the right dimensions and position could further reduce the resonant frequency; meaning that it was highly miniaturised and reduced the harmonic separation between two passbands.

A planar dual-mode microstrip bandpass filter with a square notch was designed in [36], where an inset feed was used to perturb the field of resonators, thus exciting two degenerate modes. A perturbation element at the centre of the filter was used to couple two degenerate modes, thus leading to mode splitting of the filter response. In [37], a miniaturised dual mode spiral ring resonator with asymmetrical perturbation was investigated. In the design, the overall filter size reduction was achieved by using a triple ring spiral configuration, where each of them was connected to the others by via-holes and CPW sections in the ground plane. However, the limitation of this design was observed when the design frequency was higher, in which the distance between rings became bigger due to the application of "three times the line width" rule; hence, increased the physical size of the filter. A miniaturized dual-mode ring resonator bandpass filter with a wide passband was designed in [38]. The wideband property was realized by adding an impedance transformer at the input and output feeding port where the transformer was meandered to miniaturize the circuit size. Besides, the dual-mode response was achieved by using an inductive perturbation which is asymmetrically located to the input and output feeding port.

A study on dual-mode patch resonator-based microwave filters with transmission zeros at real or imaginary frequencies was conducted in [24]. The two degenerate modes were excited by a pair of orthogonal feeding line and a circular hole that serves as the perturbation element. In the design, a few

perturbation locations were implemented on a patch resonator to observe its influence on the frequency response. As a result, transmission zeros were observed when the perturbation was located unsymmetrical with respect to the excitation ports, which improved the selectivity of the filter response. However, there was no transmission zero created if the perturbation was located symmetrically to the excitation ports, which indicates that the transmission zeros were shifted from real frequencies to imaginary frequencies. Cheab and Wong in [39] discussed the design and synthesis method of a dual mode and quasi-elliptic dual mode microwave filter. In the design, transmission and reflection polynomials for both filters were generated to obtain even and odd admittances that were used to determine the filter topology and coupling matrix. Besides, rotating matrix technique was applied to the coupling matrix to eliminate the inter-resonator coupling. Besides the past research contributed on dual-mode filters with various structures, a study on the literature related to suspended substrate stripline technology was also carried out.

1.4.2 Suspended Substrate Stripline (SSS) Filters

A large and growing body of literature has been investigated on filter design using SSS. SSS is a type of planar transmission line that is considered as a good selection of transmission line for filter design. This is because of the merits such as high selectivity, high Q values and lower insertion loss compared to other types of transmission lines. In 1983, Rhodes and Mobbs published a paper, in which they described filtering circuits designed using SSS structure [40]. A compact asymmetrical SSS filter using an open loop meandered resonator structure was designed in [41]. In this design, the cross-coupling between non-adjacent resonator was used to create transmission zero on the

side of the passband, hence enhance the out-of-band rejection and give high selectivity performance characteristics. Another compact asymmetrical SSS filter was also designed in [42] where an open loop resonator based on meandered half-wavelength topology was used. The transmission zero is created due to the cross-coupling between two resonators, thus a positive coupling creates transmission zero on the high side while a negative coupling creates transmission zero on the lower side.

In [43], an ultra-wide band SSS filter with a frequency range from 3.1 to 10.6 GHz was designed and implemented. The filter consisted of a quasi-lumped low pass filter that was capacitively coupled to the input and output port. Although this is a simple design implemented by making use of a capacitor to suppress low frequency, it gives a problem when implemented with a microstrip circuit, especially as it requires higher capacitance value. Back in 2008, a broadband suspended stripline bandpass filter using an end-coupled resonator printed on both surfaces of the substrate was designed and tested in [44]. Low insertion loss and wide passband were obtained in this design; thus, making it suitable for various applications.

An SSS bandpass filter using an H-shaped resonator was proposed in [45]. In the design, the circuit pattern was printed on both surfaces of the substrate; thus, enabling broadside coupling. The resulting output gives insertion loss of lower than 1 dB with measured group delay variation between 0.5-1.5 ns. An ultra-wide band SSS filter comprises of band rejection slot line structure, low pass and high pass filters were realised in [46]. The values of LC elements were obtained using a quasi-lumped approach and the band rejection slot line structure was introduced to avoid WLAN interference. As a result, the proposed

filter exhibits very low insertion loss with very wide stopband characteristics. A broadband suspended stripline filter with the resonators coupled by turn on both sides of the substrate is presented in [47] with a wide band from 41 to 60GHz. This design offers much wider passband and smaller volume compared to the traditional suspended stripline end-coupled filter. A good response was achieved which satisfy the objectives of the research.

An SSS bandpass filter was proposed in [48] using quasi-lumped elements with transmission zero created at the upper frequency using parallel connected inductance and capacitance. As a result, the passband imposed high selectivity frequency response with improved out-of-band rejection level. Another ultra-wide band SSS filter was designed and tested with the focus on high pass filter in [49]; providing a good agreement between simulation and measurement results. In the design, the low pass prototype was transformed into a distributed circuit using Richards frequency transformation method; thus, a broadband high pass filter at microwave frequency was obtained. Zakaria *et al.* in [11] proposed the design of low pass filter with the integration of defected stripline structure (DSS) based on an SSS structure. The results exhibit good agreement between theoretical and experiment with notch response at 3.2 GHz that acts to remove undesired signal within the passband. This design was proven to reduce the overall filter size due to the usage of DSS; hence, minimize the manufacturing cost.

1.5   Objectives of the project

The thesis is constructed around the following objectives:

1) To develop design techniques for dual-mode suspended substrate stripline (SSS) filters with harmonic suppression

2) To develop higher order dual-mode resonator filter with good mid-band performance and high selectivity on each side of the passband.

3) To develop a novel type of asymmetrical bandpass filter with transmission zero above the passband to fulfil the need for high level of rejection in the receive band of transmit filter in the RF front-end of a cellular base station.

1.6   Organisation of thesis

The project organisation is as follows. In Chapter 2, the basic concept of microwave filter design relevant to this thesis is introduced. The topics cover the insertion loss filter design method, low pass filter prototypes, filter transfer functions, type of filters, filter transformation including impedance & frequency transformations and lowpass to bandpass transformations, and losses in the filters.

Chapter 3 described the design of dual-mode SSS filter where an inductive perturbation is used to couple two degenerate modes as well as controlling the bandwidth. In this chapter, the theoretical background of the ring resonator filter was described using the transmission line model. The full-wave electromagnetic (EM) simulation results and the measured result of the fabricated filter are also presented.

Chapter 4 describes the design of dual-mode SSS filter with transmission zero control. Two methods of analysis were investigated: adding susceptance to the ground and controlling the input and output feeding port. The theoretical background of the ring resonator filter with the ability to control the transmission

zeros is also presented using the transmission line model. A second order and fourth order filter are being simulated and analysed.

Finally, a summary of the contributions of the presented works and suggestions for future research work is concluded in Chapter 5.

Chapter 2 Microwave Filter Design

2.1   Introduction

In modern communication systems, filters play an important role in passing the desired signal and preventing an unwanted signal from being transmitted or received. Therefore, designing such an effective filter bank is crucial in that it influences the whole system performance and results. In general, filter design procedure begins with specifications and progresses as follows:

- Transfer function

- Synthesis of the filter

- Scaling and conversion

- Physical implementation

This chapter describes the basic concept and theories that form the foundations of filter design. The topics cover the insertion loss filter design method, low pass filter prototype, filter transfer function, type of filters, filter transformation,

including impedance and frequency transformation and low pass to bandpass transformation, and losses in the filter.

2.2 Insertion Loss Filter Design Method

The insertion loss method is a systematic design method in filter design using a network synthesis technique to design a filter with specified frequency response. This method allows a high degree of control of the passband amplitude, stopband attenuation and phase of the filter under investigation. All types of filter responses, including low pass, bandpass, the band-stop and high pass, can be designed using the insertion loss method. A suitable filter response can be chosen depending on the design parameters, e.g., low insertion loss, cut-off and stopband attenuation, in order to satisfy the required specification performance. The order of the filter is equal to the number of reactive elements and this method also allows improvement of the filter performance, at the expense of a degree of order. In the insertion loss method, a filter response can be expressed by its power loss ratio [50], P_{LR} :

$$P_{LR} = \frac{P_{in}}{P_l} \qquad 2.1$$

where the P_{in} and P_l are the power available from the source and the power delivered to the load, respectively. The insertion loss in dB can be expressed as:

$$IL = 10 \log P_{LR} \qquad 2.2$$

2.2.1 Low Pass Filter Prototype

A low pass filter prototype is a two-port passive lumped element reciprocal filter network where the filter element is normalised in terms of its impedance and frequency. The order of the filter is determined by the number of reactive

elements in the filter and the selectivity of the filter is proportional to the filter order. The low pass filter prototype can be formed by a cascade of ladder networks consisting of the reactive elements, which are the shunt capacitors and series inductors, as shown in Figure 9.
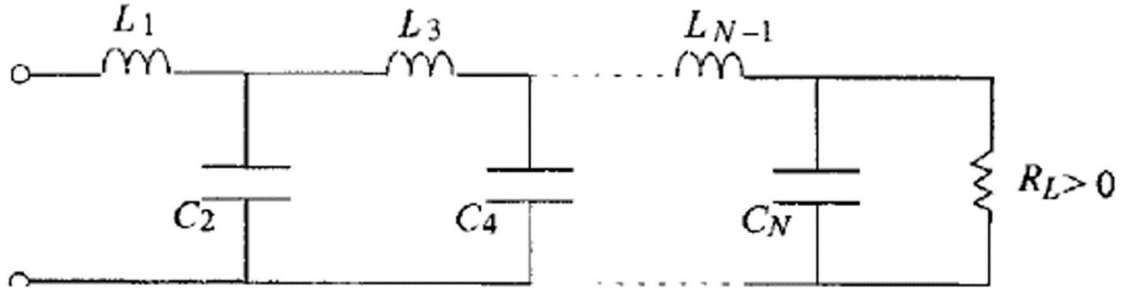
Figure 9 A Typical Low Pass Ladder Network [2]

An alternative way to realise a ladder network is to use immitance inverters. The immittance inverter is either an admittance or impedance inverter, which can be used to transform the series to a shunt connected element, and vice-versa. For most of the networks operating at microwave frequencies, the realisation of shunt and series resonators simultaneously is very difficult. Therefore, it is more convenient to use an immittance inverters where only shunt or series elements are used, depending on whether the low pass prototype filter has series inductors or shunt capacitors. Consider a circuit which is terminated in an impedance Z_L at one port, the impedance seen looking at the other port is [51]

$$Z_s = \frac{K^2}{Z_L} \hspace{4cm} 2.3$$

where K represents the characteristic impedance of the filter. The transfer matrix of ideal impedance inverters can be expressed as:

$$[T] = \begin{bmatrix} 0 & jK \\ \dfrac{j}{K} & 0 \end{bmatrix} \qquad 2.4$$

Likewise, an ideal admittance inverter is a two-port network, such that one port is terminated with an admittance Y_L, and the admittance seen looking at the other port can be expressed as [51]:

$$Y_s = \frac{J^2}{Y_L} \qquad 2.5$$

where J represents the characteristic admittance of the filter. In general, the transfer matrix of ideal impedance inverters can be expressed as:

$$[T] = \begin{bmatrix} 0 & \dfrac{j}{J} \\ jJ & 0 \end{bmatrix} \qquad 2.6$$

The conceptual representation of impedance and admittance inverted is illustrated in Figure 10.
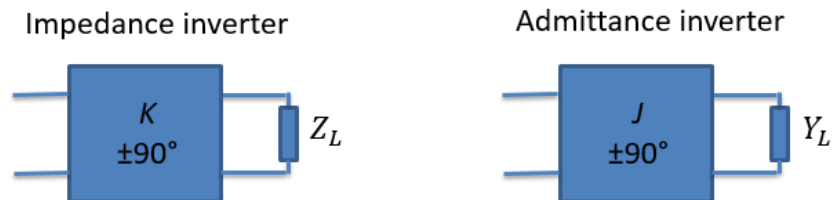
Figure 10 Impedance and Admittance Inverter

2.2.2 Transfer Functions

A two-port filter network can be represented by its transfer function, which is defined as:

$$|S_{21}(j\omega)|^2 = \frac{1}{1 + \varepsilon^2 F_N{}^2(\omega)} \qquad 2.7$$

where ε is the ripple constant, $F_N(\omega)$ represents a filtering or characteristic function and ω is the frequency variable. For a given transfer function above, the insertion loss of the filter is defined as attenuation of signal passing through the filter network and, thus, can be computed by

$$IL\ (dB) = 10\ log_{10}\ \frac{1}{|S_{21}(j\omega)|^2} \qquad 2.8$$

For a lossless, passive two-port network, $\left|S_{11}^2\right| + |S_{21}^2| = 1$, and the filter return loss can be calculated using

$$RL(dB) = 10\ log_{10}[1 - |S_{21}(j\omega)|^2] \qquad 2.9$$

In a filter network, return loss measures how perfect the power is being transferred from filter back to the source whereby a perfectly matched filter network would have a return loss value of infinity (no reflected power). In other words, return loss defines the matching level of a filter network. The insertion loss and return loss of a filter are often measured in dB.

2.3   Types of Filter

A low pass prototype is normally designed with the cut-off frequency at ω = 1. In a low pass prototype, the signal passes through from a source to the load, which is usually operated in a 1Ω system. In practice, an ideal filter with unity transmission and zero attenuation is impossible to realise. Therefore, filters are usually designed by approximations, which will make it realisable at microwave frequency. In RF and microwave filter design, each response can be characterised based on its family type or band form. The Butterworth,

Chebyshev, Generalized Chebyshev and Elliptic responses are types of filters commonly identified in most of the filter designs by their transfer function.

2.3.1 Butterworth Approximation

The Butterworth approximation is the simplest approximation to an ideal low pass filter where it is also often referred to as a "maximally flat" (no ripples) response. This is because the passband is designed to have a response which is as flat as possible with no ripple from the zero DC value to cut-off frequency - 3dB. In other words, the Butterworth approximation has no gain ripple in the passband and stopband. Higher frequencies beyond the cut-off frequency roll-off down to zero in the stopband at 20dB/decade. The approximation is defined as [52]:

$$|S_{12}(j\omega)|^2 = \frac{1}{1 + \omega^{2N}} \qquad\qquad 2.10$$

where N represents the order of the filter, where the larger the order of the filter, the more rapid the transition from passband to stopband. The insertion loss of the filter is therefore given by

$$IL = 10 \, log_{10}[1 + \omega^{2N}] \qquad\qquad 2.11$$

Figure 11 shows the Butterworth filter response for different orders of filter, in which it can be seen that the filter response gets steeper as the order of the filter is increased. In other words, the roll-off gets steeper, producing a sharp transition between passband and stopband as the order of the filter increases.
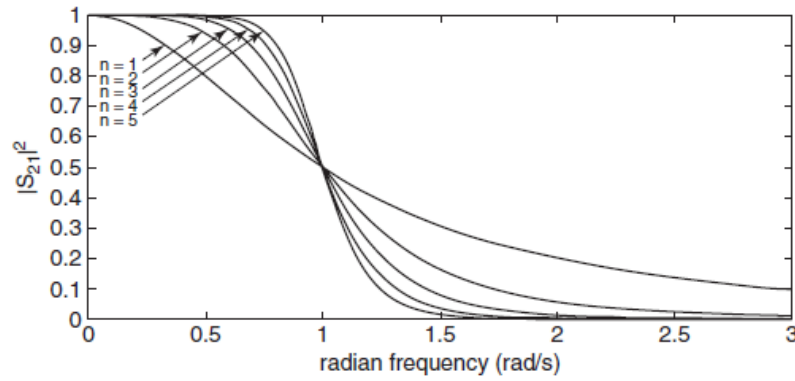
Figure 11 Butterworth Filter Response

The 3dB cut-off frequency is at $\omega = 1$, the point where the passband stops and the stopband starts. In order to meet the required specification, the order of the filter can be calculated as:

$$N \geq \frac{L_A + L_R}{20 \, log_{10}(S)} \qquad \text{2.12}$$

And

$$S = \frac{\omega_s}{\omega_p} \qquad \text{2.13}$$

where L_A, L_R, S, ω_s and ω_p are defined as insertion loss, return loss, selectivity, stopband critical frequency and passband critical frequency respectively.

2.3.2 Chebychev Approximation

The Chebychev approximation is a type of filter which exhibits equal-ripple passband up to the band-edge of $\omega=1$ before rolling off rapidly in the stopband. Chebyshev filter provides steeper and sharper filter response than in a Butterworth filter because of the presence of a ripple in the passband or stopband. The transfer function that describes this type of filter is defined as [52]:

$$|S_{12}(j\omega)|^2 = \frac{1}{1 + \varepsilon^2 T_n{}^2(\omega)} \qquad\qquad 2.14$$

where the ripple constant ε can be evaluated by

$$\varepsilon = \sqrt{10^{\frac{L_A}{10}} - 1} \qquad\qquad 2.15$$

Thus, the insertion loss of the filter is given by

$$IL = 10\,log_{10}\big[1 + \varepsilon^2 T_N{}^2(\omega)\big] \qquad\qquad 2.16$$

$T_N(\omega)$ is a Chebychev polynomial function of order N which has maximum value of 1 in the passband and can be defined as:

$$T_N(\omega) = \cos\big(N\,cos^{-1}(\omega)\big) \qquad\qquad 2.17$$

In order to meet the required specification, the order of Chebychev filter can be calculated as:

$$N \geq \frac{L_A + L_R + 6}{20\,log_{10}\left[S + (S^2 - 1)^{\frac{1}{2}}\right]} \qquad\qquad 2.18$$

where L_A, L_R and S are defined as insertion loss, return loss and selectivity, respectively. Figure 12 shows a Chebychev filter response with different values of N when ε=0.5.
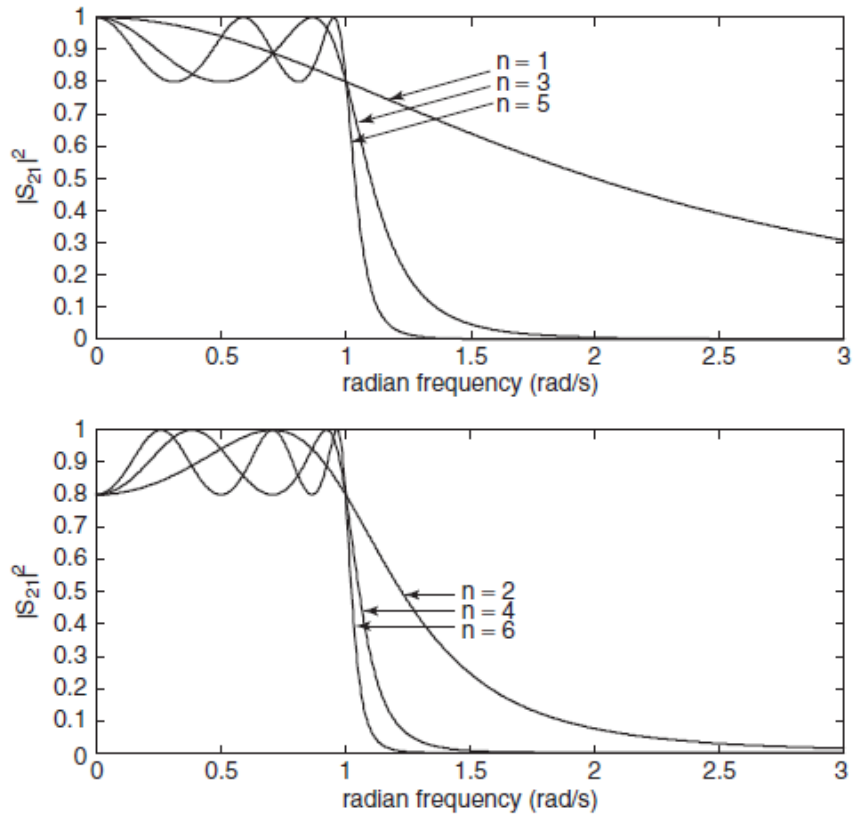
Figure 12 Chebychev Filter Response

2.3.3 Generalised Chebychev Approximation

The generalised Chebyshev low pass prototype network provides an equiripple signal at passband with arbitrarily transmission zeros in the stopband; hence, both symmetrical and asymmetrical responses can be generated with this type of approximation [52]. The presence of transmission zeros that can be placed arbitrarily in the stopband leads to high selectivity at the transition band as nearly as an Elliptic approximation. Furthermore, the transmission zeros are not restricted to be located at real frequency, but may also be located at the complex plane. Figure 13 shows a generalised Chebyshev low pass prototype circuit.
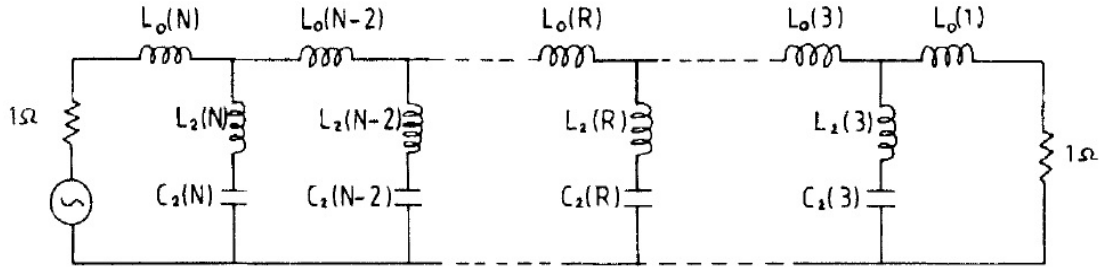
Figure 13 Generalised Chebychev Low Pass Prototype

The transfer function of a generalised Chebyshev low pass filter prototype is given by [1]

$$|S_{12}(j\omega)|^2 = \frac{1}{1 + \varepsilon^2 F_N{}^2(\omega)}$$
2.19

where

$$F_N(\omega) = \begin{cases} \cos\left[(n - n_z)\cos^{-1}\omega + \sum_{k=1}^{n_z} \cos^{-1}\dfrac{1 - \omega\omega_k}{\omega - \omega_k}\right] & -1 \leq |\omega| \leq 1 \\[4mm] \cosh\left[(n - n_z)\cosh^{-1}\omega + \sum_{k=1}^{n_z} \cosh^{-1}\dfrac{1 - \omega\omega_k}{\omega - \omega_k}\right] & 1 < |\omega| \end{cases}$$
2.20

In the above equations, n_z is the number of purely imaginary zeros that represents the transmission zeros in the stopband.

2.4 Filter Transformations

In the filter design, the low pass filter prototype was normalised, whereby the source impedance and cut-off frequency were set to 1Ω and $\omega_c = 1$, respectively. In communication systems, most of the network systems are operated with 50Ω source and terminations. Therefore, impedance and frequency scaling can be used to scale the low pass filter prototype. The low pass filter prototype can be converted into high-pass, band-stop and bandpass characteristics depending on the system requirements.

2.4.1 Impedance and Frequency Scaling

The low pass filter prototype element values are scaled to reach the impedance level of Z_o, which gives the new impedance scaled quantities of [2]:

$$R_S' = R_O \tag{2.21}$$

$$R_L' = R_O R_L \tag{2.22}$$

$$L' = R_O L \tag{2.23}$$

$$C' = \frac{C}{R_O} \tag{2.24}$$

where R_O, L and C are the original low pass prototype component values. To change the low pass cut-off frequency from unity to ω_c , the ω must be scaled by a factor of $\frac{1}{\omega_c}$; thus, ω can be replaced by $\frac{\omega}{\omega_c}$ and the resulting power loss ratio will be

$$P_{LR}'(\omega) = P_{LR}\left(\frac{\omega}{\omega_c}\right) \tag{2.25}$$

where the ω_c is the new cut-off frequency of the transformed filter, and the new element filter components after applying both impedance and frequency transformations are [2]:

$$L_k' = \frac{R_O L_k}{\omega_c} \qquad\qquad 2.26$$

$$C_k' = \frac{C_k}{R_O \omega_c} \qquad\qquad 2.27$$

2.4.2 Low Pass to Bandpass Transformation

A low pass filter prototype can be converted into a bandpass filter using the following frequency substitution [2]:

$$\omega \rightarrow \frac{1}{\Delta}\left(\frac{\omega}{\omega_0} - \frac{\omega_0}{\omega}\right) \qquad\qquad 2.28$$

where

$$\Delta = \frac{\omega_2 - \omega_1}{\omega_0} \qquad\qquad 2.29$$

and

$$\omega_0 = \sqrt{\omega_1 \omega_2} \qquad\qquad 2.30$$

The Δ and ω_0 are the fractional bandwidth and centre frequency, respectively. A series inductor L_k in the low pass prototype filter elements is converted into a low impedance series LC circuit elements using the following equations:

$$L_k' = \frac{L_k}{\Delta \omega_0} \qquad\qquad 2.31$$

$$C_k' = \frac{\Delta}{\omega_0 L_k}$$ 2.32

While a shunt capacitor C_k is transformed into a high impedance shunt LC circuit

elements using the following equations:

$$L_k' = \frac{\Delta}{\omega_0 C_k}$$ 2.33

$$C_k' = \frac{C_k}{\Delta \omega_0}$$ 2.34
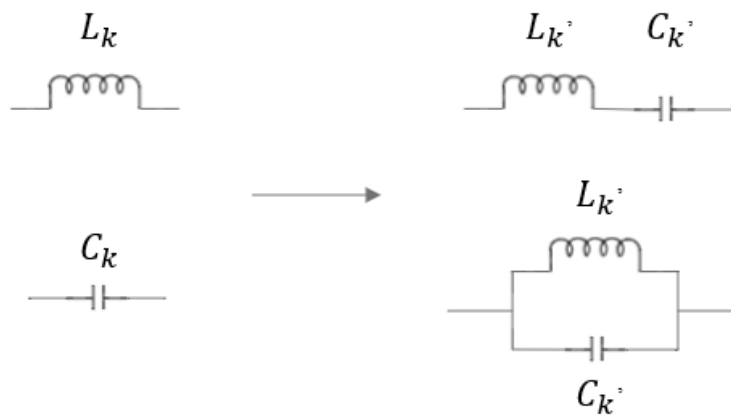
Figure 14 Low pass to bandpass network element transformations
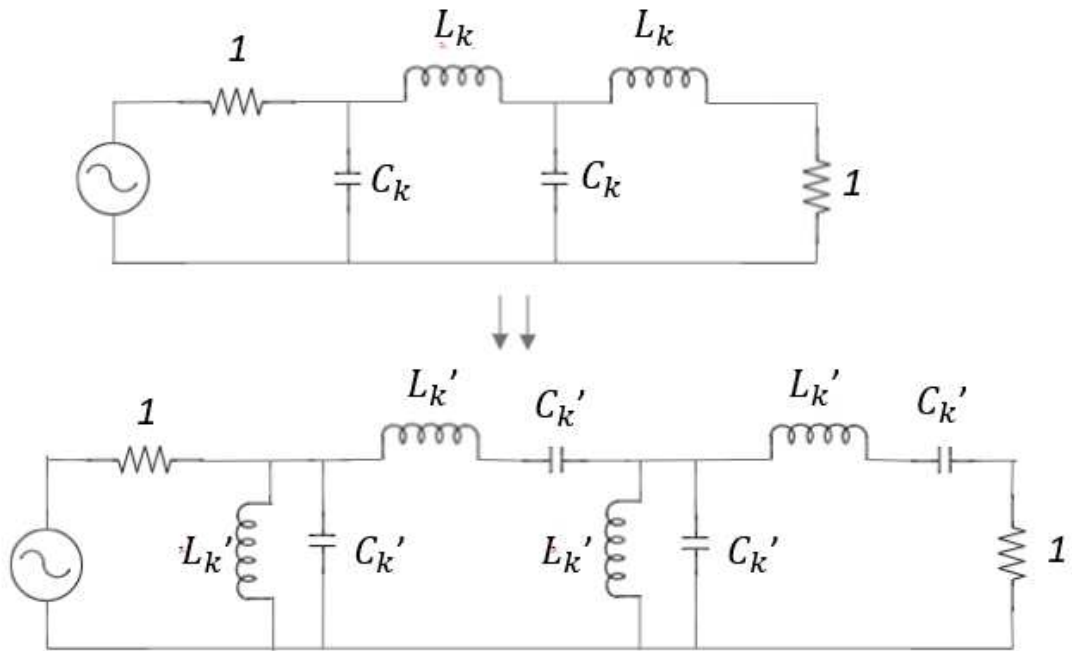
Figure 15 Low pass to bandpass network transformation circuit example

2.5   Losses in Filters

In the filter design procedure, it is commonly assumed that the filter is a lossless low pass prototype; thereby, yielding a lossless bandpass filter. However, in the real practical filter, the use of resistive components is practised and, hence, leads to the degradation of overall filter performance. The effect of this resistance represents losses and is linked directly to the quality factor of each component used in a filter circuit. The Q factor of a circuit can be expressed as:

$$Q = \frac{2\pi \ maximum \ energy \ stored \ in \ a \ cycle}{energy \ dissipated \ per \ cycle} \qquad 2.35$$

One of the main critical problems in filter design is that the passband loss is indirectly proportional to the bandwidth of the filter. Consequently, to achieve a

low passband loss in the practical filter, a high resonator Q factor must be used, which directly gives a narrow bandwidth filter response. Additionally, the passband loss is also influenced by the degree of the filter. As the degree of the filter is increased, the passband loss is also increased, as shown in the relationship below [50]:

$$L = \frac{4.343\, f_o}{\Delta f\, Q_u} \sum_{r=1}^{N} g_r \qquad\qquad 2.36$$

where g_r , Δf and Q_u represent the element values in the bandpass filter, bandwidth and unloaded quality factor, respectively. Figure 16 shows a simulation of a bandpass filter with various resonator Q factors.
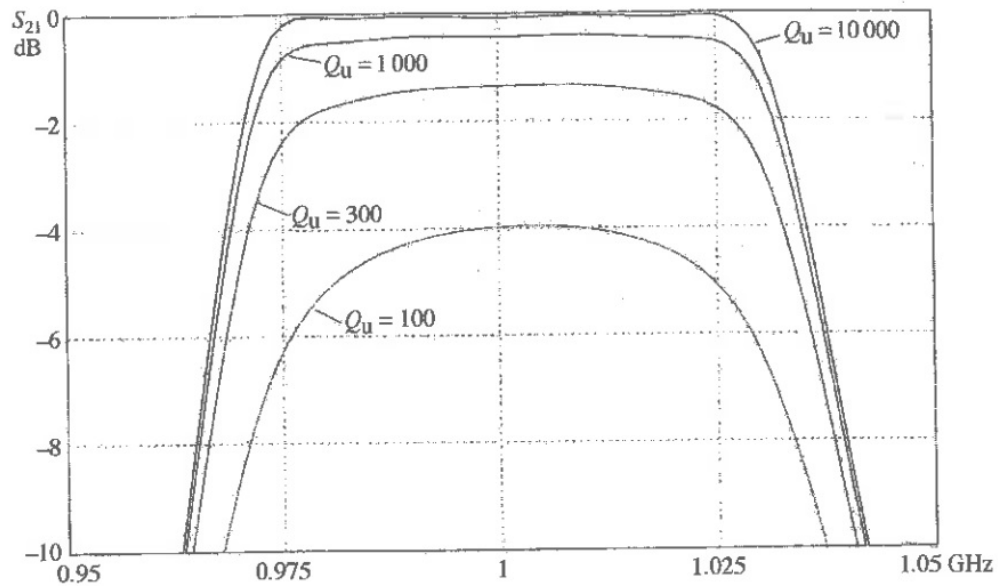
Figure 16 Simulation of Bandpass Filter with Various Q Factors [50]

It can be clearly seen that the passband losses are obviously influenced by the value of the Q factor. In this regard, the passband losses increased as the Q factor was reduced, whereby the bandwidth became narrower. Therefore, it can be concluded that the lower the losses, the response becomes sharper, as

energy is stored better in the circuit; thus, improving the selectivity of a filter response.

Chapter 3 Dual Mode Suspended Substrate Stripline (SSS) Filters

3.1   Introduction

Simple filtering functions, such as Chebychev and Butterworth, can be implemented by a low pass prototype network using a simple ladder structure. With this structure, a filter response where all transmission zeros are at infinity and without cross-coupling between resonators can be achieved. A more complicated filter with transmission zeros at finite frequency and cross-coupling between resonators can be realised, which significantly improves the filter performance compared to the latter structure. For instance, the dual mode resonant cavities, which involve the concept of coupling matrix as equivalent circuit, are widely used in filtering structure design. This contains normalised values of the coupling coefficients between the resonant cavities and the input/output port. This kind of structure can greatly minimise overall filter size as compared to using the single mode filter structure. Figure 17 shows an example

of coupling topology of a fourth order filter with its coupling matrix. Using these two, a fourth order triangular dual-mode filter was successfully designed in [31].

$$\begin{bmatrix} 0 & 0.4130 & -0.4130 & 0.6039 & -0.6039 & 0 \\ 0.4130 & 1.3242 & 0 & 0 & 0 & 0.4130 \\ -0.4130 & 0 & -1.3242 & 0 & 0 & 0.4130 \\ 0.6039 & 0 & 0 & -0.6277 & 0 & 0.6039 \\ -0.6039 & 0 & 0 & 0 & 0.6277 & 0.6039 \\ 0 & 0.4130 & 0.4130 & 0.6039 & 0.6039 & 0 \end{bmatrix}$$
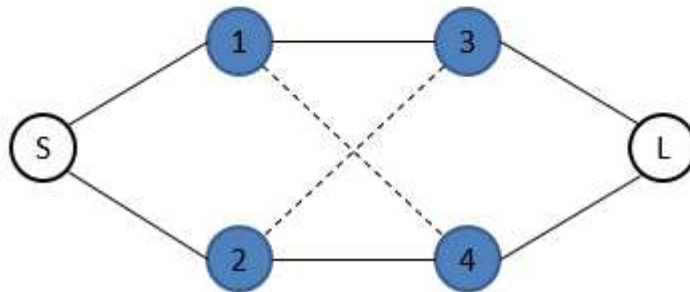
Figure 17 Example of coupling matrix and coupling topology of a fourth order filter

Dual mode excitation can be achieved by introducing a perturbation in the cavity, such as iris and notch, which disturbs the electromagnetic fields and creates two split resonance frequencies. The larger in size the perturbation is, the higher is the frequency shift between the two modes. In other words, the size of perturbation controls the bandwidth of the filter response. Filters with a dual-mode operation were investigated due to their ability to produce two degenerate modes using a single physical structure; therefore, the size and cost of the filter can be reduced without compromising any figure-of-merits.

There are many research works addressing improving the design of the transmit filter by using a dual-mode design technique. The microstrip technology

often attracts researchers in designing dual-mode filters due to such advantage as low fabrication cost. In [27], a dual-mode rotational symmetric resonator filter was designed with two transmission zeros generated near the upper and lower passband. Additionally, a fourth order dual-mode microstrip filter with interdigital capacitive loading element was designed in [28]. In [29] and [30], compact dual-mode microstrip filters were designed, fabricated and tested using parallel coupled resonator and meander loop resonator, respectively. A triangular microstrip dual-mode filter based on the coupling matrix synthesis method was designed in [31] with a good rejection performance obtained. Also, a dual-mode filter with source-load coupling was designed in [32] and [33], which demonstrated good filter performance. Some of the above mentioned dual-mode filter are shown in Figure 18. All the above-mentioned filters offered good return loss values and sharp skirt selectivity due to the ability to generate transmission zeros. Nonetheless, they suffered high insertion loss, which was greater than 1 dB at the mid-band frequency, thus resulting in lower Q. Therefore, this research was proposed to produce high selectivity filter response without using any cross coupling connection and lower insertion loss thus resulting in higher Q factor.

In this chapter, another type of technology is utilised to design the dual mode ring resonator filter, namely, using suspended substrate stripline (SSS). The major advantages of using this technology compared to other planar filters are high selectivity, higher Q, non-dispersiveness and good temperature stability.
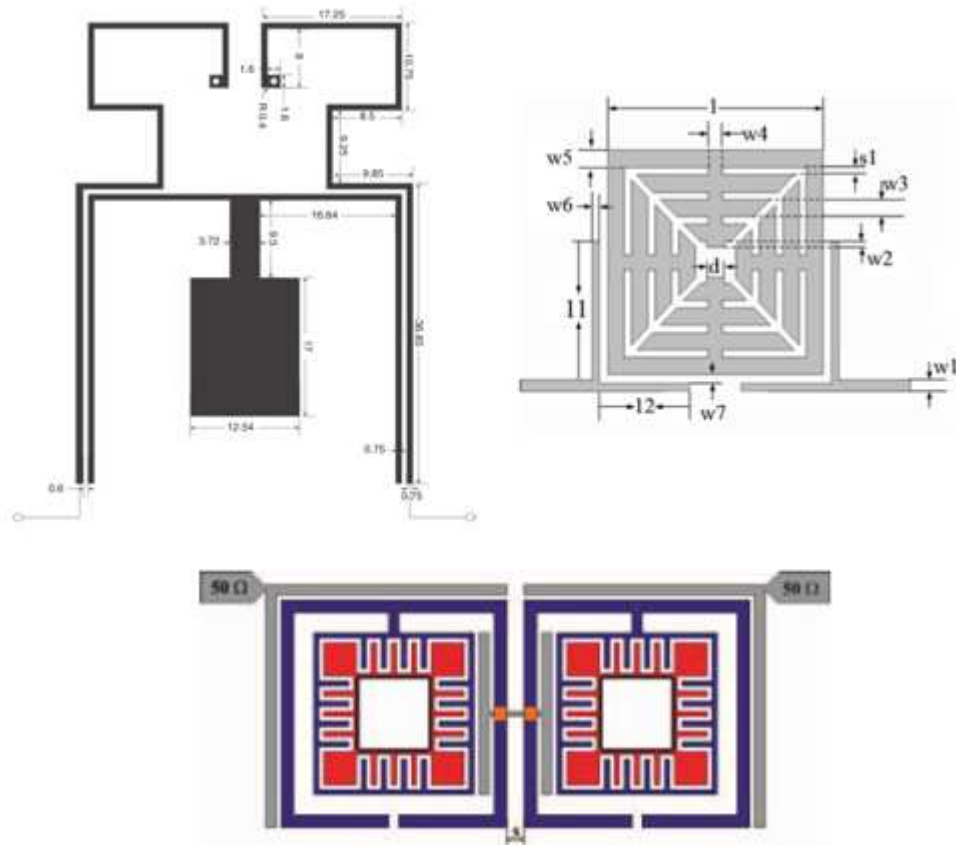
Figure 18 Examples of Past Dual-Mode Filters [28][32][33]

3.2   The Ring Resonator

A ring resonator, one wavelength long at frequency 2.07 GHz, was simulated and evaluated using a full-wave electromagnetic (EM) simulator. The radius of the ring is calculated as follows:

$$2\pi r = \frac{c}{f\sqrt{\varepsilon_r}} \qquad\qquad 3.1$$

where c, f and ε_r are the speed of light, operating frequency and effective permittivity constant, respectively. The calculated radius of the ring resonator was 24.77 mm.
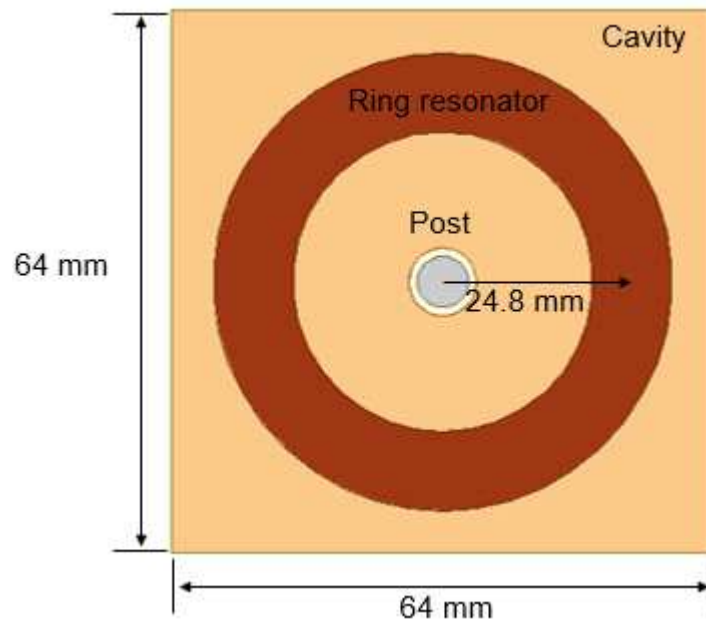
Figure 19 Top View of Ring Resonator Filter
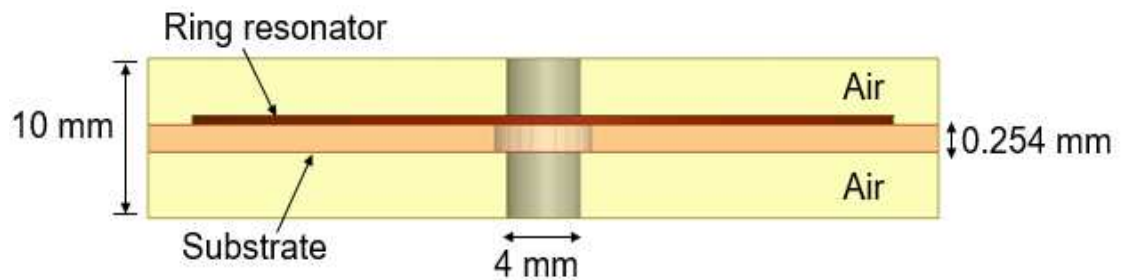
Figure 20 Side View of Ring Resonator Filter

Figure 19 and Figure 20 show the top and side view of the ring resonator filter, respectively. The filter was designed and fabricated on a 0.254 mm thickness RT/Duroid 5880 substrate with a relative dielectric constant ε_r= 2.2. The ring resonator filter is printed on the substrate which is suspended in the air and enclosed by a metal cavity. Using air as the dielectric has the advantage that it avoids the transmission losses associated with dielectric materials. The metal post, which is shorted to ground, is placed at the centre of the cavity and is used to improve the first harmonics of the filter. In designing a filter, the dimension is

an important parameter since it affects the filter's electrical performance. Maintaining the box height $b < \lambda/2$ can avoid higher order modes [50]; hence, the height of box 'b' was chosen as 10 mm. As the height of box chosen was 10mm with the substrate thickness 't' of 0.254 mm, the ring resonator impedance of 58 Ω was obtained from the graph of t/b versus Z_o in [53], with t/b and w/b are 0 and 1.2, respectively.

Table 1 Eigenmode Solution of The Ring Resonator Without Metal Post

Eigenmode	Frequency (GHz)	Q-factor
Mode 1	2.07	1486.26
Mode 2	2.07	1496.46
Mode 3	3.34	4654.81
Mode 4	4.03	2214.26

Table 2 Eigenmode Solution of The Ring Resonator with Metal Post

Eigenmode	Frequency (GHz)	Q-factor
Mode 1	2.07	1569.43
Mode 2	2.07	1528.28
Mode 3	4.06	2211.79
Mode 4	4.11	2244.16

Figure 21 Electric Field Distribution for Mode 1 Without and With a Metal Post
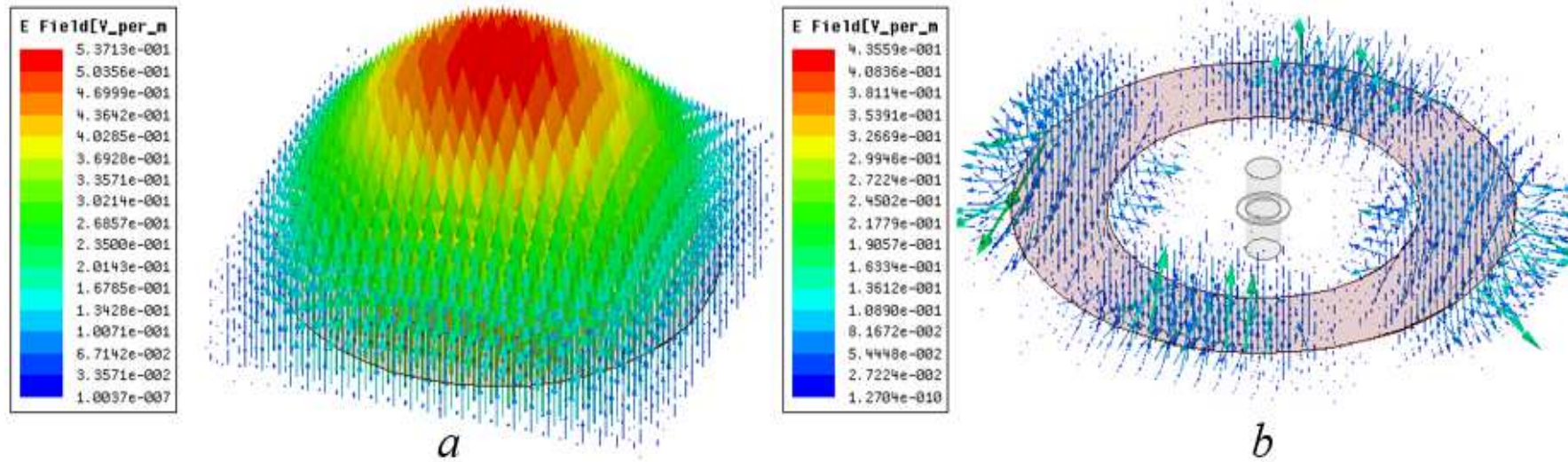
Figure 22 Electric Field Distribution for First Harmonic Without and With a Metal Post

Table 1 and Table 2 represent the eigenmode solutions of the ring resonator without and with a metal post shorted to the ground, respectively. Both solutions have dual mode 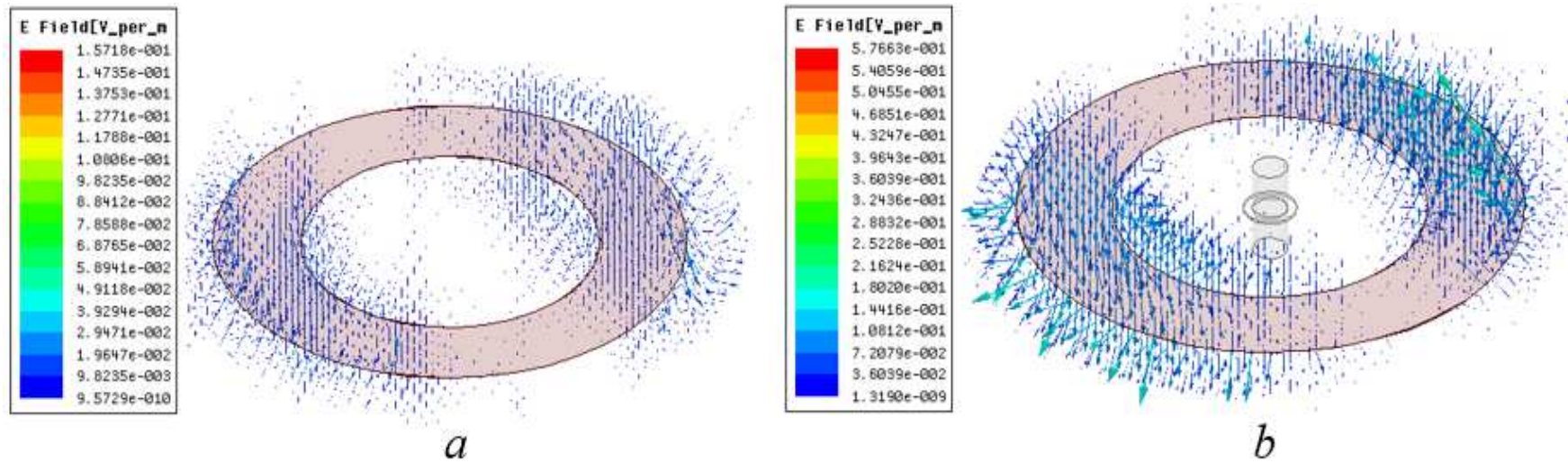resonances at approximately 2.07 GHz. It was observed that the Q-factor of the first resonance is improved from 1486.26 to 1569.43 by using a metal post shorted to the ground. The first harmonic was also improved from 3.34 GHz to 4.06 GHz when a metal post was inserted at the centre of the cavity. Figure 21 demonstrates the electric field distributions of the first resonance for both structures, which are nearly identical for both conditions except that the magnitude of the fields was more intense when a metal post was applied. This agrees well with the eigenmode solutions whereby the Q-factor of the first harmonics is higher when a metal post is applied at the centre of the cavity; hence, lower insertion loss can be obtained. Figure 22 illustrates the electric field distribution of the first harmonics of the filter structure without and with a metal post applied. It was observed that the field distributions were pushed away from the centre of the cavity when a metal post was applied shorted to the ground, which, in turn, pushed the first harmonic to a higher frequency. This result showed that a wider out-of-band rejection, as well as better spurious, is achieved by applying a metal post. Therefore, a filter structure with the metal post is used in the following filter design.

3.3   Transmission Line Equivalent Circuit Analysis

The ring resonator was analysed as two transmission lines wherein electrical lengths of θ_1 and θ_2 are connected in parallel, as shown in Figure 23. The characteristic impedances Z_o of the transmission lines are assumed as 1 Ω.
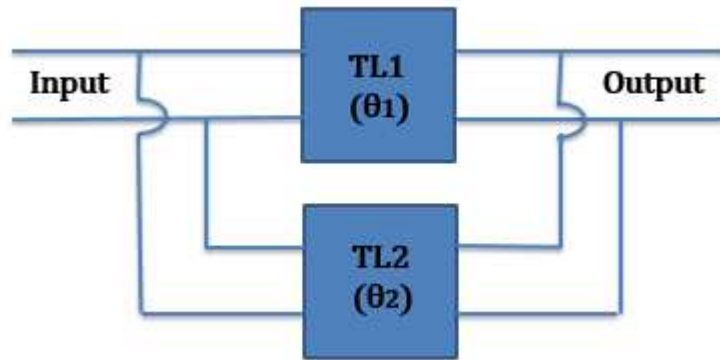
Figure 23 Equivalent Circuit Representation of a Ring Resonator

The transfer matrix of a single transmission line is:

$$[T] = \begin{bmatrix} \cos\theta & j\sin\theta \\ j\sin\theta & \cos\theta \end{bmatrix} \qquad 3.2$$

And the Y matrix of a unit impedance is:

$$[Y] = \begin{bmatrix} \dfrac{-j}{\tan\theta} & \dfrac{j}{\sin\theta} \\ \dfrac{j}{\sin\theta} & \dfrac{-j}{\tan\theta} \end{bmatrix} \qquad 3.3$$

Since the two transmission lines are connected in parallel, therefore,

$$[Y] = [Y_1] + [Y_2], \qquad 3.4$$

$$[Y] = j \begin{bmatrix} -\dfrac{1}{\tan\theta_1} - \dfrac{1}{\tan\theta_2} & \dfrac{1}{\sin\theta_1} + \dfrac{1}{\sin\theta_2} \\ \dfrac{1}{\sin\theta_1} + \dfrac{1}{\sin\theta_2} & -\dfrac{1}{\tan\theta_1} - \dfrac{1}{\tan\theta_2} \end{bmatrix} \qquad 3.5$$

So, let's represent the Y-matrix as π network, as shown in Figure 24:
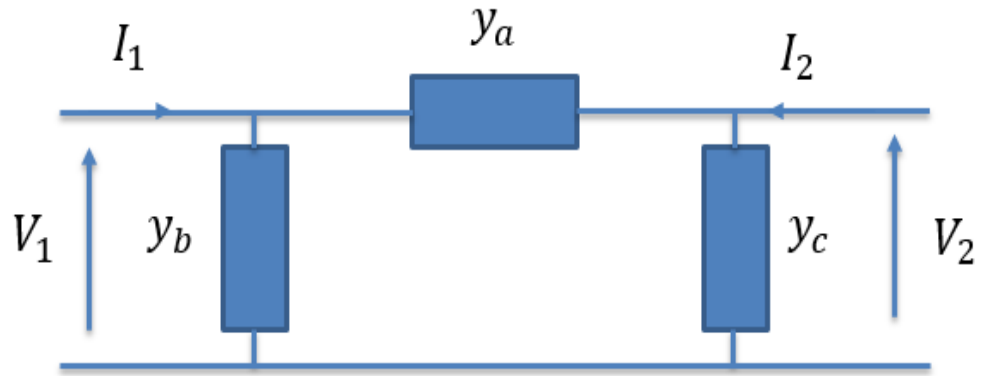
Figure 24 Two Port π Network

where

$$\begin{bmatrix} I_1 \\ I_2 \end{bmatrix} = \begin{bmatrix} y_{11} & y_{12} \\ y_{21} & y_{22} \end{bmatrix} \begin{bmatrix} V_1 \\ V_2 \end{bmatrix} \qquad 3.6$$

$$y_{11} = \frac{I_1}{V_1} \text{ when } V_2 = 0$$

$$y_{11} = y_a + y_b \qquad 3.7$$

Thus,

$$y_b = y_{11} - y_a \qquad 3.8$$

$$y_{12} = \frac{I_1}{V_2} \text{ when } V_1 = 0$$

Thus,

$$y_a = y_{12} \qquad 3.9$$

$$y_{22} = \frac{I_2}{V_2} \text{ when } V_1 = 0$$

$$y_{22} = y_c + y_a \qquad 3.10$$

Thus,

$$y_c = y_{22} - y_a \qquad\qquad 3.11$$

For the two-port transmission lines which are connected in parallel, the equivalent circuit can be represented as a π network, as follows:
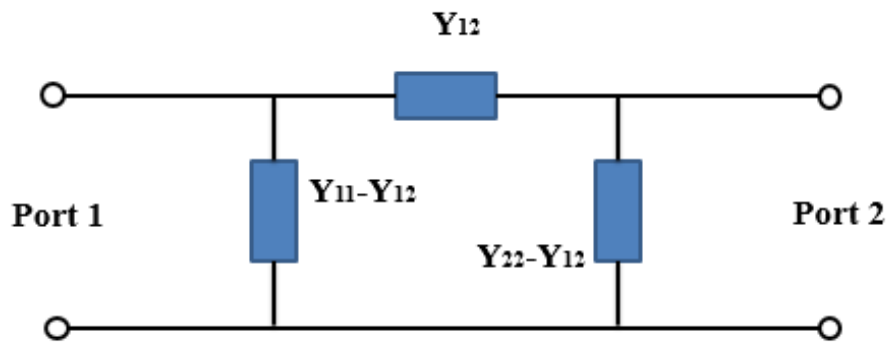
Figure 25 π Network Representation of Two Transmission Lines Connected in Parallel

Therefore, rearranging the two-port equivalent circuit, as shown in Figure 26, where the π network can be seen as admittance inverter K_{12}.
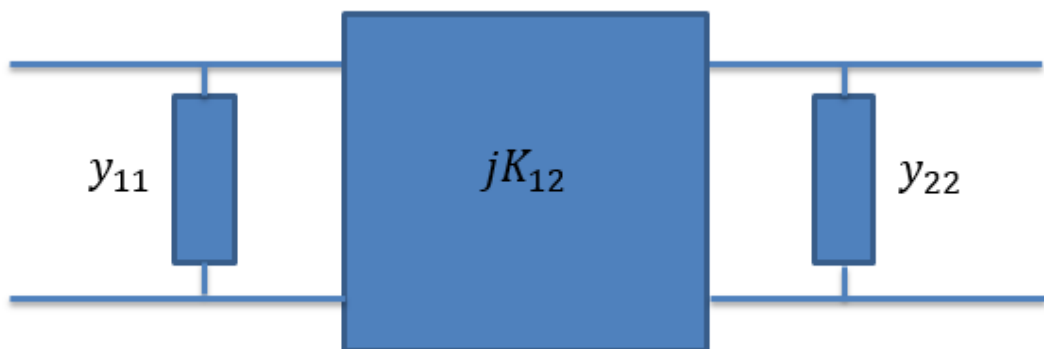
Figure 26 Equivalent Circuit Representation of the π Network with Admittance Inverter K_{12}

Therefore,

$$jK_{12} = y_{12} \qquad\qquad 3.12$$

And from 3.5

$$y_{12} = \frac{j}{\sin\theta_1} + \frac{j}{\sin\theta_2} \qquad\qquad 3.13$$

Hence, the transmission zeros are the zeros of y_{12} and occur when

$$\sin\theta_1 + \sin\theta_2 = 0 \qquad\qquad 3.14$$

3.4 Second Order Filter Design

A second order ring resonator filter was designed with the specifications as follows:

Table 3 Bandpass Filter Specifications

Centre Frequency (f_o)	2.08 GHz
20 dB Bandwidth (BW)	80 MHz
Return Loss (RL)	>20 dB
Insertion Loss (IL)	<0.5 dB
System Impedance 'Z_O'	50 Ω

Figure 27 shows the structure of a one wavelength long dual-mode ring resonator filter with 90° input and output feed separation. The filter is designed at 2.08 GHz with a bandwidth of 80 MHz and it is capacitively coupled to the input and output port. Since the output feeding line is the mirror image of the input feeding line, the coupling values at both locations are the same. A notch is located 135° from both input and output feeding and is used to couple two degenerates' modes, which represent the dual-mode response. Without a notch, only a single mode

excitation can be achieved. The proposed dual-mode filter is initially arranged under weak capacitive coupling with a perturbation located 135° to the input and output port to investigate the influence of varying the notch radius to the frequency response. The location and size of the notch are two important design parameters, whereby it influences the electrical filter performance. Figure 28 depicts the movement of the first three resonant modes versus notch radius. As notch radius increases, mode 2 remains unchanged while mode 1 moves down, thus separating these two modes from each other. Therefore, it shows that the notch radius controls the mode splitting of the degenerates' modes.
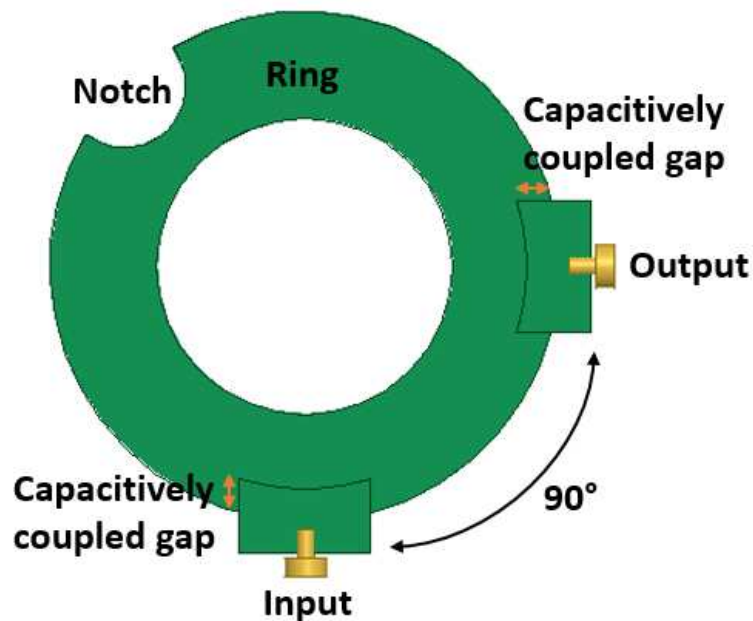
Figure 27 Ring Resonator Filter with 90° Separation of Input and Output Port
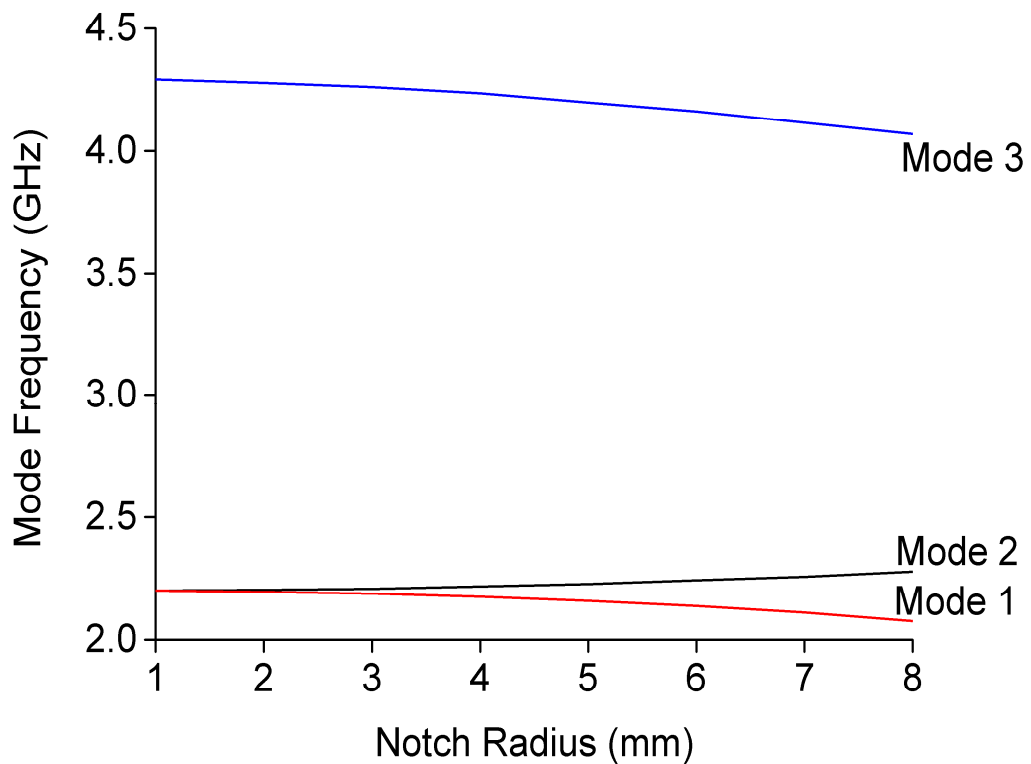
Figure 28 Mode Splitting Frequency for Various Notch Radii

3.4.1 Input/output Coupling Analysis

In designing a filter, coupling plays an important role in connecting the two parts of a filter. For example, to connect two transmission lines, the coupling value is needed to avoid a mismatch, which may lead to more losses, thus, degrading the electrical filter performance. Input/output coupling, also known as external coupling, connects the filter to the outside world and is often expressed as external Q (Q_e). Figure 29 illustrates the arrangement setup of a single ring resonator filter to find the external coupling, Q_e, where the value of Q_e is determined by the overlap between the input transmission line and the ring resonator filter. Figure 30 shows the cross section of a single ring resonator where the overlap is shown clearly in the figure.
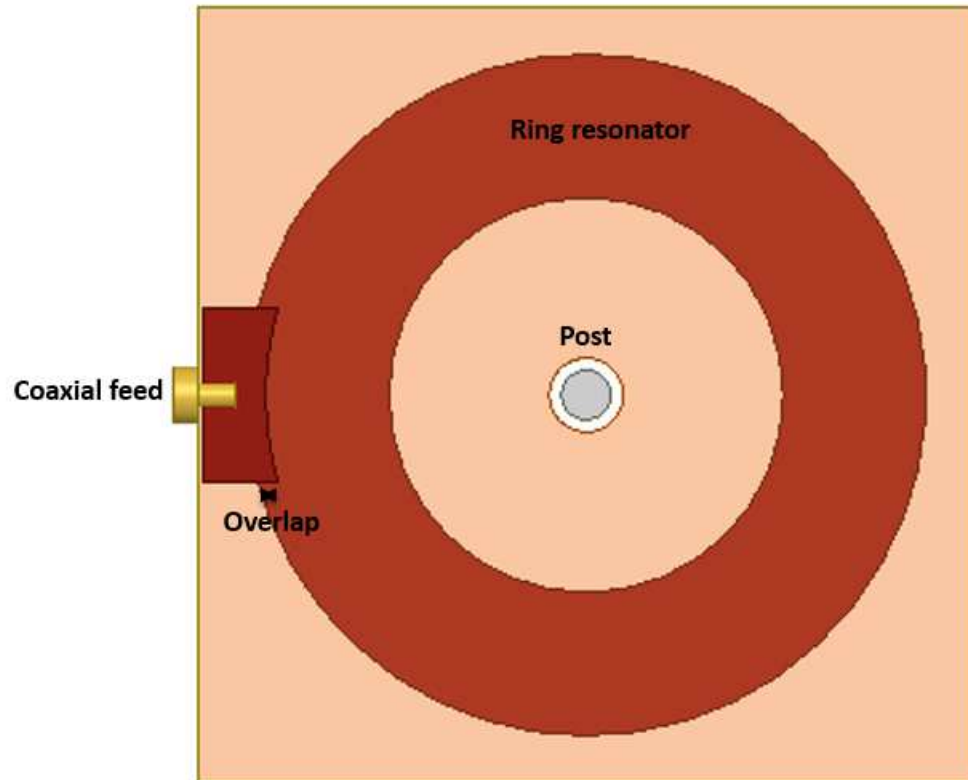
Figure 29 Single Ring Resonator Layout to Find the External Q (Q_e)
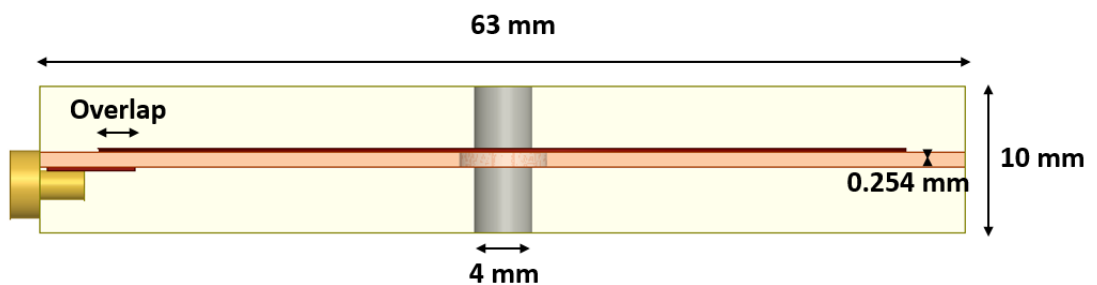
Figure 30 Cross Section of a Single Ring Resonator

In this design, the correct value of coupling is needed to couple the input transmission line to the ring resonator filter to avoid mismatch. Based on the specification requirements, the input/output coupling coefficient is first extracted from the Coupling Matrix Synthesis (CMS) [54], which is a filter and coupling matrix synthesis software developed by Guided Wave Technology. The extracted normalised coupling coefficients are stated in Table 4, as follows:

Table 4 Normalised Coupling Coefficients M_{ij} of the Second Order Filter

	S	1	2	L
S	0	1.2247	0	0
1	1.2247	0	1.6583	0
2	0	1.6583	0	1.2247
L	0	0	1.2247	0

Coupling coefficient is a dimensionless value that characterizes the interaction between two resonators. From Table 4, the normalised coupling coefficient between source and the first resonator was identified with the value of 1.2247. The external Q (Q_e) can be expressed by the normalised coupling coefficient M_{01}

$$Q_e = \frac{f_0}{BW \; M_{01}{}^2} \qquad\qquad 3.15$$

where f_0 and BW are the operating frequency and ripple bandwidth of the filter, respectively. The calculated Q_e is 17.38 and the filter is simulated to find its group delay response so that the exact overlap distance can be determined. Figure 31 demonstrates the group delay responses versus frequency for various overlap distance, ranging from 0 to 1.6 mm, while Figure 32 represents the graph of Q_e versus overlap distance, which was extracted based on the data obtained from Figure 31. An overlap distance of 0.5 mm was extracted from the graph in Figure 32, which satisfies the Q_e value of 17.38.
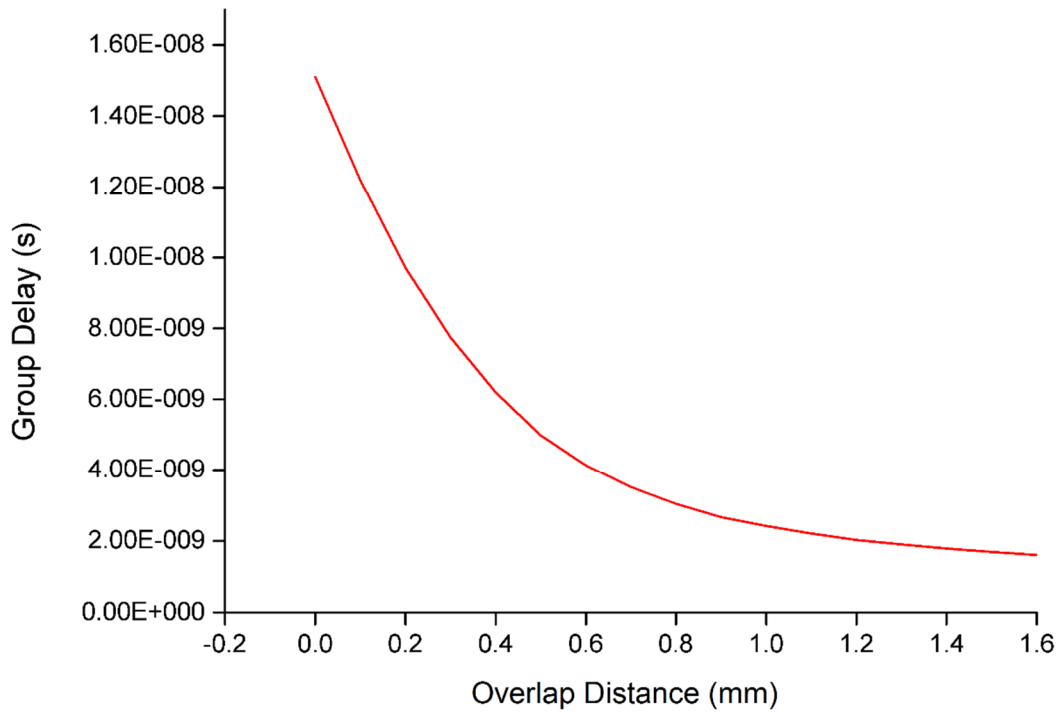
Figure 31 Group Delay vs. Frequency for Various Overlap Distance
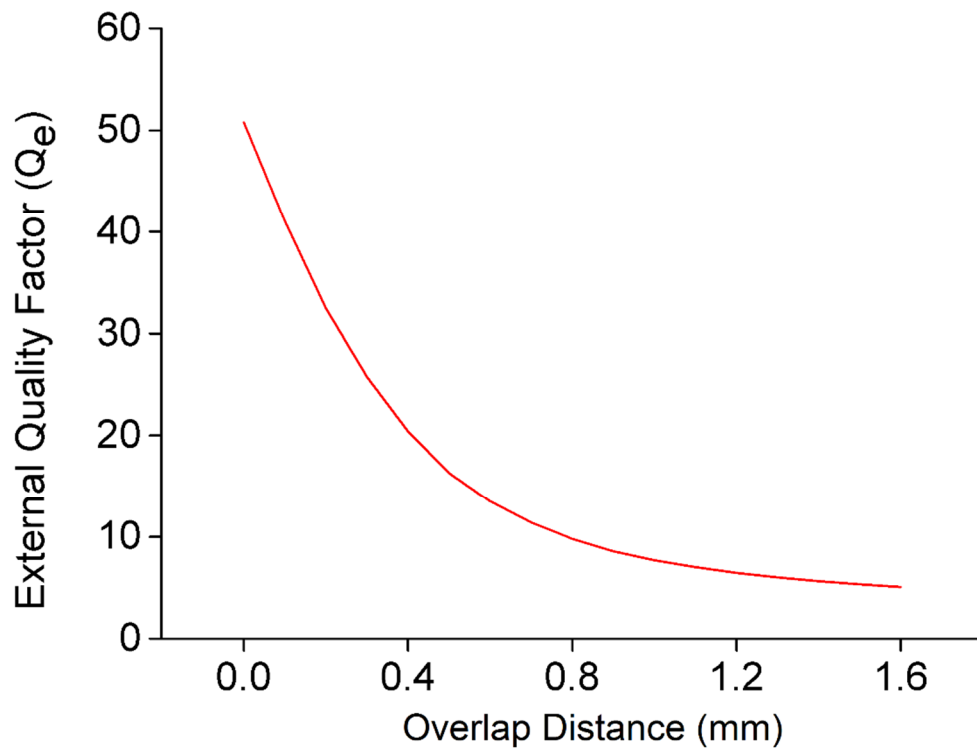
Figure 32 Graph of External Q (Q_e) vs. Overlap Distance

3.4.2 Inter-Resonator Coupling Analysis

Inter-resonator coupling is executed by elements which can provide the exchange of energy between resonators. These can be constructed by posts, irises, septa, perturbations and by other means. In this design, the coupling between resonators is realised using a notch, which is perturbed on the ring resonator filter, as shown in Figure 33 . The notch not only controls the coupling between resonators, but also controls the bandwidth of the filter response. Figure 34 demonstrates the graph of coupling bandwidth M_{12} versus notch radius, where the coupling bandwidth was extracted from [54]. From the graph, it can be seen that the coupling bandwidth is increased as the notch radius increases. Based on the specification requirements, the coupling bandwidth M_{12} obtained

from [54] is 132.66 MHz; thus, the notch radius matched with M_{12} extracted from

Figure 34 is 6.6 mm.
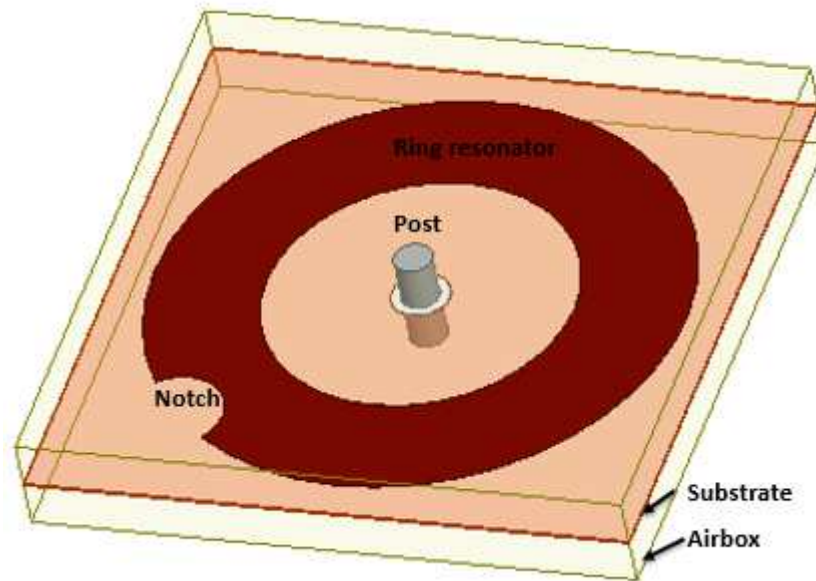
Figure 33 Ring Resonator Filter With a Notch Perturbed on The Ring
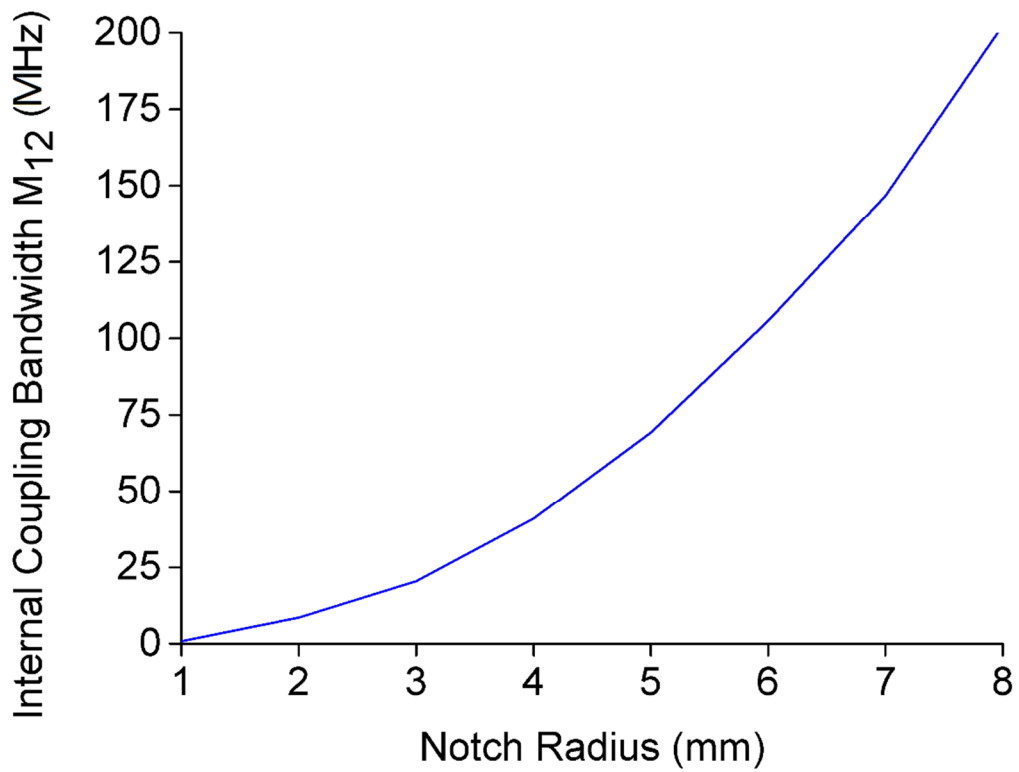
Figure 34 Graph of Coupling Bandwidth M_{12} vs. Notch Radius

3.4.3 Result and Discussion

Figure 35 depicts the top view of a dual mode ring resonator filter with a notch located 135° from the input and output feeding location. The substrate used for this filter is Rogers/Duroid 5880 with a relative dielectric constant ε_r= 2.2 and thickness of 0.254 mm. The length and width of the filter cavity are 63 mm while the height chosen is 10 mm. The input and output ports are capacitively coupled to the ring resonator, which, in this design, was represented by the overlap between the ring resonator and the input/output transmission lines. A return loss value of 20 dB with 84 MHz bandwidth and insertion loss value of 0.13 dB was obtained from the simulation outcome, as depicted in Figure 36. Figure 37 shows the wideband frequency response of the simulated designed filter, which shows that the first harmonic appears at $1.8 f_0$, which is at 3.87 GHz. Simulation and analysis also show that increasing the notch radius leads to greater bandwidth, but weakens the return loss value. Meanwhile, the notch location is a great influencer to the transmission zero location. In this design, a pair of transmission zeros is located at the imaginary axis of the complex s-plane, whereas, in Figure 38, the simulation result shows that transmission zeros were seen below and above the passband. This is due to the notch, which is asymmetrically located to the input and output port; thus, the transmission zeros are moved to the real axis of the complex s-plane.
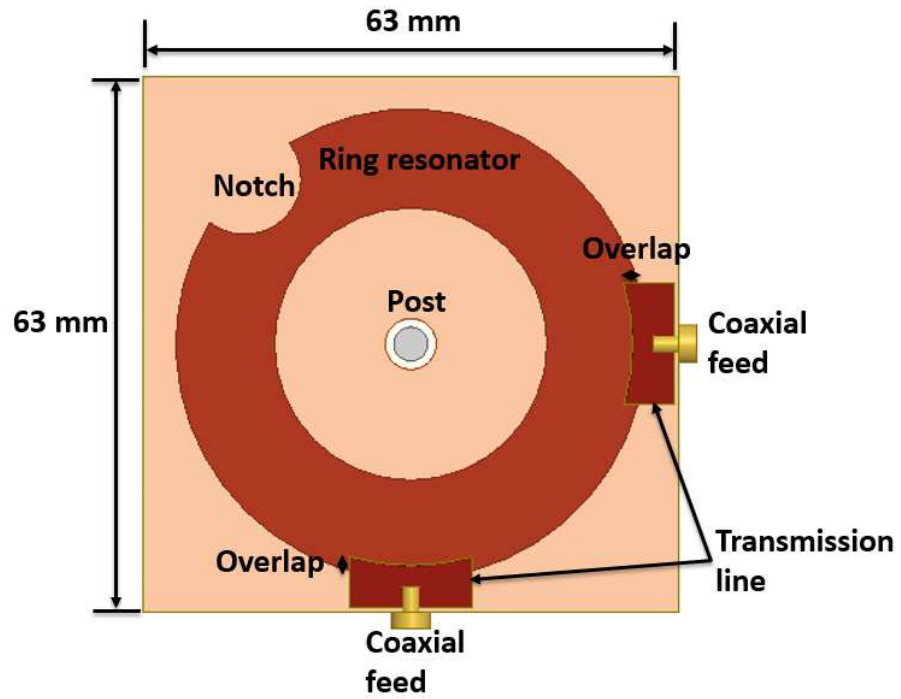
Figure 35 Top View of a Dual Mode Ring Resonator Filter
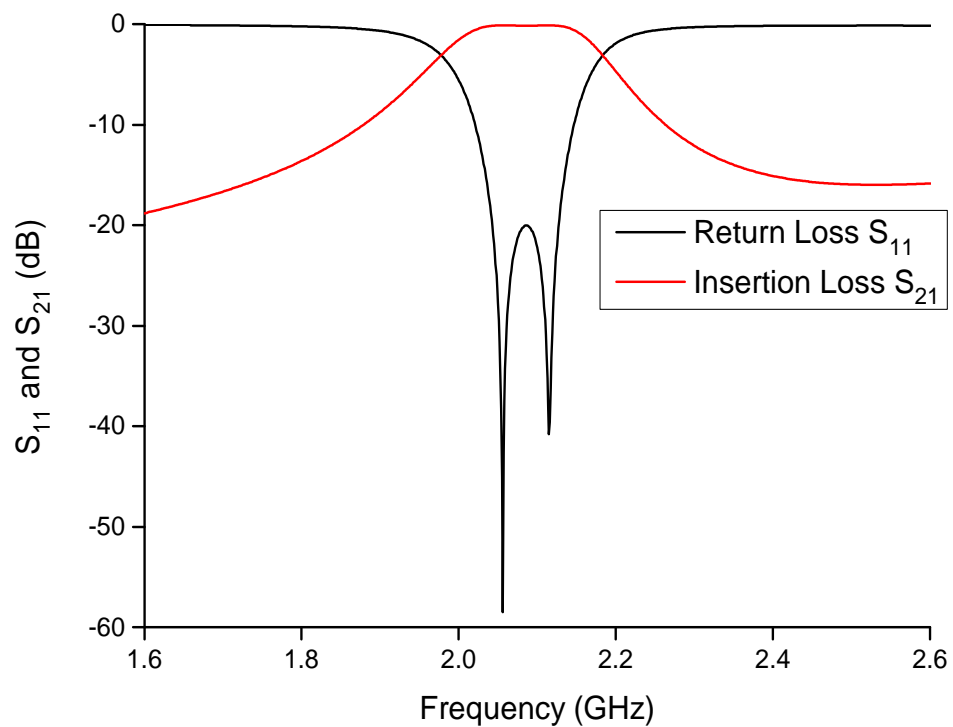
Figure 36 Simulated Response of Second Order Filter
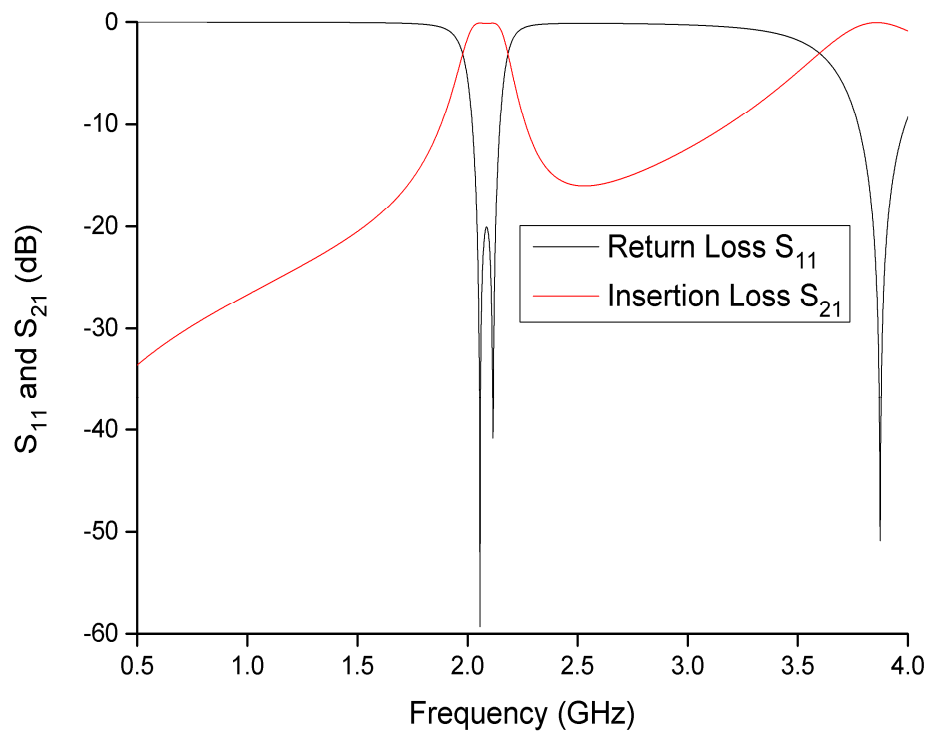
Figure 37 Wideband Frequency Response with Symmetrical Notch Location
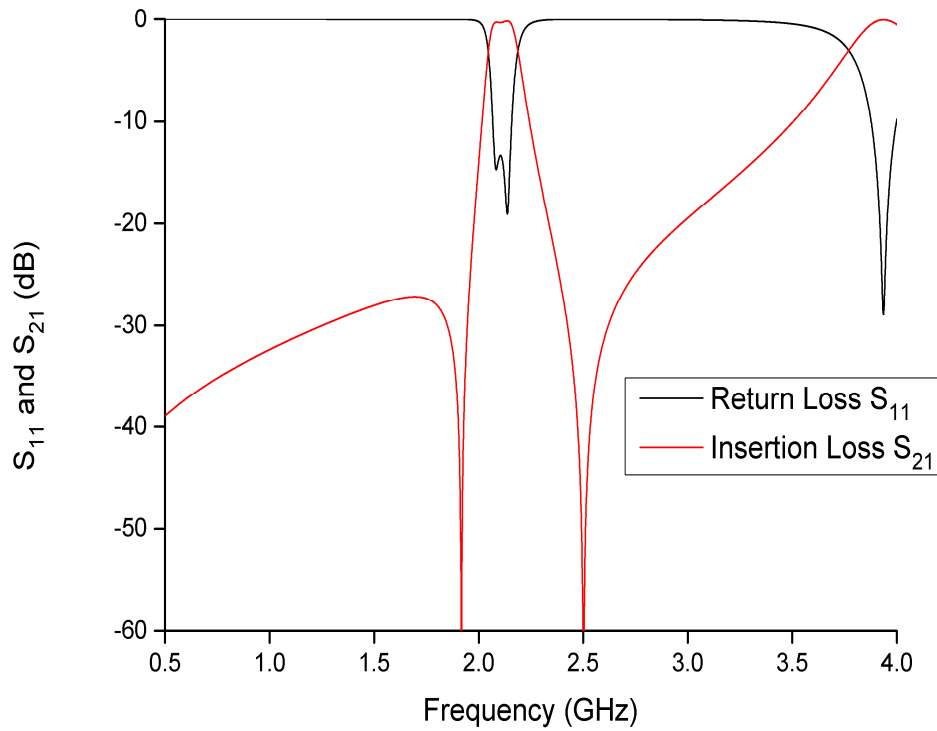
Figure 38 Wideband Frequency Response with Asymmetrical Notch Location

3.5 Fourth Order Filter Design

This section gives an overview of higher order filter development, from design to fabrication, with the proposed dual-mode filter through a design example of a fourth order bandpass filter. The filter specifications are summarised as follows:

Centre Frequency (f_o)	2.08 GHz
20 dB Bandwidth (BW)	50 MHz
Return Loss (RL)	>20 dB

Insertion Loss (IL)	<1 dB
System Impedance ' Z_O '	50Ω

Figure 39 and Figure 40 depicts the structure of a fourth order filter and the side view of the fourth order filter respectively. The two cavities were separated by a wall with a small iris in which the wall separator was used to avoid cross-coupling between non-adjacent modes. A metal strip was located between the two rings passing through the wall separator to couple mode 2 and mode 3 and a metal post placed in each cavity to improve the first harmonics of the filter frequency response. Dual modes are excited in both cavities using a semi-circular notch, which inductively perturbed each ring.
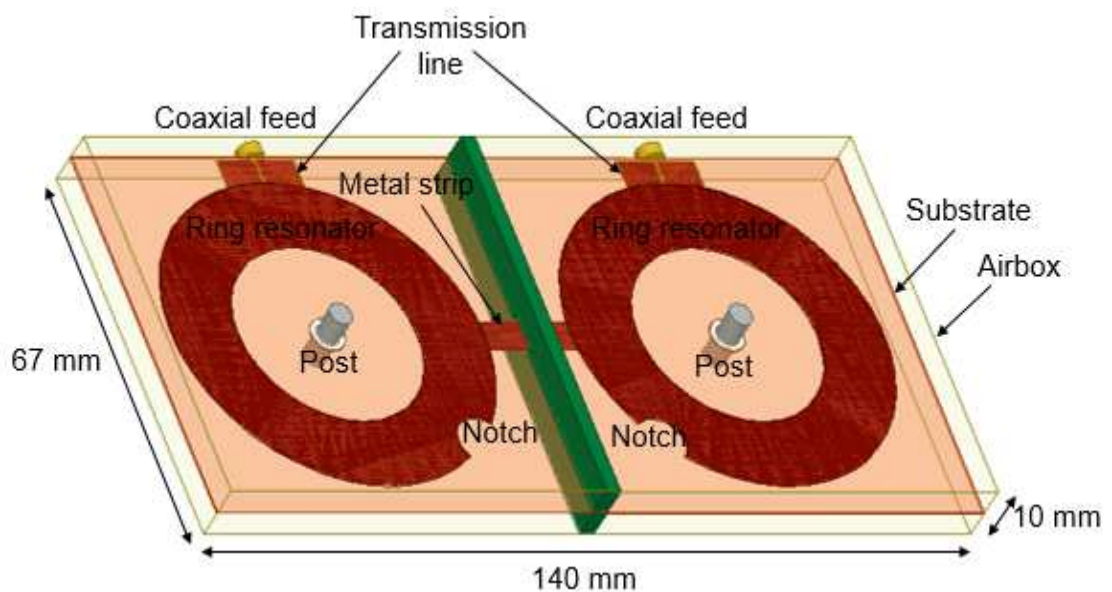
Figure 39 Fourth Order Filter Structure
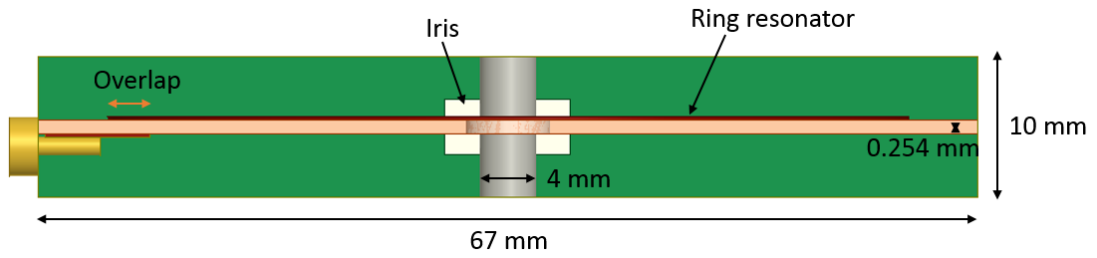
Figure 40 Side View of The Fourth Order Filter

3.5.1 Input/output Coupling Analysis

The input/output coupling was analysed the same way as in Section 3.4.1. Based on the specification requirements, the input/output coupling coefficient was first extracted from [54] and the extracted normalised coupling coefficients are as featured in Table 5.

Table 5 Normalised Coupling Coefficients M_{ij} of the Four Order Filter

	S	1	2	3	4	L
S	0	1.0352	0	0	0	0
1	1.0352	0	0.9106	0	0	0
2	0	0.9106	0	0.6999	0	0
3	0	0	0.6999	0	0.9106	0
4	0	0	0	0.9106	0	1.0352
L	0	0	0	0	1.0352	0

From Table 5, the normalised coupling coefficient of the source to the first resonator is 1.0352. Therefore, the Q_e is 38.97, which is calculated using

equation 3.15 while the overlap distance obtained from Figure 32 to match with the calculated Q_e , is 0.18 mm.

3.5.2   Inter-Resonator Coupling Analysis

3.5.2.1 M_{12} and M_{34}

The coupling in each cavity is referred to as M_{12} and M_{34}, which also represents the coupling between resonators in a single ring resonator filter. M_{12} and M_{34} are realised in the same way as in Section 3.4.2. The normalised coupling bandwidth of M_{12} and M_{34} extracted from Table 5 is 0.9106; thus, for 50 MHz ripple bandwidth, the coupling bandwidth of 45.53 MHz is calculated for M_{12} and M_{34}. Since the notch radius represents the coupling of M_{12} and M_{34}, Figure 34 is, therefore, also used to extract the notch radius, which is 4.4 mm, to match with the coupling bandwidth obtained.

3.5.2.2 M_{23}

In this design, M_{23} is referred to as inter-ring resonator coupling whereby the coupling depends on the overlap distance between the metal strip and the ring resonator filter. To demonstrate the concept of inter-ring resonator coupling, the ring resonator filter structure in Figure 41 was used. Two ring resonators were enclosed in a metallic housing and loosely coupled to the input and output ports. The coupling of M_{23} was determined by the overlap distance whereby the metal strip length was varied to evaluate the corresponding transmission characteristic (S_{21}), as shown in Figure 42. The two ring resonators are identical with both resonating at the operating frequency, f_o. For each value of strip length, two peaks were observed in the frequency response. The metal strip length, which controls the inter-ring resonator coupling, was adjusted until S_{21} between

two peaks was roughly -30 dB to -40 dB to guarantee loose coupling. The actual coupling value was first extracted from [54] to match with the inter-ring resonator coupling value of 0.0172, which was calculated from expression [52]

$$K = \frac{f_H{}^2 - f_L{}^2}{f_H{}^2 + f_L{}^2} \qquad 3.16$$

where f_H is the frequency of the upper peak, while f_L is the frequency of the lower peak. Figure 43 shows the graph of inter-ring resonator coupling versus strip length, where the strip length is 13.4 mm to match with the calculated coupling value of 0.0172.
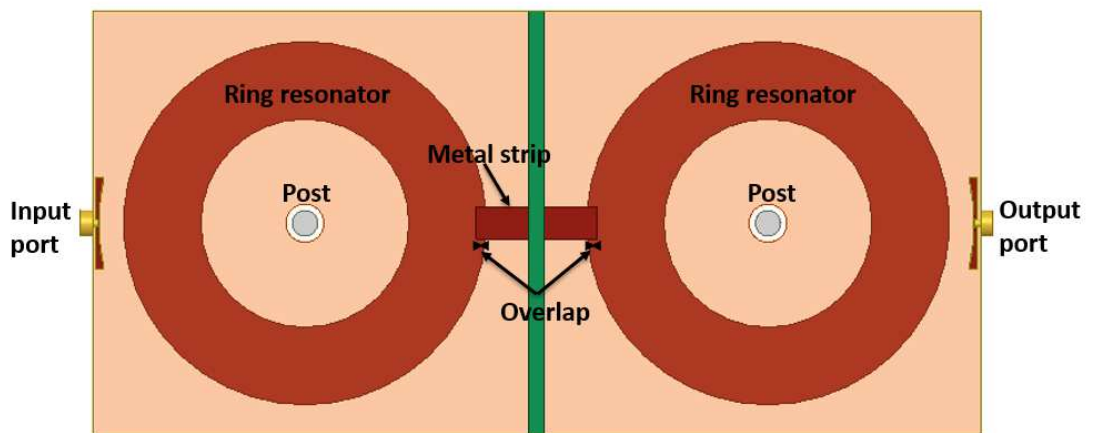
Figure 41 Top View of a Loosely Coupled Four Order Filter
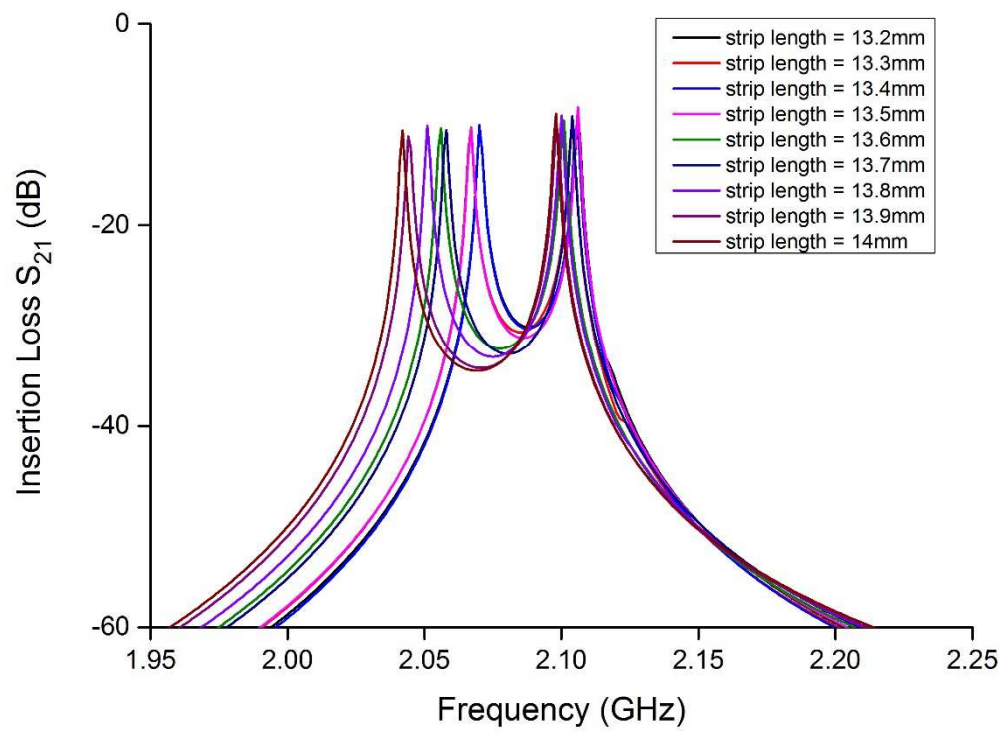
Figure 42 Graph of Insertion Loss vs. Frequency for Various Strip Length
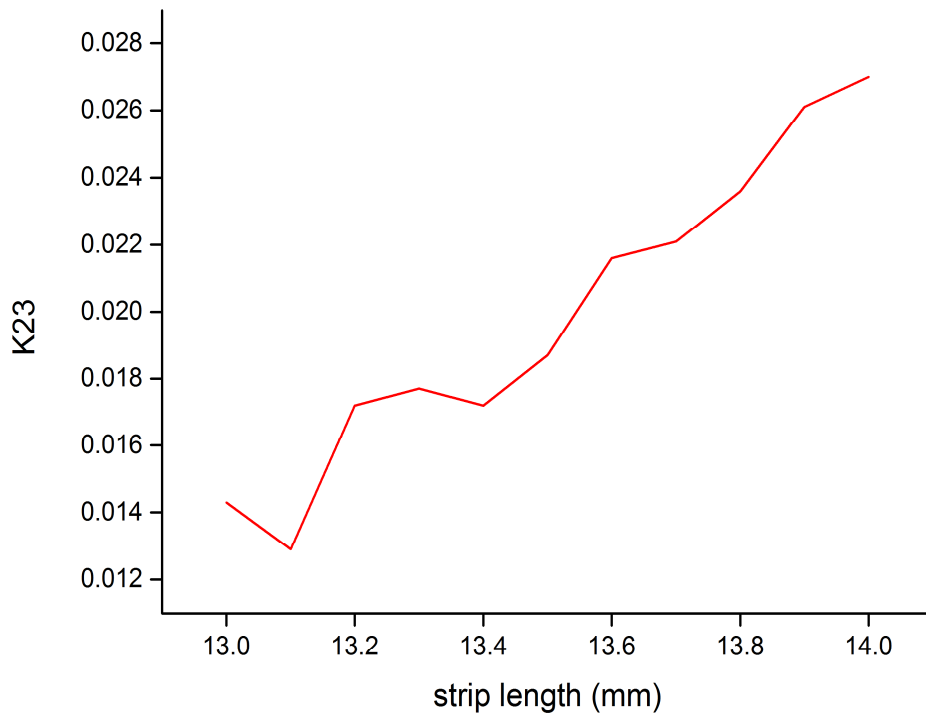
Figure 43 Graph of Inter-Ring Resonator Coupling vs. Strip Length

3.5.3 Simulation and Measurement Results and Discussions

A fourth order dual-mode filter was designed using suspended substrate stripline technology. Figure 44 shows the simulated response of the designed filter with a return loss value of 15.33 dB and insertion loss value of 0.66dB obtained at the operating frequency of 2.088 GHz. Additionally, four transmission zeros appeared, two below and two above the passband, with the shoulder level of 74 dB. This is because when a ring was fed at 90°, two separate paths exist, with one of $\lambda/4$ while the other one is $3\lambda/4$, which creates a 180° phase difference. The 180° phase difference thus naturally creates transmission zeros by phase cancellation. Therefore, the selectivity of the filter response is improved on both sides of the passband. Although the size of the two rings are identical, the

transmission zeros appeared at four different frequencies. This is because there are more than one solutions available for the transmission zero which referred to equation 3.14. This is proven by the transmission line equivalent circuit of the fourth order filter as shown in Figure 45. The difference in the electrical length of both rings has led to the formation of four transmission zeros, even though the value of the characteristic impedance of both rings are the same. The simulated frequency response of the transmission line equivalent circuit is shown in Figure 46 where four transmission zeros were observed. The top and bottom view of the fabricated fourth order filter having transmission zeros above and below the passband are shown in Figure 47 and Figure 48, respectively. The substrate was enclosed in a metal enclosure at top and bottom, which was suspended by the airgaps. The two ring resonators were printed on the top side while the input/output feeding line and the metal strip were printed on the bottom side of the substrate, which ensured broadside coupling. The top and bottom enclosure of the designed filter is shown in Figure 49.

Figure 50 shows the measurement result of the fabricated filter with return loss value of 16.42 dB, insertion loss of 0.926 dB at 2 GHz and bandwidth of 57.7 MHz. Two transmission zeros were observed below the passband while another two were observed above the passband. Although there was a shifting in the resonance frequency which was mainly caused by the tuning screws, the designed filter gives good response which agreed well with the EM simulated outcome. Figure 51 represents the wideband frequency response of the fabricated fourth order filter. The outcome showed a wideband spurious free response wherein the first harmonic frequency appeared at $1.8 f o$, which is nearly double the fundamental frequency.
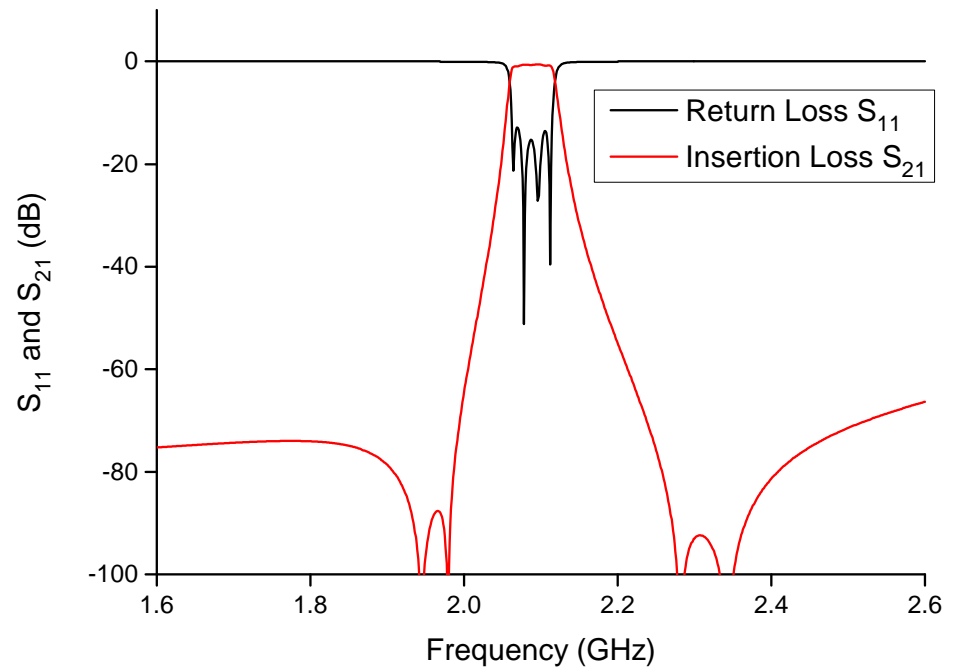
Figure 44 Simulated Response of The Fourth Order Filter
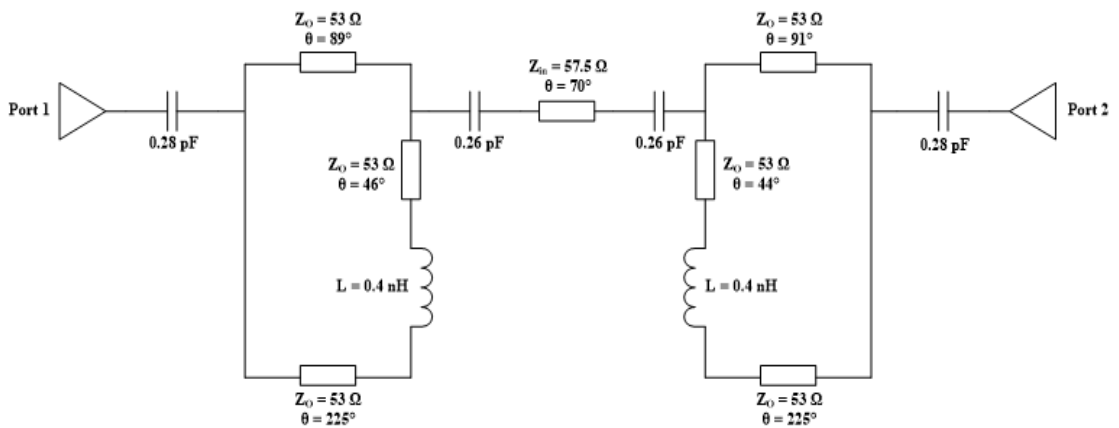
Figure 45 Transmission line equivalent circuit of the fourth order filter
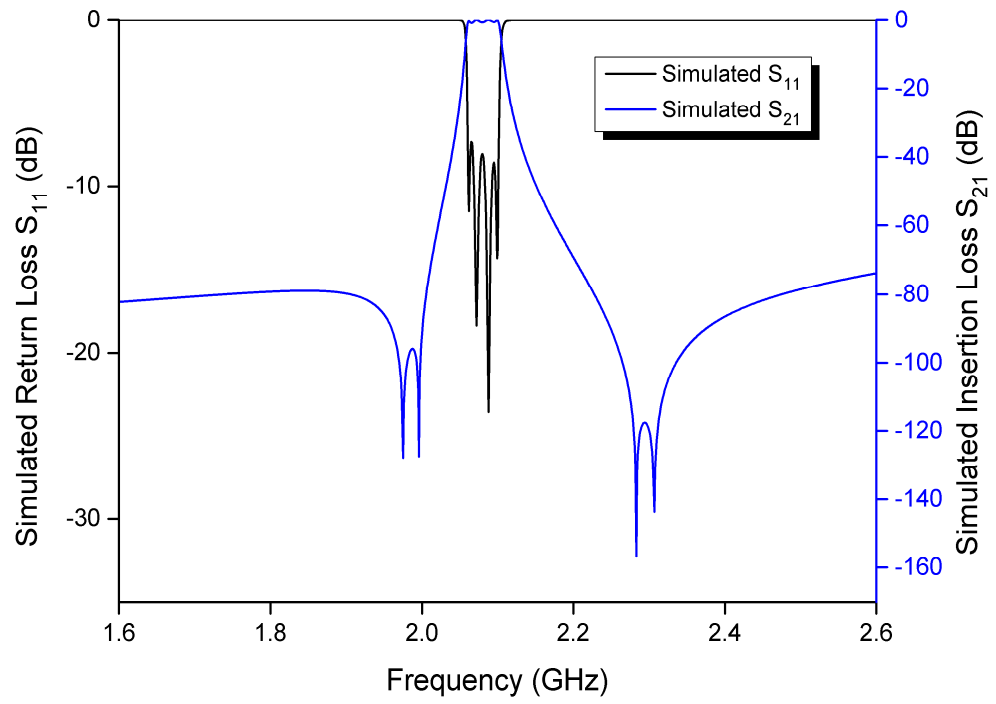
Figure 46 Simulated frequency response of the transmission line equivalent circuit
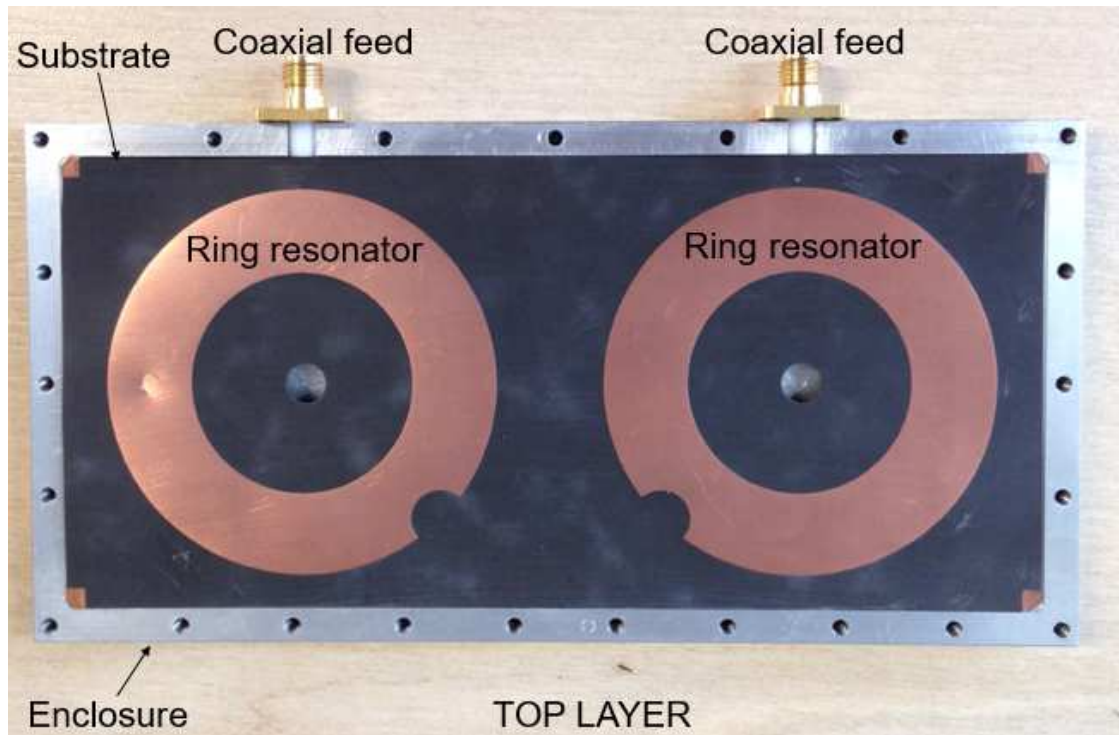
Figure 47 Top View of The Fabricated Fourth Order Filter
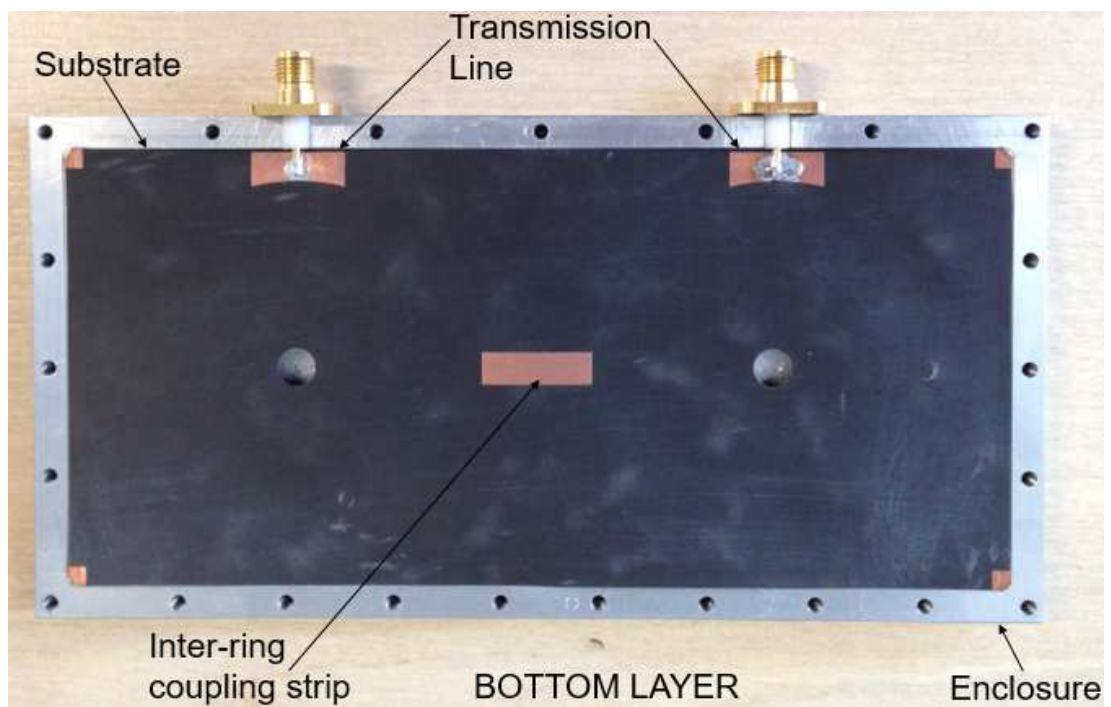
Figure 48 Bottom View of The Fabricated Fourth Order Filter
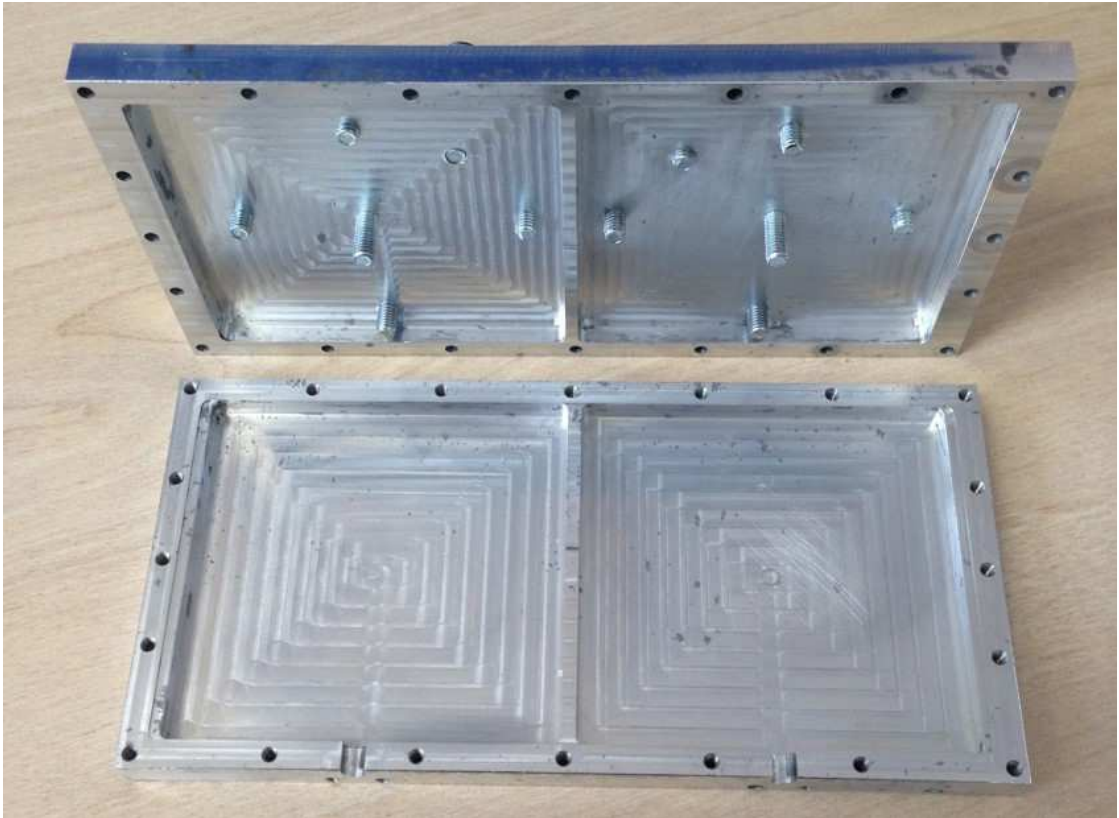
Figure 49 Top and Bottom Enclosure of The Designed Filter
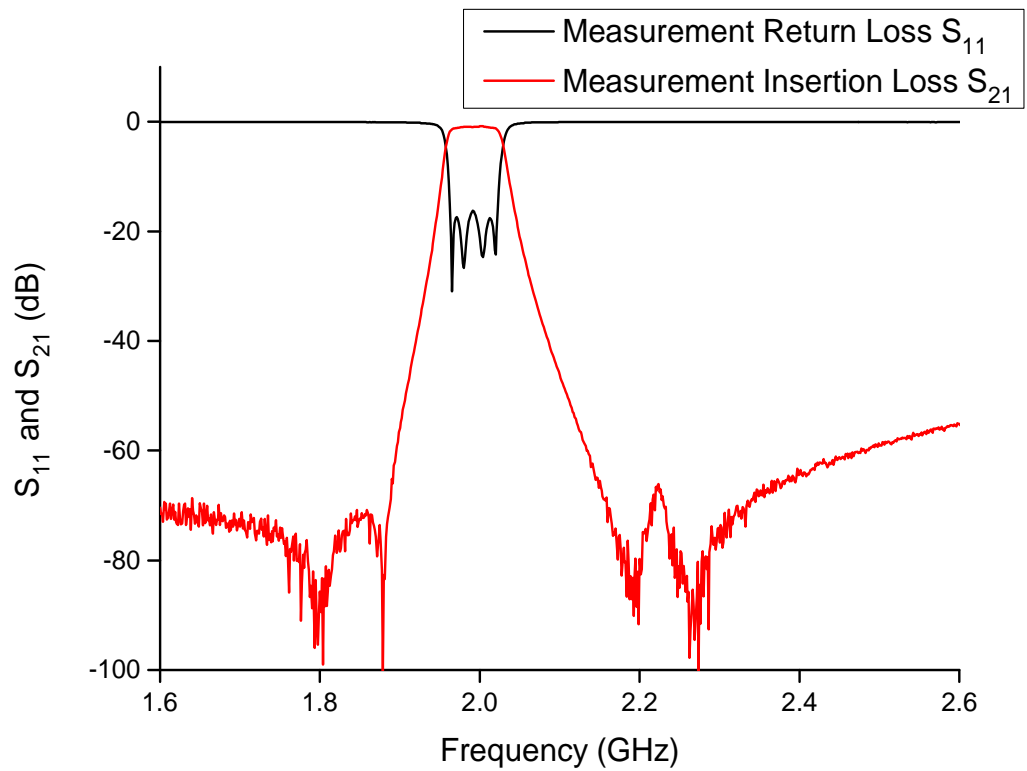
Figure 50 Measurement Result of The Fabricated Fourth Order Filter
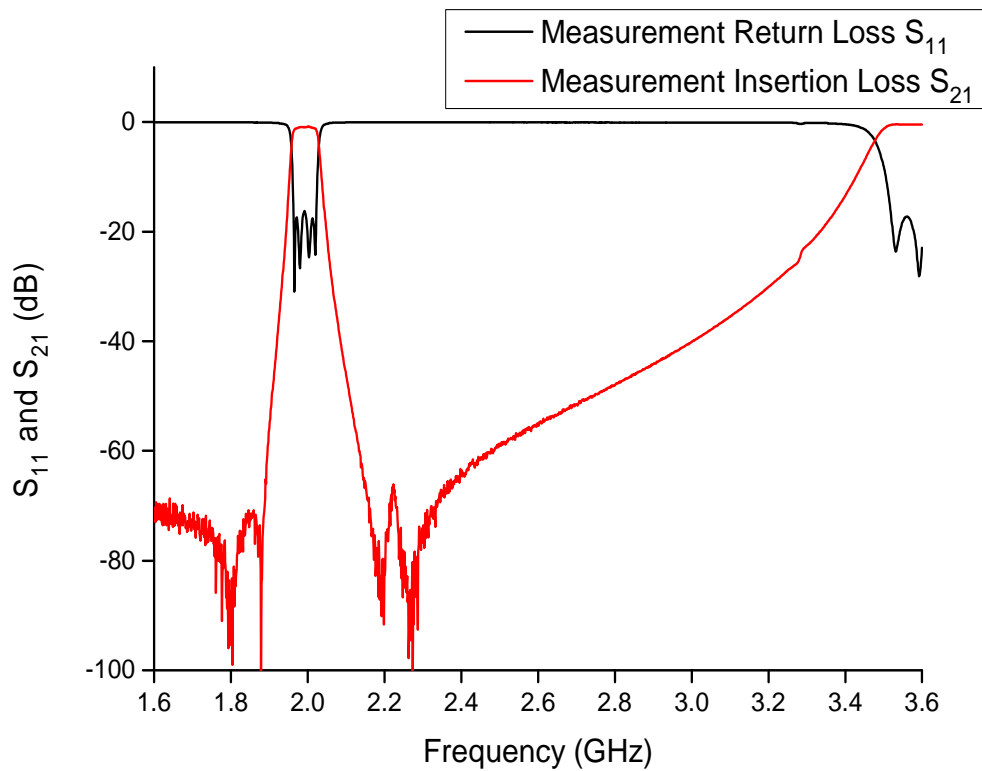
Figure 51 Wideband Response of The Fabricated Fourth Order Filter

3.6 Summary

A second order and fourth order dual mode suspended substrate stripline filter were presented whereby the influence of a metal post was first investigated. The first harmonic was suppressed and nearly doubled the fundamental frequency by adding the metal post. Using 90° input and output port arrangement, transmission zeros were obtained due to phase cancellation between two paths in the ring. In other words, no cross-coupling is needed to achieve a sharp skirt filter response. The notch radius is an important parameter, since it controls the bandwidth of the filter response as well as the coupling of two degenerates' modes, in which it generates a dual mode response. The obtained frequency response indicated that the dual mode SSS bandpass filter

enables the achievement of low-loss filter response, a good spurious, high Q factor as well as high selectivity filter response without using any cross-coupling connection.

Chapter 4 Dual Mode Suspended Substrate Stripline (SSS) Filters With Transmission Zero Control

4.1   Introduction

Wireless communication systems demand efficient utilisation of the frequency spectrum to satisfy the ever-increasing rigid specification requirements, including higher performance and lower cost. It is essential for RF and microwave filters to possess a sharp skirt selectivity in the transition band. A high selectivity filter can be realised by using more resonators, but this method has some drawbacks, such as higher losses and larger size. To overcome this problem, a high selectivity filter can be realised by introducing transmission zero near the passband. However, it is crucial to some of the applications which require transmission zeros only on one side or both sides of the passband based on their stringent rejection requirements. In the past, there has been considerable research conducted, mainly to control the transmission zeros' location in microwave bandpass filters [55]–[62]. In this chapter, two methods of

controlling the transmission zero location are explored, which is by adding susceptance to the ground and by controlling the degree of input and output feeding location.

4.2 Method 1: Adding Susceptance to the Ground

4.2.1 Transmission Line Equivalent Circuit Analysis

Figure 52 shows a ring resonator with susceptance which is directly connected to the ground at the input and output port. The ring resonator was analysed as two transmission lines with electrical length of θ_1 and θ_2 which are connected in parallel. The characteristic impedances Zo of the transmission lines are assumed as 1Ω.
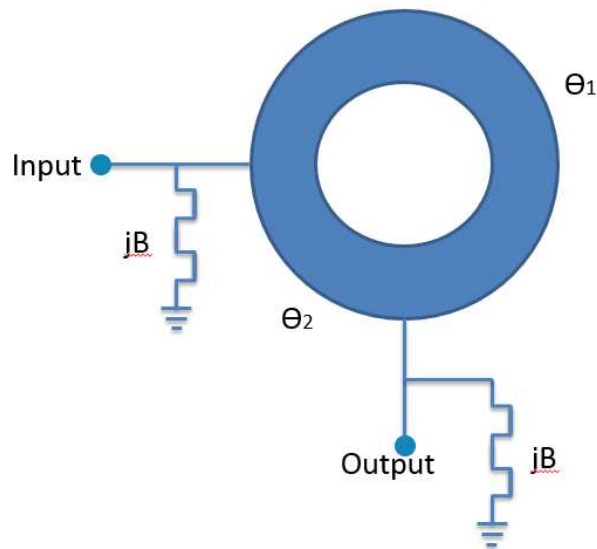
Figure 52 Ring Resonator with Susceptance to Ground at the Input and Output Port
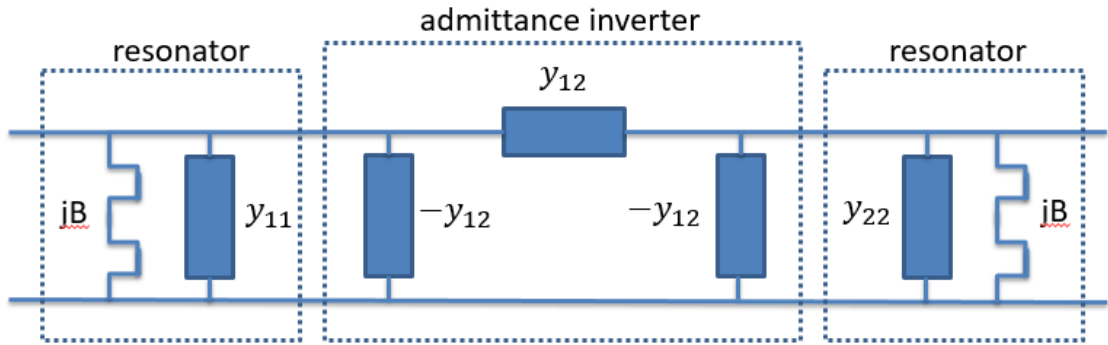
Figure 53 Transmission Line Equivalent Circuit
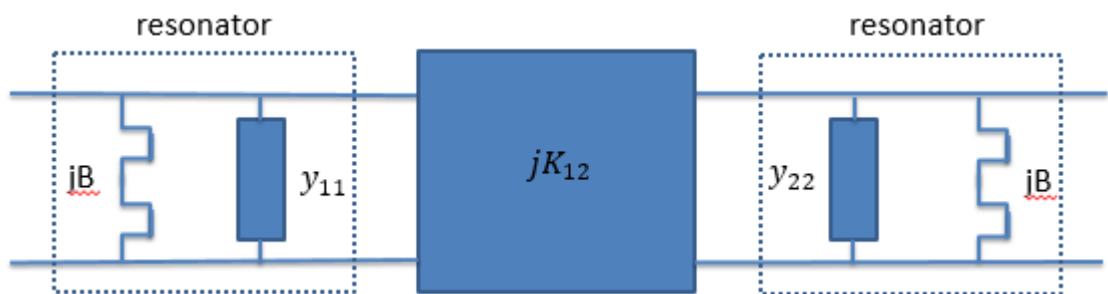
Figure 54 Simplified Transmission Line Equivalent Circuit with Admittance Inverter K_{12}

The two-port network is analysed the same as in the previous chapter and the final equivalent circuit, including the susceptance to the ground, is visualised in Figure 53. From the figure, it is demonstrated that the susceptance and the shunt impedance, y_{11}/y_{22}, are seen as two resonance circuits shunted to the ground, which are separated by a π network represented by an admittance inverter. Therefore, the equivalent circuit can be simplified, as in Figure 54.

And,

$$jK_{12} = y_{12} \qquad\qquad 4.1$$

From equation 3.5

$$y_{12} = \frac{j}{\sin \theta_1} + \frac{j}{\sin \theta_2} \qquad\qquad 4.2$$

Hence, the transmission zeros are the zeros of y_{12} and occur when

$$\sin \theta_1 + \sin \theta_2 = 0 \qquad\qquad 4.3$$

While, for the resonant circuits

$$jB - y_{11} = 0 \qquad\qquad 4.4$$

where $y_{11} = y_{22}$

Thence,

$$jB - j\left[\frac{1}{\tan \theta_1} + \frac{1}{\tan \theta_2}\right] = 0 \qquad\qquad 4.5$$

From equation 4.5, it is observed that the susceptance influences the passband response. For instance, if a capacitive susceptance is applied at the input and output port, the resonance will be shifted to a lower frequency and the bandwidth of the filter response will also increase; thus, the transmission zeros will appear on the higher side of the passband. In contrast, if an inductive susceptance is applied at the input and output port, the resonance will be shifted to the higher frequency and the bandwidth of the filter response will also increase; thus, the transmission zeros will appear on the lower side of the passband.

4.2.2 Second Order Filter Design

A second order filter was designed and simulated with the following specifications:

Table 6 Second Order Filter With Controllable Transmission Zero

Centre Frequency (f_o)	2.08 GHz
20 dB Bandwidth (BW)	100 MHz
Return Loss (RL)	>20 dB
Insertion Loss (IL)	<0.5 dB
System Impedance 'Z_O'	50Ω
Transmission zero	Above the passband

Figure 55 shows a second-order bandpass filter with a capacitive susceptance shunted to the ground at the input and output port. The transmission lines represent the ring resonator, and it is capacitively coupled to the input and output port. The circuit was simulated and optimised until it reaches the desired filter performance. Figure 56 depicts the filter response of the designed filter where the transmission zero is observed located at 2.08GHz, while the resonance is shifted to lower frequency which is contributed by the susceptance. In this design, no notch is needed as the dual mode response is initiated by the combination of input capacitance coupling and the capacitive susceptance, while

the bandwidth depends on the susceptance value. Therefore, the higher the capacitance value, the larger the bandwidth of the filter, thus leading the resonance frequency to be shifted further down.
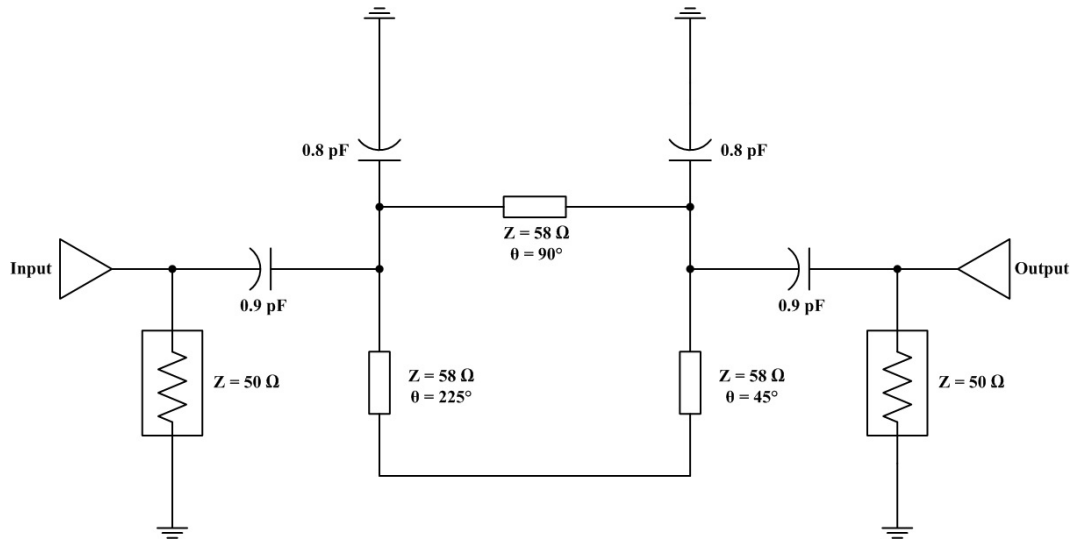
Figure 55 Circuit Diagram of The Second Order Asymmetrical Bandpass Filter With Capacitive Susceptance
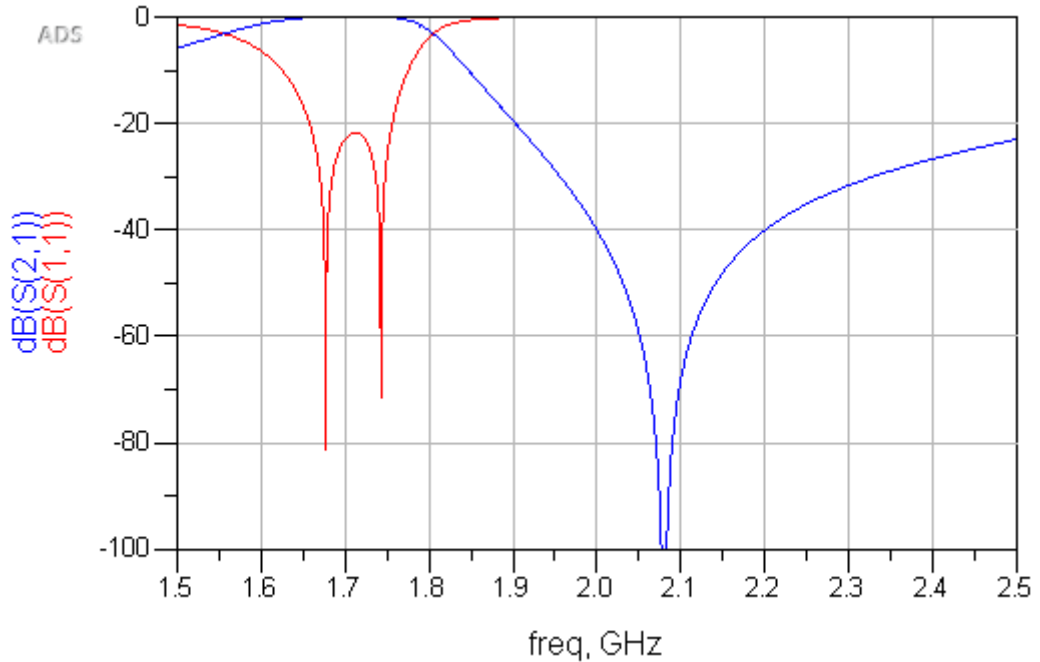
Figure 56 Simulated Result of The Second Order Asymmetrical Bandpass Filter With Capacitive Susceptance
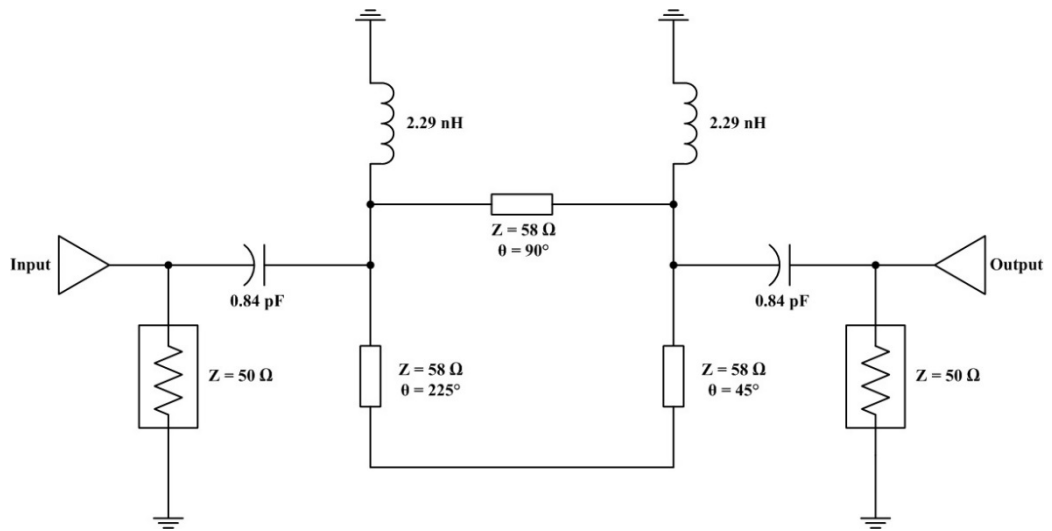
Figure 57 Circuit Diagram of The Second Order Asymmetrical Bandpass Filter With Inductive Susceptance
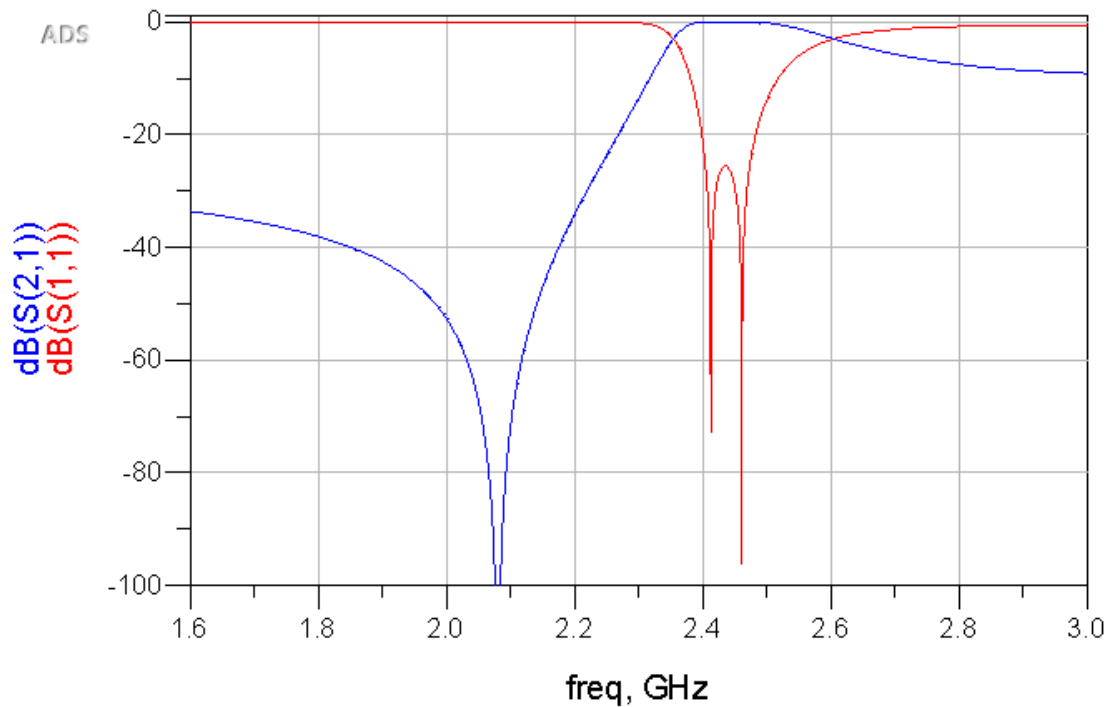
Figure 58 Simulated Result of The Second Order Asymmetrical Bandpass Filter With Inductive Susceptance

Figure 57 demonstrates the second order asymmetrical bandpass filter with an inductive susceptance shunted to the ground, while Figure 58 is the frequency response of the filter. Due to the different type of susceptance used, which is

now inductive, the resonance frequency is pushed to the higher frequency, thus moving the transmission zeros below the passband. Comparing the results in Figure 56 and Figure 58, it was observed that the location of transmission zeros were static at 2.08 GHz, and the type of susceptance has led the resonance to be shifted, thus making the transmission zero appear above or below the passband. This is consistent with the theory presented in Section 4.2.1, whereby the transmission zero position can be controlled by using susceptance shunted to the ground. However, in practice, a filter with inductive susceptance is difficult to realise using SSS; thus, a filter with capacitive susceptance was analysed further using the electromagnetic (EM) simulator.
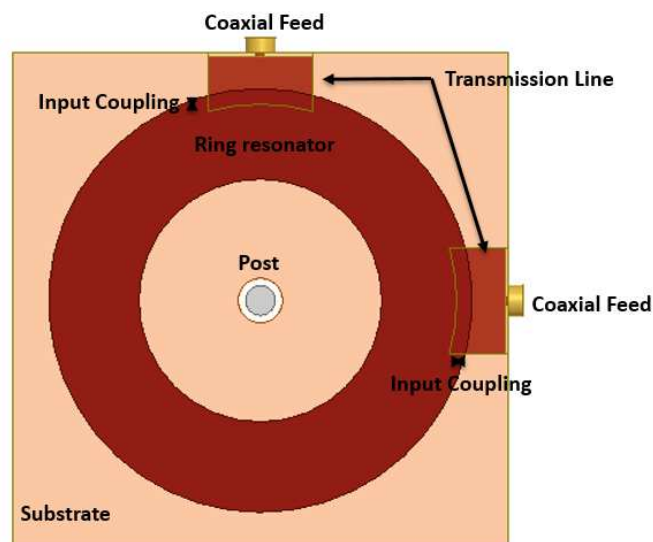
Figure 59 Top View of An Asymmetrical Second Order Bandpass Filter With Capacitive Susceptance
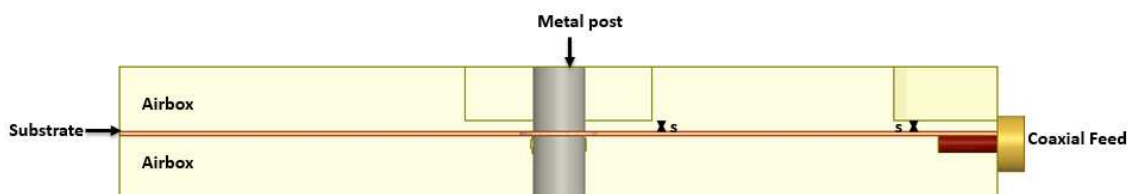
Figure 60 Front View of An Asymmetrical Second Order Bandpass Filter With Capacitive Susceptance

Figure 59 and Figure 60 show the top view and front view of the asymmetrical second order filter with capacitive susceptance, respectively. The filter is designed on a 0.254 mm thickness RT/Duroid 5880 substrate with a relative dielectric constant, ε_r= 2.2. The structure layout is the same as the one used in the previous chapter, except that the airbox was cut from the top of the cavity towards near the input and output transmission line to represent the capacitive susceptance, which is labelled as "s" in Figure 60. The initial coupling values were first extracted from [54] and the capacitive susceptance was assumed the same value as the input and output coupling value. Table 7 shows the extracted coupling value of the second order filter.

Table 7 Normalised Coupling Coefficients M_{ij} of the Second Order Filter

	S	1	2	L
S	0	1.2247	0	0
1	1.2247	0	1.6583	0
2	0	1.6583	0	1.2247
L	0	0	1.2247	0

The external coupling Q_e is calculated using equation 3.15 and the coupling value is 17.38. The filter is then simulated to find its group delay response so that the exact gap distance can be determined. The gap distance extracted is 0.5 mm and the impedance of the transmission line is 58 Ω, which is extracted from the graph of t/b versus Z_O [53], in which the t/b and w/b are 0 and 1.2, respectively.
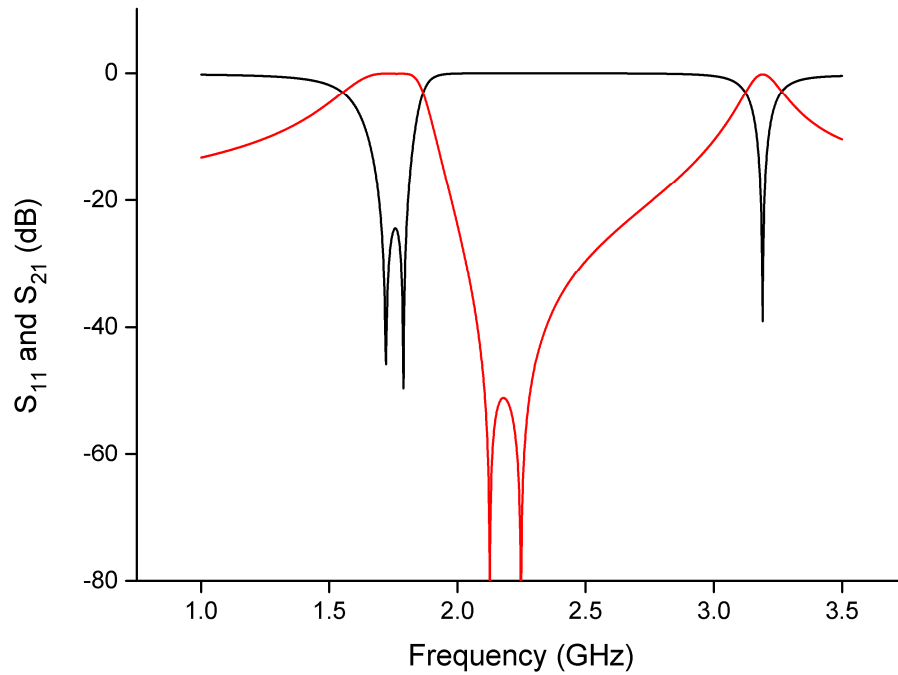
Figure 61 EM Simulated Response of The Asymmetrical Second-Order Filter With Capacitive Susceptance

The EM simulation result is shown in Figure 61 wherein a return loss of 24.7 dB and insertion loss of 0.07 dB were observed at 1.77 GHz. The bandwidth of the filter is 102 MHz and two transmission zeros were observed at 2.13 GHz and 2.25 GHz. The separation of the transmission zeros was due to more than one solution available for the transmission zero, where the transmission zero occurs when

$$\sin \theta_1 + \sin \theta_2 = 0 \qquad\qquad 4.6$$

where

$$\theta_1 = \frac{\omega_1 l_1}{v} \qquad\qquad 4.7$$

and

$$\theta_2 = \frac{\omega_2 l_2}{v} \qquad \qquad 4.8$$

Then, from the sine wave transmission zero equations, two solutions are obtained

$$\frac{\omega_1(l_2 - l_1)}{v} = \pi \qquad \qquad 4.9$$

And

$$\frac{\omega_2(l_2 + l_1)}{2v} = \pi \qquad \qquad 4.10$$

For instance,

Let $l_2 = 7l_1$,

Then, putting $l_2 = 7l_1$ into equation 4.9 and 4.10

$$\frac{\omega_1(6l_1)}{v} = \pi \qquad \qquad 4.11$$

And

$$\frac{4\omega_2(l_1)}{v} = \pi \qquad \qquad 4.12$$

Equating 4.11 and 4.12

$$\frac{\omega_1(6l_1)}{v} = \frac{4\omega_2(l_1)}{v} \qquad \qquad 4.13$$

Therefore,

$$\omega_2 = 1.5\omega_1 \qquad \qquad 4.14$$

where the second transmission zero ω_2 occurs at $1.5\omega_1$, thus making both transmission zeros further apart from each other. From the example given, it can

be concluded that there are two solutions obtained from the sine wave equation, which separate the location of two transmission zeros.
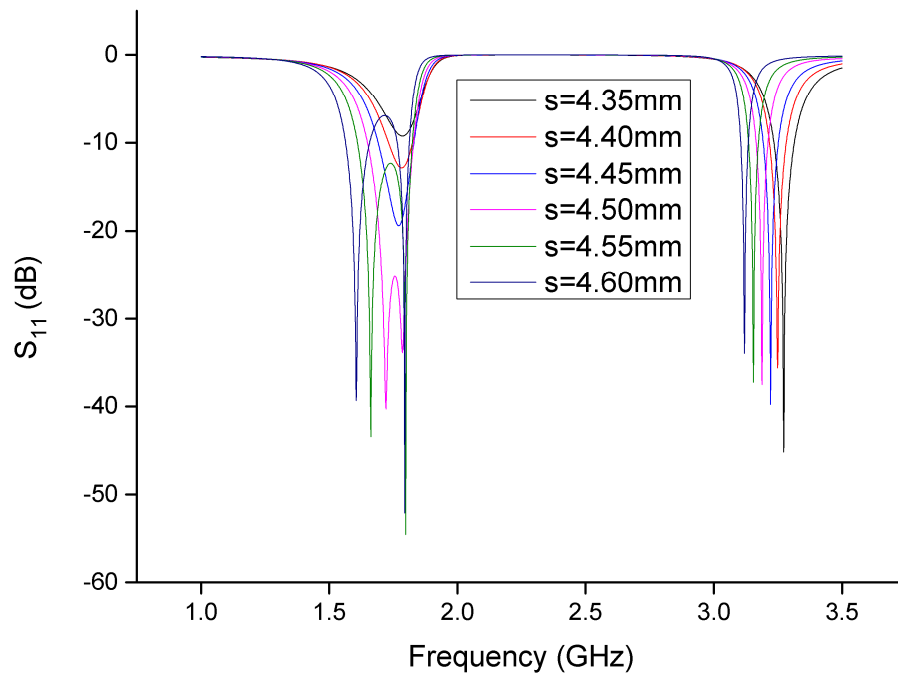
Figure 62 EM S$_{11}$ Frequency Response of The Asymmetrical Second-Order Filter With Capacitive Susceptance Varied

Figure 62 shows the return loss response of the designed filter with the capacitive susceptance varied and labelled as 's'. In the analysis, the gap distance 's' is varied from 4.35 mm to 4.60 mm. Results shows that the bandwidth of the filter response increases as the gap distance increases. In other words, as the capacitance of the susceptance is increased, the bandwidth of the filter becomes larger, thus shifting the resonance further down to the lower frequency. It is also observed that dual-mode response can be easily realised whenever there is sufficient coupling applied.

4.2.3 Fourth Order Filter Design

Fourth order filter with capacitance susceptance to the ground is shown in Figure 63. The two rings are identical, which is one wavelength long at 2.08 GHz, and both rings are located in-between a metal strip with a wall used to avoid cross coupling between the two cavities. A small iris is used to let the electromagnetic field pass and allow enough coupling between the two rings. The size of the filter is 136.5 mm length, 67 mm width and 10 mm height. The capacitive susceptances are represented by the gap which was cut from the top of the cavity towards near the top of the input transmission lines and the metal strip, as shown with the arrows in Figure 63. The side view of the fourth order asymmetrical filter is shown in Figure 64. The filter was simulated and optimised to get the desired performance, as presented in Figure 65.
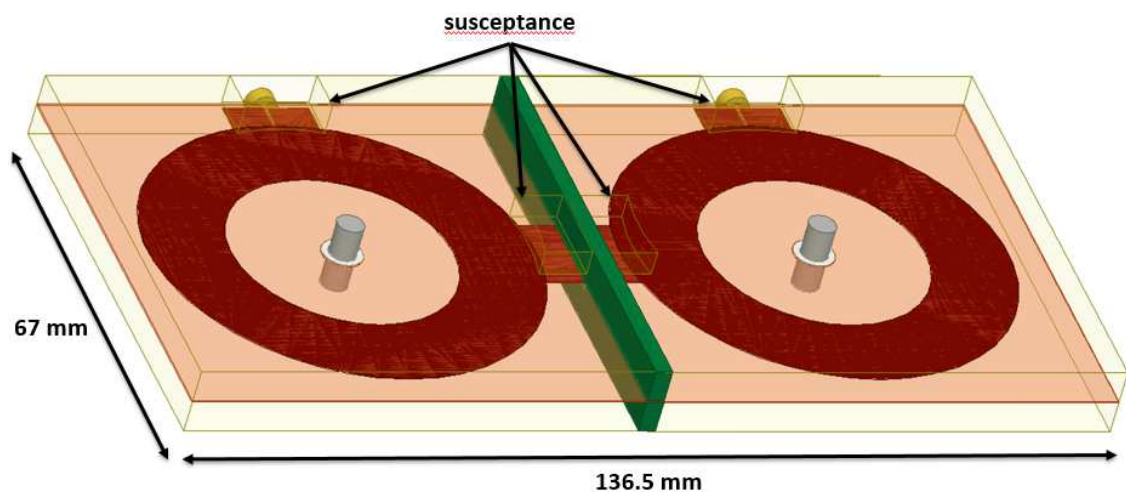
Figure 63 Asymmetrical Fourth Order Filter With Capacitive Susceptance
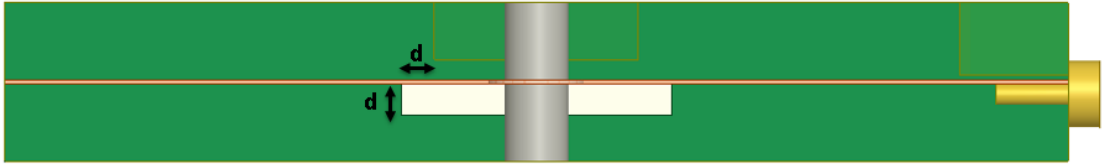
Figure 64 Side View of The Fourth Order Filter
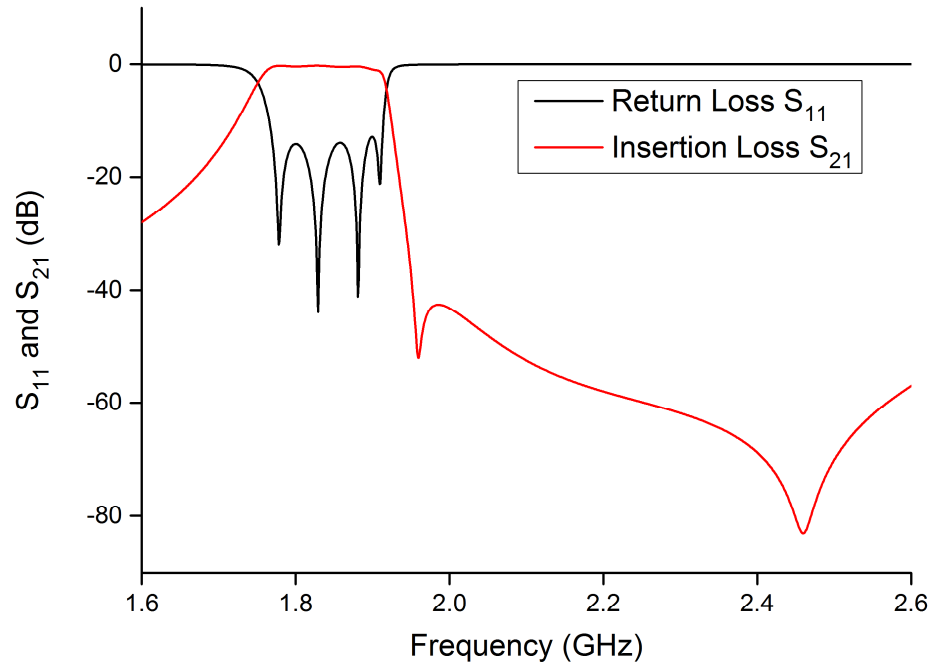
**Figure 65 EM Simulated Response of The Asymmetrical Fourth Order
Filter**
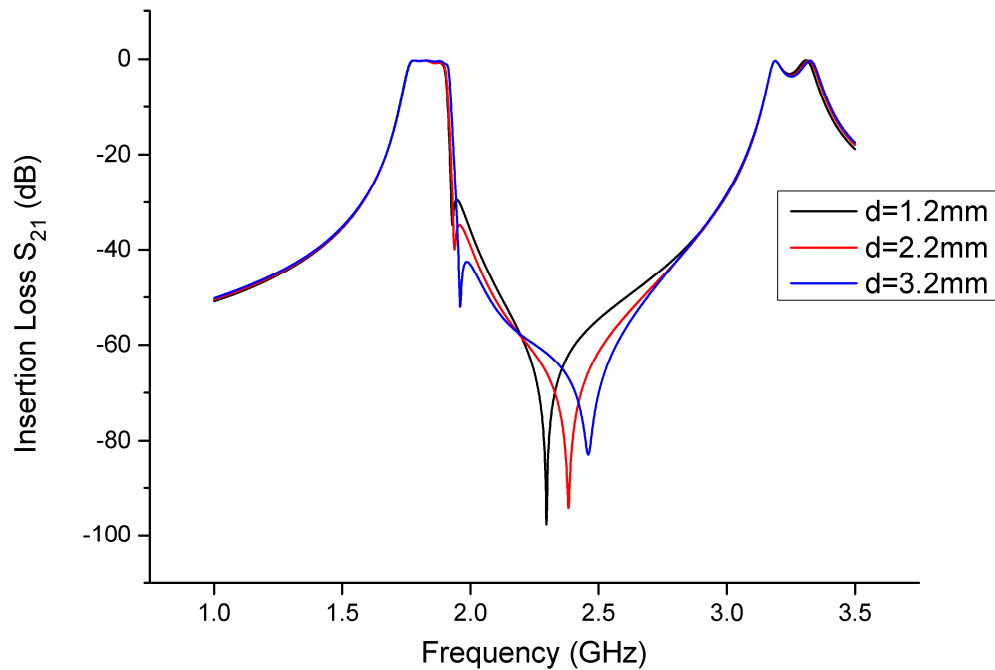
Figure 66 Effect of Varying Iris

A return loss of 14.6 dB, insertion loss of 0.33 dB and bandwidth of 130 MHz was obtained from the simulation outcome. In addition, two transmission zeros were observed at 1.96 GHz and 2.46 GHz, which increased the selectivity of the filter at the higher side of the passband. Figure 66 illustrates the effect of varying the size of the iris to the distance between the two transmission zeros while Figure 64 shows the location of the iris, which is located at the wall separator. It was observed that the distance of the transmission zeros was controlled by the size of the iris. The bigger the size of the iris, the further the distance between the two transmission zeros.

4.3   Method 2: Controlling the Input / Output Feed Location

A method of controlling the transmission zeros by adding susceptance connected to the ground was explained in detail in the previous sub-topic. However, there is another method explored which can also control the appearance of the transmission zero location and, hence, improve the selectivity of the filter response at the desired guard band. By changing the phase difference between the input and output port, the location of the transmission zeros appearance can be controlled. Using this method, no notch is needed, as the dual mode response is achieved using a suitable input coupling value. Additionally, the phase difference does not only control the transmission zero location, but also influences the passband response, such as the bandwidth, insertion loss and return loss. Therefore, a suitable coupling value must be applied at the input and output port so that the desired filter performance can be achieved.

4.3.1   Second Order Filter Design

A second order filter was designed and simulated with the following specifications:

Table 8 Second Order Filter With Input Feeding Control

Centre Frequency (f_o)	2.16 GHz
20 dB Bandwidth (BW)	65 MHz
Return Loss (RL)	>20 dB
Insertion Loss (IL)	<0.5 dB
System Impedance 'Z_O'	50 Ω

Transmission Zero	Above
	passband

Figure 67 shows the transmission line equivalent circuit for the second order filter with input feed control, which was designed at 2.16 GHz. The normalised coupling values were calculated from the low pass prototype g values, which were taken from [63] and the normalised external couplings are calculated as follows:

$$q_1 = g_0 g_1 \qquad \qquad 4.15$$

where $g_0 = 1$ and $g_1 = 0.4881$

$$q_1 = 0.4881 \qquad \qquad 4.16$$

Therefore, the coupling bandwidth is

$$K_{01} = \frac{BW}{q_1} \qquad \qquad 4.17$$

$$K_{01} = \frac{65\ MHz}{0.4881} \qquad \qquad 4.18$$

$$K_{01} = 133.17\ MHz \qquad \qquad 4.19$$

For the external coupling,

$$J_{01} = \frac{(\pi \frac{K_{01}}{2f_0})^{\frac{1}{2}}}{Z_0} \qquad \qquad 4.20$$

$$J_{01} = 6.22\ x\ 10^{-3} \qquad \qquad 4.21$$

And

$$J_{01} = 2\pi f_0 C_{01} \qquad \qquad 4.22$$

Therefore,

$$C_{01} = \frac{J_{01}}{2\pi f_0} \tag{4.23}$$

$$C_{01} = 0.4586 \, pF \tag{4.24}$$

Figure 67 shows the transmission line equivalent circuit for a one wavelength long second order filter with input feed control where the impedance of the transmission lines are extracted from [53]. The electrical length of the first path of the transmission line was set to 120°, while the second path was set to 240°. The circuit was simulated and optimised until it approached the desired filter performance. Figure 68 shows the simulated frequency response of the second-order designed filter. It was observed that two transmission zeros appeared after the passband, one of which is located at 2.16 GHz and the other at 3.16 GHz. The insertion loss, return loss and bandwidth obtained are 0.015 dB, 24.57 dB and 65 MHz, respectively.
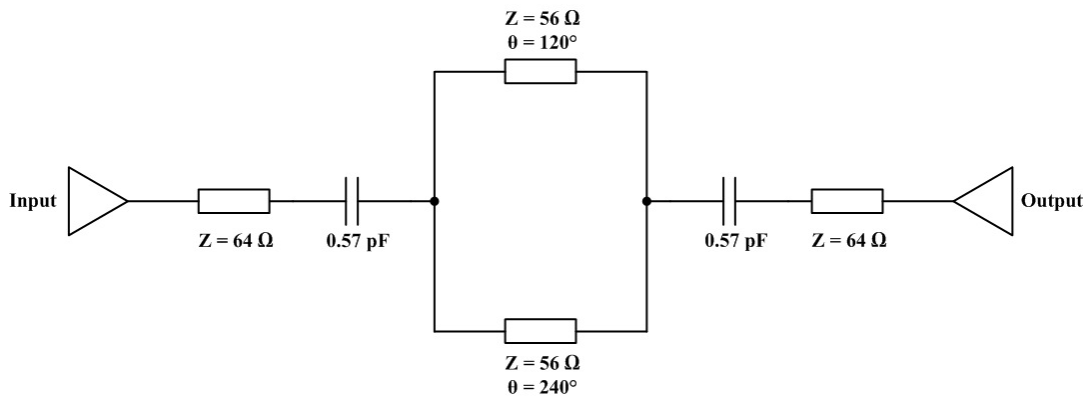
Figure 67 Second Order Filter With Input Feed Control
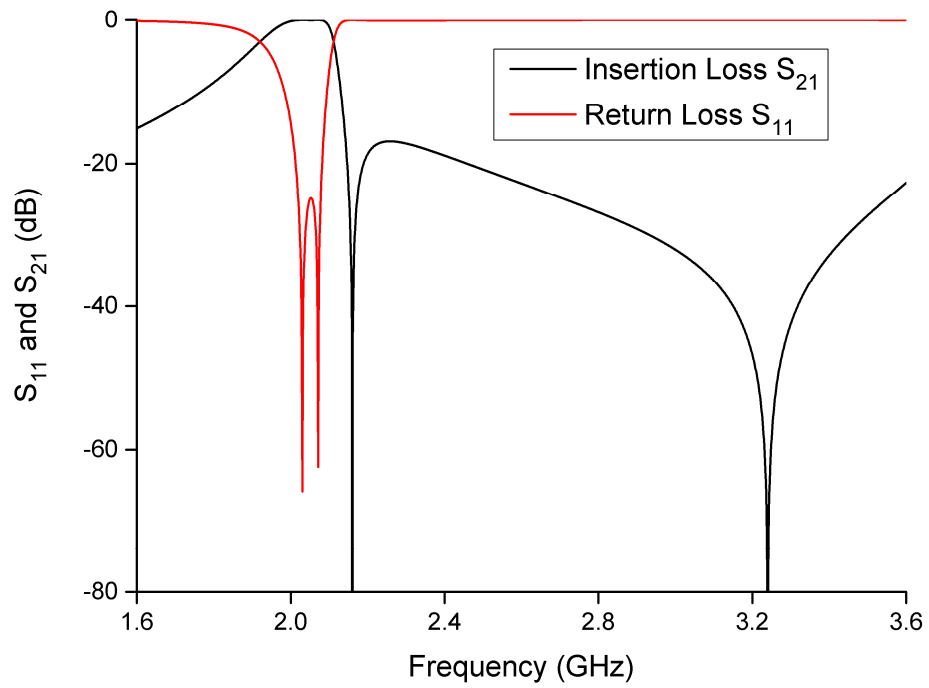
Figure 68 Frequency Response of the Second Order Filter With Input Feeding Control
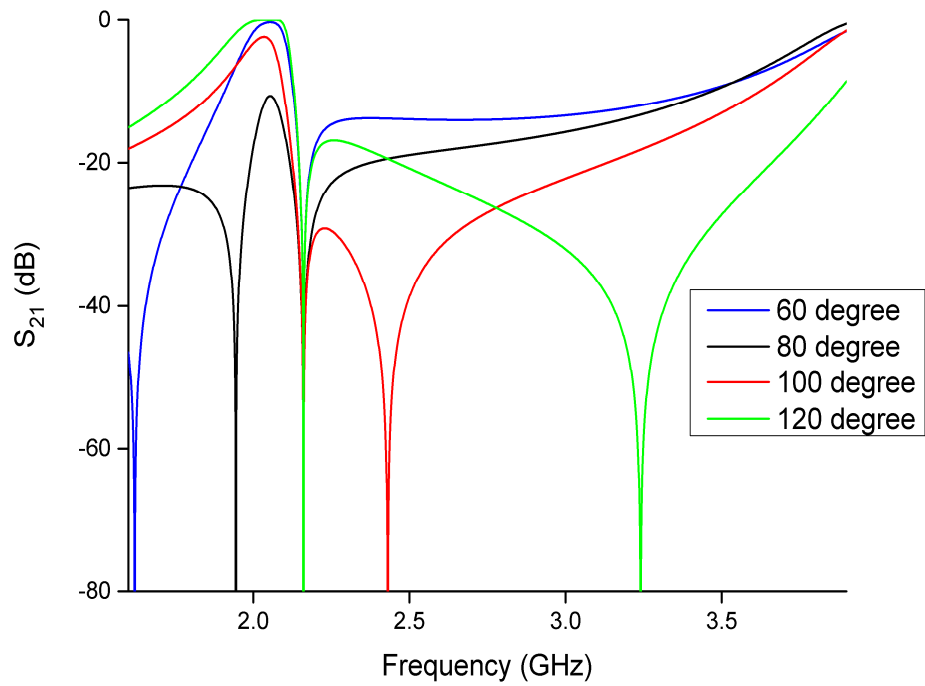
Figure 69 EM Simulation Responses by Varying The Electrical Length of the First Path of The Transmission Line

Figure 69 shows the frequency response of the designed filter with the electrical length of the first path is varied from 60°, 80°, 100° to 120°. From the analysis, it was observed that one transmission zero was seen constant at 2.16 GHz while the other transmission zero location depends on the electrical length of the first path of the transmission line. When the electrical length of the first path is lower than 90°, the transmission zeros are located at both sides of the passband and, when the electrical length is greater than 90°, both transmission zeros appear above the passband, thus making the sharp skirt selectivity on the higher side. The top view of the designed one wavelength long second order filter with input feed control is presented in Figure 70. The electrical length between the input and output feed port of the first path is 120°, while the second path is 360°-120°=240°. The substrate chosen is Rogers RT/Duroid 5880 with a relative dielectric constant ε_r= 2.2 and thickness of 0.254 mm.
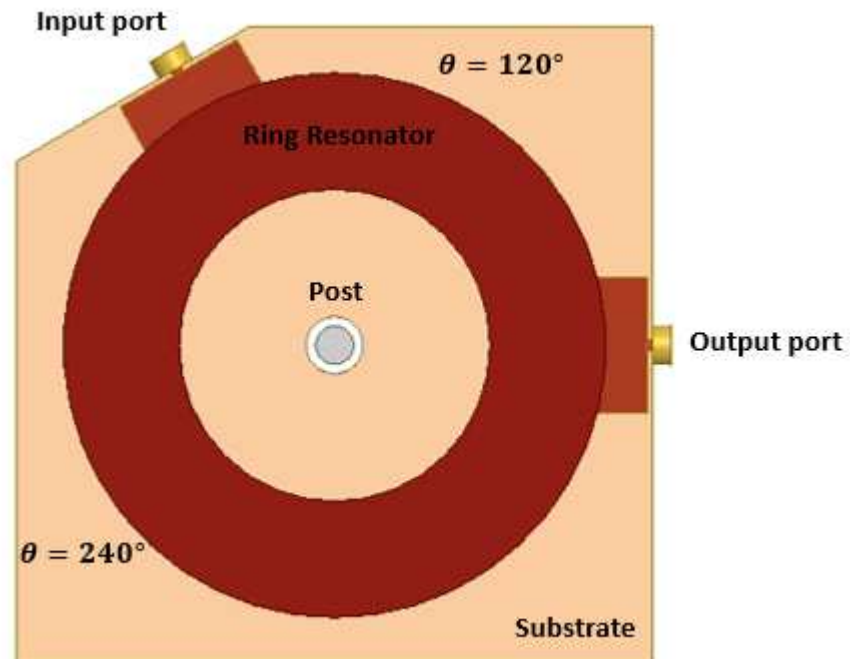
Figure 70 Top View of the Second Order Filter With Input Feed Control
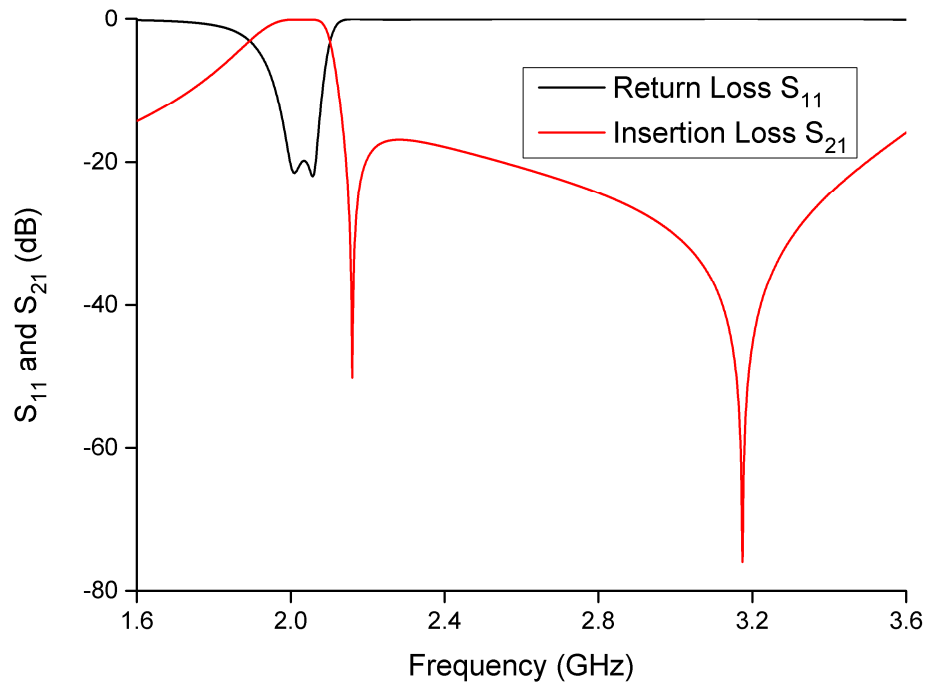
Figure 71 EM Simulated Response of the Second Order Filter With Input Feed Control

Figure 71 depicts the EM simulated response of the second order filter with input feed control. Two transmission poles are observed within the passband with a return loss of 20 dB and insertion loss of 0.12 dB at frequency 2.04 GHz. The bandwidth of the filter is 65 MHz and two transmission zeros were observed after the passband, which agreed well with the simulation results obtained from the transmission line equivalent circuit, as shown in Figure 68. From the simulation outcomes, it can be concluded that the transmission zero location appearance can be controlled by the electrical length between the input and output feed port.

4.3.2 Fourth Order Filter Design

A higher order filter was designed and simulated to observe the effect of controlling the input and output feeding port position. A fourth order filter was designed and the specifications are as follows:

Table 9 Fourth Order Filter With Input and Output Feed Control

Centre Frequency (f_o)	2.16 GHz
20 dB Bandwidth (BW)	50 MHz
Return Loss (RL)	>15 dB
Insertion Loss (IL)	<0.5 dB
System Impedance 'Z_O'	50 Ω
Transmission Zero	Above Passband

Figure 72 shows the transmission line equivalent circuit for a fourth order filter with input and output feed control where the impedance of the transmission lines are extracted from [53]. The normalised coupling values are calculated from the low pass prototype g values, which were taken from [63], and the normalised external couplings are calculated using equation 4.15 to 4.24, and the calculated C_{01} is 0.32 pF.

For the internal coupling,

$$k_{23} = \frac{1}{\sqrt{g_2 g_3}}$$

4.25

where $g_2 = 1.2252$ and $g_3 = 1.3712$

$$k_{23} = 0.7715 \qquad\qquad 4.26$$

Therefore, the coupling bandwidth is

$$K_{23} = k_{23}BW \qquad\qquad 4.27$$

$$K_{23} = 38.58\ MHz \qquad\qquad 4.28$$

And

$$J_{23} = \frac{\pi K_{23}}{f_0 Z_0} \qquad\qquad 4.29$$

$$J_{23} = 1.12\ x\ 10^{-3} \qquad\qquad 4.30$$

And

$$J_{23} = 2\pi f_0 C_{23} \qquad\qquad 4.31$$

Therefore,

$$C_{23} = 0.08\ pF \qquad\qquad 4.32$$

The length of the transmission line is one wavelength long each and was designed at 2.16 GHz. The electrical length of the first path was set to 110°, while the second path was set to 250°. The circuit was simulated and tuned until obtaining the desired filter performance.
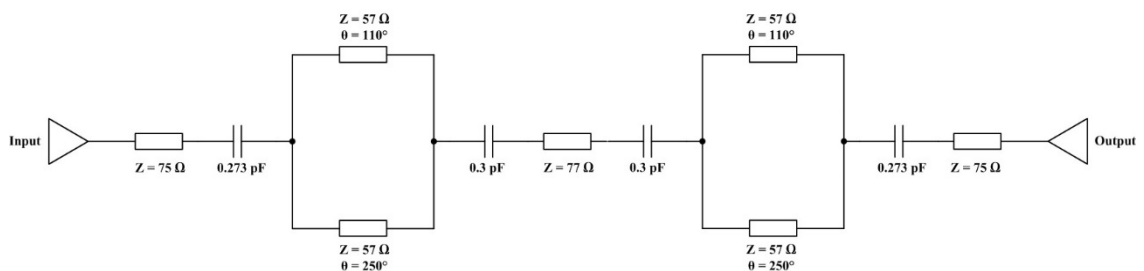
Figure 72 Fourth Order Filter With Input and Output Feed Control
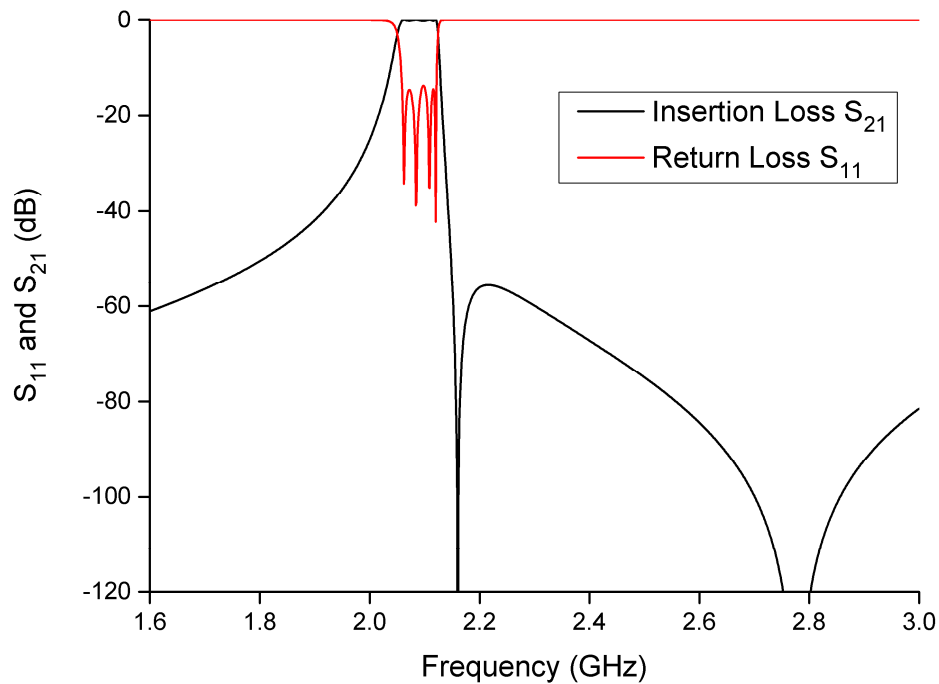
Figure 73 Simulated Frequency Response of the Fourth Order Filter With Input and Output Feed Control

Figure 73 represents the simulated frequency response of the fourth order filter with input and output feed control. Two transmission zeros appeared above the passband at 2.16 GHz and 2.78 GHz, thus sharp skirt response was achieved. The return loss, insertion loss and bandwidth are 15 dB, 0.02 dB and 50 MHz, respectively. Figure 74 shows the frequency response of the designed filter with electrical length of the first path of the transmission line was varied from 60° to 120°. It was observed that one transmission zero was located at 2.16 GHz while the other transmission zero location depended on the electrical length of the first path of the transmission line. For electrical length greater than 90°, both transmission zeros are observed after the passband, whereas, for the electrical length which is smaller than 90°, one transmission zero is located below the passband while another transmission zero is located after the passband. The

further the degree away from 90°, the further the distance between the transmission zeros.
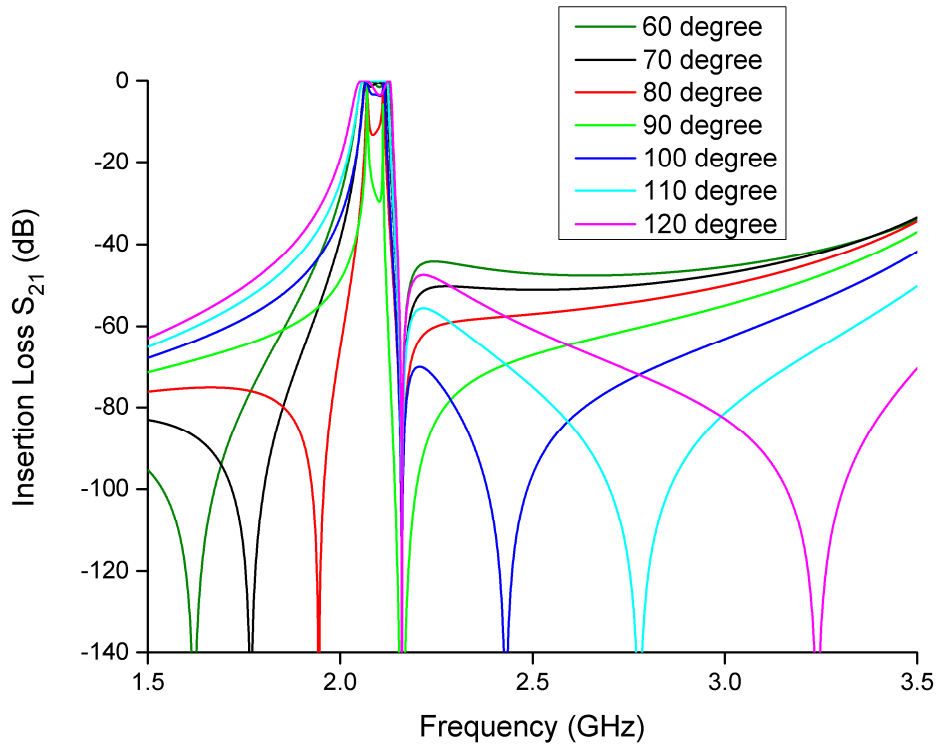
Figure 74 Simulated Frequency Response with Varied Phase Difference
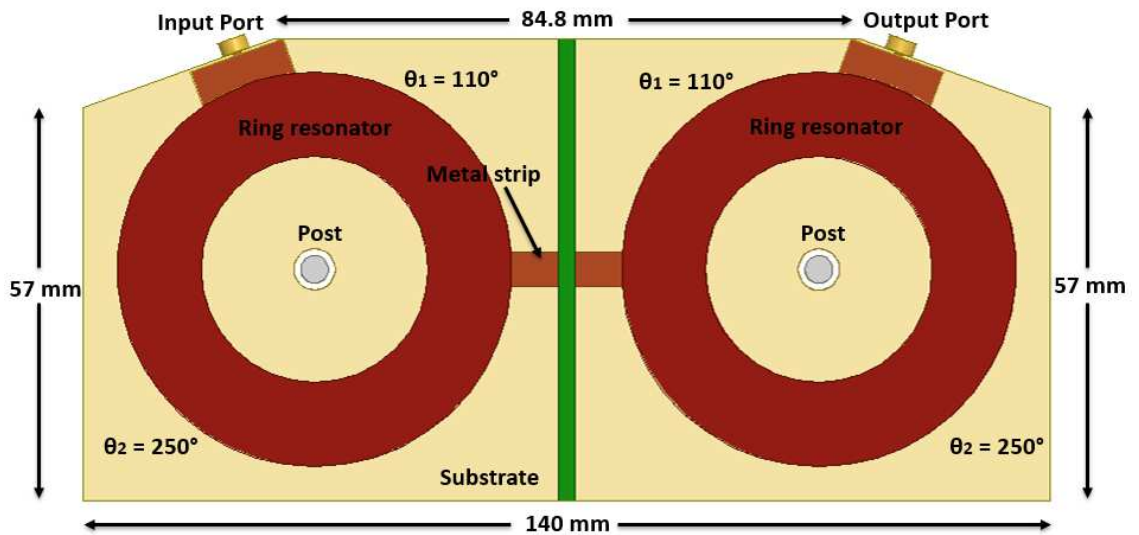
Figure 75 Top View of Fourth Order Filter With Input and Output Feed Control
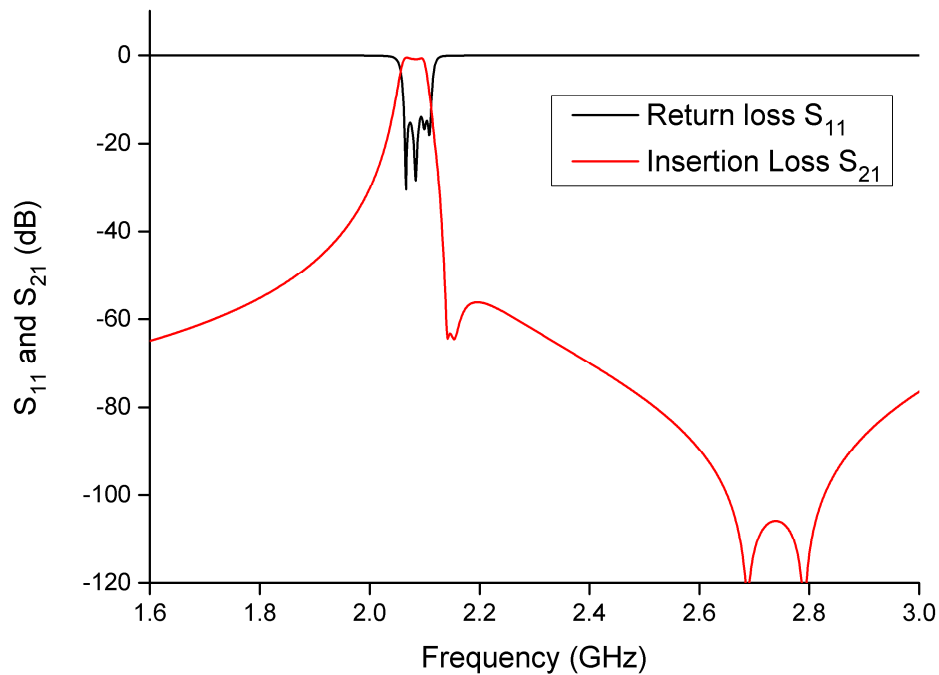
Figure 76 EM Simulated Response of the Fourth Order Filter With Input and Output Feed Control

Figure 75 depicts the top view of the fourth order filter with input and output feed control. The electrical length of the first path of the ring resonator was set to 110° while the second path was set to 250°, which made a total length of 360° for each ring resonator. The size of both ring resonators is identical, with a mean radius of 22.5 cm. The input and output couplings, as well as the coupling between two rings, were determined using the same method as stated in the previous chapter. The substrate chosen is Rogers RT/Duroid 5880 with a relative dielectric constant ε_r= 2.2 and thickness of 0.254 mm. Figure 76 shows the frequency response of the designed fourth order asymmetrical filter. The return loss, insertion loss and bandwidth obtained are 14 dB, 0.84 dB and 48 MHz, respectively. Four transmission poles were observed in the passband while four transmission zeros were observed after the passband. The transmission zeros

were located at 2.14 GHz, 2.15 GHz, 2.68 GHz and 2.79 GHz. The simulation result showed that the location of the transmission zeros can be controlled by changing the electrical length between the input and output feed, thus the sharp selectivity filter response was achieved at the higher side.

4.4   Summary

In this chapter, second order and fourth order dual mode suspended substrate stripline filters with controllable transmission zeros were designed and simulated. Two methods were studied in this chapter, namely, by using the susceptance to the ground and by controlling the input and output feeding location. Simulation results showed that both methods work well whereby the transmission zeros locations can be controlled successfully and appeared after the passband. As a consequence, sharp skirt selectivity filter response was achieved.

Chapter 5 Conclusions

5.1   Contributions to dissertation

In this dissertation, design techniques for dual-mode SSS bandpass filters have been investigated. Using this technique, several filters were designed and constructed. A ring structure was chosen due to its simplicity to model and fabricate. A study on the eigenmode solution and its field distributions was carried out using a full-wave electromagnetic (EM) simulator. In the study, it was proven that adding a metal post in the middle of the cavity shorted at both end to ground improves the first harmonic up to nearly double the fundamental frequency. It has also shown that a wider out-of-band rejection is achievable when a metal post is applied in the middle of the cavity.

The ring resonator was then analysed as a two-port network with two transmission lines, which were connected in parallel. The two-port network was rearranged and analysed as a π network, which can be viewed as an admittance inverter. The transmission zero was analysed and calculated using the solution obtained from the two-port network equivalent circuit. A second and fourth order filter was designed to demonstrate the discussed theory. In the second order

designed filter, the ring resonator was one wavelength long with 90° input and output feed separation. An inductive notch, which was represented by a semi-circular cut, was located 135° from both input and output feeding port. The analysis on the radius change on the notch had an effect on the mode splitting of the degenerate modes. In other words, the radius of the notch controls the dual-mode response, as well as the bandwidth of the filter. A good frequency response was obtained, which resulted in a good return loss and insertion loss value without compromising any other design parameters. In addition, the wideband response showed that the first harmonic occurred at nearly double the fundamental frequency.

As for the fourth order filter, two rings were cascaded whereby each ring generated a dual-mode response; thus, four reflection zeros were observed in the passband. Four transmission zeros were observed, with two below and another two above the passband. This is because when the input and output ports are at 90° to each other, there were two separate paths existing, with one path of λ/4 long and the other 3λ/4 long, which created a 180° phase difference. The 180° phase difference naturally creates zero transmission; thus, the skirt selectivity was improved. In other words, *no cross-coupling configuration is needed with this design to achieve a sharp skirt selectivity response*. The measured frequency response indicated that the dual mode suspended substrate stripline filter enables the achievement of low-loss filter response, a good spurious, high Q factor as well as high selectivity filter response without any cross-coupling connection.

For the filter with controllable transmission zero, two methods were approached. The first method was using susceptance, which was connected to

the ground, while the second method was by controlling the input and output feeding location. For the first method of adding susceptance to the ground, two transmission lines were connected in parallel with one susceptance each, connected to the input and output port to the ground, respectively. The two-port network was then analysed whereby the susceptance and the shunt impedance y_{11}/y_{22} were seen as two resonant circuits shunted to the ground, which were separated by a π network represented by an admittance inverter. Therefore, the resonant circuit, which comprises of susceptance and shunt impedance, influenced the passband response. For instance, if a capacitive susceptance was applied, the resonance was shifted to lower frequency and the bandwidth of the filter response increased; thus, the transmission zeros appeared on the higher side of the passband. In contrast, when an inductive susceptance was applied, the resonance was shifted to the higher frequency and the bandwidth of the filter response also increased; thus, the transmission zeros appeared on the lower side of the passband. A second and fourth order filter with capacitive susceptances were designed and simulated, showing good frequency responses and transmission zeros location above the passbands were obtained, thus verifying the theoretical background discussed.

For the second method, changing the electrical length between the input and output port influenced the location of the transmission zeros' appearance. Using this method, no notch was needed, as the dual mode response was achieved using a suitable input coupling value. A second order and fourth order filter were designed and simulated to demonstrate the ability to control the transmission zero location. Simulation results showed that the transmission zero appeared above the passband when the electrical length of the first path of the

ring was greater than 90°; thus, sharp selectivity was achieved at the higher side of the passband. In contrast, when the electrical length was ≤ 90°, the transmission zero appeared on both sides of the passband. Therefore, the smaller the electrical length, the further the location of transmission zeros from each other.

5.2   Future Development

A dual-mode suspended substrate stripline filter was studied extensively in this dissertation. However, the design of dual mode SSS filter can be further extended into dual passband filter which can greatly increase its applications. Another possible extension is the investigation of dual mode SSS filter at higher frequency, thus make it usable for many other applications.

In the case of the asymmetrical frequency response filter, it is imperative that the designed filter is fabricated to confirm the concept discussed in theory and to compare with the simulated results to adjust any fabrication errors that may occur. Furthermore, the filter can also be improved by using a different technique of coupling to minimise the losses. This might be possible by using a direct connection input coupling or other coupling technique at the input and output of the ring. Another possible way of designing an asymmetrical frequency response filter is by using two different values of characteristic impedance in a single ring; thus, the transmission zero location can be controlled

REFERENCES

[1]   N. Binti Mohd Najib, N. Somjit, and I. Hunter, "Design and Characterisation of Dual-Mode Suspended-Substrate Stripline Filter," *IET Microwaves, Antennas Propag.*, pp. 1–7, 2018.

[2]   I. Hunter, *Theory and Design of Microwave Filters.* London: The Institution of Electrical Engineers, 2001.

[3]   M. K. M. Salleh, G. Prigent, O. Pigaglio, and R. Crampagne, "Quarter-Wavelength Side-Coupled Ring Resonator for Bandpass Filters," *IEEE Trans. Microw. Theory Tech.*, vol. 56, pp. 156–162, 2008.

[4]   S. Sun and L. Zhu, "Wideband Microstrip Ring Resonator Bandpass Filter With Asymmetrically-loaded Stubs," *Proc. 2008 Asia Pacific Microw. Conf. APMC 2008*, vol. 55, no. 10, pp. 2176–2182, 2008.

[5]   L. H. Hsieh and K. Chang, "Dual-Mode Quasi-Elliptic-Function Bandpass Filters Using Ring Resonators With Enhanced-Coupling Tuning Stubs," *IEEE Trans. Microw. Theory Tech.*, vol. 50, no. 5, pp. 1340–1345, 2002.

[6]   K. Chang, S. Martin, F. Wang, and J. L. Klein, "On The Study of Microstrip Ring and Varactor-Tuned Ring Circuits," *IEEE Trans. Microw. Theory Tech.*, vol. 35, no. 12, pp. 1288–1295, 1987.

[7]   H. Ishida and K. Araki, "Design and Analysis of UWB Band Pass Filter With Ring Filter," *2004 IEEE MTT-S Int. Microw. Symp. Dig. (IEEE Cat. No.04CH37535)*, vol. 3, pp. 1307–1310, 2004.

[8]   C. Kai and H. Lung-Hwa, *Microwave Ring Circuits and Related Structures.* United States of America: John Wiley & Sons, Inc., 2004.

[9]   D. Preetha and T. Jayanthy, "Analysis of Different Types of Coupling For Microstrip Ring Resonator," *Int. Conf. Sci. Eng. Manag. Res. ICSEMR 2014*, pp. 1–5, 2014.

[10]   L. G. Maloratsky, "Reviewing The Basics of Suspended Striplines," *Microw. J.*, 2002.

[11]   Z. Zakaria *et al.*, "Design of Generalized Chebyshev Lowpass Filter With Defected Stripline Structure (DSS)," in *2013 IEEE Symposium on Wireless Technology & Applications (ISWTA)*, 2013, pp. 230–235.

[12]   W. J. Getsinger, "Coupled Rectangular Bars Between Parallel Plates," *IRE Trans. Microw. Theory Tech.*, vol. M, no. 1, pp. 65–72, 1962.

[13]   C. Sovuthy and W. P. Wen, "Stepped Impedance Dual Mode Coaxial Filter," in *2013 IEEE International RF and Microwave Conference (RFM)*, 2013, pp. 165–167.

[14]   C. Sovuthy and W. P. Wen, "High Q, Miniaturized Dual-Mode Coaxial Bandpass Filter," in *2014 Asia-Pacific Microwave Conference*, 2014, pp. 1294–1296.

[15]   C. Bingjie and B. Chen, "A Novel Class of Compact Dual-Mode Coaxial Filter Using Stepped Impedance Resonators," in *2015 IEEE International Conference on Communication Problem-Solving (ICCP)*, 2015, pp. 204–207.

[16]   Z. Zheng, J. Hu, S. Liu, and Y. Zhang, "WR-1.5 Band Waveguide Bandpass Dual-mode Filter on Silicon Micromachining Technique," in *IEEE International Conference on Communication Problem-Solving (ICCP)*, 2015, no. 1, pp. 112–114.

[17] Y. Su, X. Lin, S. Member, P. Pang, and S. Liu, "A Dual Mode Substrate Integrated Waveguide Filter With Capacitive I/O Coupling Structure," in *IEEE MTT-S International Microwave Workshop Series on Advanced Materials and Processes for RF and THz Applications (IMWS-AMP)*, 2016, pp. 101–103.

[18] C. Guo, J. Li, J. Xu, and H. Li, "An X -Band Lightweight 3-D Printed Slotted Circular Waveguide Dual-Mode Bandpass Filter," in *IEEE International Symposium on Antennas and Propagation & USNC/URSI National Radio Science Meeting*, 2017, pp. 2645–2646.

[19] A. Moran-Lopez, J. Corcoles, J. A. Ruiz-Cruz, J. R. Montejo-Garai, and J. M. Rebollar, "Dual-Mode Filters in Equilateral Triangular Waveguides With Wide Spurious-Free Response," *IEEE MTT-S Int. Microw. Symp. Dig.*, no. 3, pp. 1192–1195, 2017.

[20] H. Hu and K.-L. Wu, "A TM11 Dual-Mode Dielectric Resonator Filter With Planar Coupling Configuration," *IEEE Trans. Microw. Theory Tech.*, vol. 61, no. 1, 2013.

[21] C. Y. Li and Q. X. Chu, "A Dual-Mode Dielectric Resonator Filter With Metal Patches," in *2016 IEEE International Workshop on Electromagnetics, iWEM 2016 - Proceeding*, 2016, pp. 1–2.

[22] J. X. Chen, W. J. Zhou, and W. Qin, "Miniaturized Balanced Bandpass Filter Using Dual-Mode Dielectric Resonator," in *2016 IEEE International Conference on Ubiquitous Wireless Broadband, ICUWB 2016*, 2016, pp. 1–3.

[23] Y. Cheng, L. Zeng, and W. Lu, "A Compact CSRR-based Dual-Mode Patch

Bandpass Filter," in *2015 IEEE MTT-S International Microwave Workshop Series on Advanced Materials and Processes for RF and THz Applications, IEEE MTT-S IMWS-AMP 2015 - Proceedings*, 2015, pp. 3–5.

[24] J. L. Li, J. P. Wang, X. S. Yang, and B. Z. Wang, "A Study of Dual-Mode Patch Resonator-based Microwave Filters," in *2010 International Conference on Microwave and Millimeter Wave Technology*, 2010, pp. 48–51.

[25] B. Jeon, H. Nam, K. Yoon, B. Jeon, Y. Kim, and J. Lee, "Design of A Patch Dual-Mode Bandpass Filter With Second Harmonic Suppression Using Open Stubs," in *Proceedings of Asia-Pacific Microwave Conference 2010*, 2010, pp. 1106–1109.

[26] I. Wolff, "Microstrip Bandpass Filter Using Degenerate Modes of A Microstrip Ring Resonator," *Electron. Lett.*, vol. 8, pp. 302–303, 1972.

[27] S. S. Gao, H. L. Liu, J. Li, and W. Wu, "A Compact Dual-Mode Bandpass Filter For GPS, Compass (Beidou) and GLONASS," *10th Glob. Symp. Millimeter-Waves, GSMM 2017*, pp. 28–30, 2017.

[28] C. Karpuz, P. Ö. Özdemir, and G. B. Fırat, "Design of Fourth Order Dual-Mode Microstrip Filter by Using Interdigital Capacitive Loading Element with High Selectivity," in *2016 46th European Microwave Conference (EuMC)*, 2016, pp. 461–464.

[29] C. J. Chen, "Design of Parallel-Coupled Dual-Mode Resonator Bandpass Filters," *IEEE Trans. Components, Packag. Manuf. Technol.*, vol. 6, pp. 1542–1548, 2016.

[30] T. Y. Y. Xiang, T.Lei, M. Peng, T. Lei, and M. Peng, "Miniature Dual-Mode Bandpass Filter Based On Meander Loop Resonator With Source-Load Coupling," in *Asia-Pacific Microwave Conference (APMC)*, 2015, vol. 3, pp. 1–3.

[31] L. Zhang, Z. Qi, J. Chu, and X. Li, "Design of Triangular Microstrip Dual Mode Filter Based on The Coupling Matrix Synthesis Method," *2016 IEEE Int. Conf. Microw. Millim. Wave Technol.*, vol. 1, no. 1, pp. 235–237, 2016.

[32] J. Wang, J. Li, J. Ni, S. Zhao, W. Wu, and D. Fang, "Design of Miniaturized Microstrip Dual-Mode Filter With Source-Load Coupling," *IEEE Microw. Wirel. Components Lett.*, vol. 20, no. 6, pp. 319–321, 2010.

[33] L. Li and Z.-F. Li, "Application of Inductive Source-Load Coupling in Microstrip Dual-Mode Filter Design," *Electron. Lett.*, vol. 46, no. 2, p. 141, 2010.

[34] B.-B. Wu, B.-R. Guan, and Z.-H. Zhang, "A Novel Compact Microstrip Dual-Mode Bandpass Filter," in *2011 International Conference on Electronics, Communications and Control (ICECC)*, 2011, pp. 650–652.

[35] Y. K. Singh and A. Chakrabarty, "Miniaturized Dual-Mode Circular Patch Bandpass Filters With Wide Harmonic Separation," *IEEE Microw. Wirel. Components Lett.*, vol. 18, pp. 584–586, 2008.

[36] L. Suping, C. Hongtao, W. Wei, L. Ying, and W. Zihua, "New Dual-Mode Microstrip Bandpass Filter With A Square Notch," in *2010 IEEE 12th International Conference on Communication Technology*, 2010, pp. 656–658.

[37] T. W. Lin, J. T. Kuo, and S. J. Chung, "Miniaturized Dual-Mode Spiral-Ring

Resonator Bandpass Filter," in *2012 Asia Pacific Microwave Conference Proceedings*, 2012, pp. 1127–1129.

[38] T. W. Lin, J. T. Kuo, S. C. Tang, and S. J. Chung, "Miniaturized Dual-Mode Ring Resonator Bandpass Filter With A Wide Passband," in *2014 IEEE International Wireless Symposium (IWS 2014)*, 2014, pp. 1–3.

[39] C. Sovuthy and W. P. Wen, "Design and Synthesis of Microwave Dual Mode Filter," in *IEEE Asia-Pacific Conference on Applied Electromagnetics (APACE 2012)*, 2012, pp. 226–229.

[40] C. I. Mobbs and J. D. Rhodes, "A Generalized Chebyshev Suspended Substrate Stripline Bandpass Filter," *IEEE Trans. Microw. Theory Tech.*, vol. 31, pp. 397–402, 1983.

[41] J. M. Pham, P. Jarry, E. Kerherve, and E. Hanna, "A Novel Compact Suspended Stripline Bandpass Filter Using Open-Loop Resonators Technology With Transmission Zeroes," in *2007 SBMO/IEEE MTT-S International Microwave and Optoelectronics Conference*, 2007, pp. 937–940.

[42] E. Hanna, P. Jarry, E. Kerherve, and J. M. Pham, "Cross-Coupled Suspended Stripline Trisection Bandpass Filters With Open-Loop Resonators," in *SBMO/IEEE MTT-S International Conference on Microwave and Optoelectronics, 2005.*, 2005, pp. 42–46.

[43] A. Balalem, W. Menzel, J. Machac, and A. Omar, "A Simple Ultra-Wideband Suspended Stripline Bandpass Filter With Very Wide Stop-Band," *IEEE Microw. Wirel. Components Lett.*, vol. 18, pp. 170–172, 2008.

[44] O.-S. Kim, N.-S. Kim, W.-G. Moon, and G.-B. Lee, "A Novel Broadband

Suspended Substrate Stripline Filter Using Dual-Mode Resonators," *2008 IEEE 19th Int. Symp. Pers. Indoor Mob. Radio Commun.*, 2008.

[45] J. S. Kim, Y. J. Kim, W. G. Moon, and S. G. Byeon, "A Novel Suspended Substrate Bandpass Filter Using H-Shaped Resonator," in *2006 Asia-Pacific Microwave Conference*, 2006, pp. 1181–1184.

[46] X. J. Liao, W. H. Hsu, and M. H. Ho, "Design of The UWB Band-Pass Filter With A Notch Response Using The Suspended Stripline," in *2009 Asia Pacific Microwave Conference*, 2009, pp. 902–904.

[47] Y. Chen, Y. Guo, M. Zhan, and R. Xu, "A Broadband Suspended Stripline Bandpass Filter," in *2009 3rd IEEE International Symposium on Microwave, Antenna, Propagation and EMC Technologies for Wireless Communications*, 2009, pp. 804–806.

[48] L.-J. Lin, M.-H. Ho, and W.-Q. Xu, "Design of Compact Suspended Stripline Bandpass Filters With Wide Stopband," *Microw. Opt. Technol. Lett.*, vol. 50, pp. 865–868, 2008.

[49] X. Tan, B. Jin, and R. Zhang, "Well-Designed of UWB Suspended Substrate Stripline Highpass Filters," in *2010 IEEE International Conference on Ultra-Wideband*, 2010, vol. 2, pp. 1–3.

[50] D. M. Pozar, *Microwave Engineering*. United States of America: John Wiley & Sons, Inc., 2005.

[51] P. J. J. Beneat, *Advanced Design Techniques and Realisations of Microwave and RF Filters*. Wiley-IEEE Press , 2008.

[52] H. Jia-Sheng and M. J. Lancaster, *Microstrip Filters for RF/Microwave Applications*. United States of America: John Wiley & Sons, Inc., 2001.

[53] G. L. Matthaei, L.Young, and E. M. T. Jones, *Microwave filters, impedance-matching networks, and coupling structures*. McGraw-Hill, 1980.

[54] G. W. Technology, *CMS-Filter & Coupling Matrix Synthesis Software*. 2013.

[55] S. C. Tang, J. T. Kuo, and S. J. Chung, "Bandwidth and Transmission Zero Control For Compact Dual-Mode Resonator Filter by Extraction of EM Coupling," in *2012 Asia Pacific Microwave Conference Proceedings*, 2012, pp. 661–663.

[56] A. Gorur, C. Karpuz, G. M. Eryilmaz, A. Gruir, C. Karpuz, and G. M. Eryilmaz, "Asymmetric Dual-Mode Microstrip Filters With Adjustable Transmission Zero," in *2007 Asia-Pacific Microwave Conference*, 2007, pp. 1–4.

[57] Y. Zaifeng, Z. Luhong, M. Zhewang, and Y. Xuexia, "Design of A Compact Dual-Band Dual-Mode Microstrip Filter With An Adjustable Transmission Zero," in *2012 IEEE/MTT-S International Microwave Symposium Digest*, 2012, pp. 1–3.

[58] Z. Yao and N. Y. Kim, "A Dual-Mode Bandpass Filter With Tuning Transmission-Zero and Harmonic Suppression For RFID and WiMax Applications," in *2013 Asia-Pacific Microwave Conference Proceedings (APMC)*, 2013, pp. 905–907.

[59] A. K. S. Rathore, A. R. Harish, A. Kumar, S. Rathore, and A. R. Harish, "A Novel Printed Dual Mode Resonator Filter Based on Radial Stub," in *IEEE MTT-S International Microwave and RF Conference*, 2013, pp. 1–4.

[60] W. Menzel and M. Berry, "Quasi-Lumped Suspended Stripline Filters With

Adjustable Transmission Zeroes," in *2004 IEEE MTT-S International Microwave Symposium Digest (IEEE Cat. No.04CH37535)*, 2004, pp. 1601–1604.

[61] C.-L. Wei, B.-F. Jia, Z.-J. Zhu, and M.-C. Tang, "Design of Different Selectivity Dual-Mode Filters With E-Shaped Resonator," *Prog. Electromagn. Res.*, vol. 116, pp. 517–532, 2011.

[62] Q. X. Chu and H. Wang, "A Compact Open-Loop Filter With Mixed Electric and Magnetic Coupling," *IEEE Trans. Microw. Theory Tech.*, vol. 56, no. 2, pp. 431–439, 2008.

[63] P. Martin and J. Ness, "Coupling Bandwidth and Reflected Group Delay Characterization of Microwave Bandpass Filters," *Appl. Microw. Wirel.*, vol. 11, 1999.